INNOV 2019

The Eighth International Conference on Communications, Computation, Networks and Technologies

ISBN: 978-1-61208-758-0

November 24 - 28, 2019

Valencia, Spain

INNOV 2019 Editors

Jaime Lloret, Universitat Politecnica de Valencia, Spain

Pascal Lorenz, University of Haute-Alsace, France

INNOV 2019

Forward

The Eighth International Conference on Communications, Computation, Networks and Technologies (INNOV 2019), held on November 24 - 28, 2019- Valencia, Spain, aimed at addressing recent research results and forecasting challenges on selected topics related to communications, computation, networks and technologies.

Considering the importance of innovative topics in today's technology-driven society, there is a paradigm shift in classical-by-now approaches, such as networking, communications, resource sharing, collaboration and telecommunications. Recent achievements demand rethinking available technologies and considering the emerging ones.

The conference had the following tracks:

☐ Communications
☐ Networking
☐Computing
☐Web Semantic and Data Processing
☐Security, Trust, and Privacy

We take here the opportunity to warmly thank all the members of the INNOV 2019 technical program committee, as well as the numerous reviewers. The creation of such a high quality conference program would not have been possible without their involvement. We also kindly thank all the authors that dedicated much of their time and effort to contribute to INNOV 2019. We truly believe that, thanks to all these efforts, the final conference program consisted of top quality contributions.

Also, this event could not have been a reality without the support of many individuals, organizations and sponsors. We also gratefully thank the members of the INNOV 2019 organizing committee for their help in handling the logistics and for their work that made this professional meeting a success.

We hope that INNOV 2019 was a successful international forum for the exchange of ideas and results between academia and industry and to promote further progress in the areas of communication, computation, networks and technologies. We also hope Valencia provided a pleasant environment during the conference and everyone saved some time for exploring this beautiful city.

INNOV 2019 General Chair
Jaime Lloret, Universitat Politecnica de Valencia, Spain

INNOV 2019 Steering Committee

Yu-Chen Hu, Providence University, Taiwan
Carlos Becker Westphall, University of Santa Catarina, Brazil
Shih-Chang Huang, National Formosa University, Taiwan
Kiriakos Patriarcheas, Hellenic Open University, Greece
Jaime Lloret Mauri, Universitat Politècnica de València, Spain

Juan Carlos Bennett, SPAWAR Systems Center Pacific, USA

INNOV 2019 Industry/Research Advisory Committee

Igor Kotenko, ITMO University and Russian Academy of Sciences (SPIIRAS), Russia
Sung-soon Park, Anyang University and Gluesys Co. LTD, Republic of Korea
Binod Kumar, JSPM Jayawant Institute of Computer Applications, Pune, India

INNOV 2019 Publicity Chair
Pedro Luis González, Universidad Central. Colombia

INNOV 2019

Committee

INNOV General Chair
Jaime Lloret, Universitat Politecnica de Valencia, Spain

INNOV Steering Committee
Yu-Chen Hu, Providence University, Taiwan
Carlos Becker Westphall, University of Santa Catarina, Brazil
Shih-Chang Huang, National Formosa University, Taiwan
Kiriakos Patriarcheas, Hellenic Open University, Greece
Jaime Lloret Mauri, Universitat Politècnica de València, Spain
Juan Carlos Bennett, SPAWAR Systems Center Pacific, USA

INNOV Industry/Research Advisory Committee
Igor Kotenko, ITMO University and Russian Academy of Sciences (SPIIRAS), Russia
Sung-soon Park, Anyang University and Gluesys Co. LTD, Republic of Korea
Binod Kumar, JSPM Jayawant Institute of Computer Applications, Pune, India

INNOV Publicity Chair
Pedro Luis González, Universidad Central. Colombia

INNOV 2019 Technical Program Committee

Manal Abdullah, King Abdulaziz University, KSA
Kishwar Ahmed, Florida International University, USA
Suayb S. Arslan, MEF University, Maslak-Sariyer, Istanbul, Turkey
Carlos Becker Westphall, University of Santa Catarina, Brazil
Juan Carlos Bennett, SPAWAR Systems Center Pacific, USA
Saman Biookaghazadeh, Arizona State University, USA
Eugen Borcoci, University "Politehnica"of Bucharest (UPB), Romania
YK Chang, National Cheng Kung University, Taiwan
DeJiu Chen, KTH Royal Institute of Technology, Sweden
Yung-Yao Chen, National Taipei University of Technology, Taiwan
Albert M. K. Cheng, University of Houston, USA
Enrique Chirivella, University of the West of Scotland, UK
Salimur Choudhury, Lakehead University, Canada
Cosmin Copot, University of Antwerp, Belgium
Poonam Dharam, Saginaw Valley State University, USA
Sanjay Dwivedi, Babasaheb Bhimrao Ambedkar University, India
Luca Ferretti, University of Modena and Reggio Emilia, Italy
Panagiotis Fouliras, University of Macedonia, Thessaloniki, Greece
Marco Furini, University of Modena and Reggio Emilia, Italy
Antoine Gallais, Inria LNE / Université de Strasbourg, France

Copyright Information

For your reference, this is the text governing the copyright release for material published by IARIA.

The copyright release is a transfer of publication rights, which allows IARIA and its partners to drive the dissemination of the published material. This allows IARIA to give articles increased visibility via distribution, inclusion in libraries, and arrangements for submission to indexes.

I, the undersigned, declare that the article is original, and that I represent the authors of this article in the copyright release matters. If this work has been done as work-for-hire, I have obtained all necessary clearances to execute a copyright release. I hereby irrevocably transfer exclusive copyright for this material to IARIA. I give IARIA permission or reproduce the work in any media format such as, but not limited to, print, digital, or electronic. I give IARIA permission to distribute the materials without restriction to any institutions or individuals. I give IARIA permission to submit the work for inclusion in article repositories as IARIA sees fit.

I, the undersigned, declare that to the best of my knowledge, the article is does not contain libelous or otherwise unlawful contents or invading the right of privacy or infringing on a proprietary right.

Following the copyright release, any circulated version of the article must bear the copyright notice and any header and footer information that IARIA applies to the published article.

IARIA grants royalty-free permission to the authors to disseminate the work, under the above provisions, for any academic, commercial, or industrial use. IARIA grants royalty-free permission to any individuals or institutions to make the article available electronically, online, or in print.

IARIA acknowledges that rights to any algorithm, process, procedure, apparatus, or articles of manufacture remain with the authors and their employers.

I, the undersigned, understand that IARIA will not be liable, in contract, tort (including, without limitation, negligence), pre-contract or other representations (other than fraudulent misrepresentations) or otherwise in connection with the publication of my work.

Exception to the above is made for work-for-hire performed while employed by the government. In that case, copyright to the material remains with the said government. The rightful owners (authors and government entity) grant unlimited and unrestricted permission to IARIA, IARIA's contractors, and IARIA's partners to further distribute the work.

Table of Contents

Internet of Underground Things ESP8266 WiFi Coverage Study

Laura García, Lorena Parra, Jose M. Jimenez, Jaime Lloret
Integrated Management Coastal Research Institute
Universitat Politècnica de València
Valencia, Spain
email: laugarg2@teleco.upv.es, loparbo@doctor.upv.es, jojiher@dcom.upv.es, jlloret@dcom.upv.es

Abdelhafid Abouaissa, Pascal Lorenz
Network and Telecommunication Research Group
University of Haute Alsace
Colmar, France
email: abdelhafid.abouaissa@uha.fr, lorenz@ieee.org

***Abstract*— The Internet of Underground Things (IoUT) is a novel concept regarding Internet of Things (IoT). It could have countless applications, particularly in agriculture as buried devices do not interfere with the machinery. Furthermore, wireless communication among buried and above ground devices would allow a significant cost reduction as wires would not need to be deployed and wires would not be destroyed by machinery or impede the correct performance of the activities performed by the workers of the field. In this paper, we perform a WiFi coverage study of ESP8266 nodes placed both underground and above ground so as to assess the current lack of knowledge in IoUT and the performance of low-cost controller boards for IoUT applications. Tests were performed with ESP8266 nodes buried at depths of 10 cm, 20 cm, 30 cm and 40 cm in a field located in an area of citrus fields. A node programmed as an AP (Access Point) was placed at several distances at a height of 50 cm. Results showed that the coverage was better for the node buried at a depth of 20 cm.**

Keywords- IoUT; WiFi; coverage; ESP8266; agriculture

I. INTRODUCTION

The forecasts of the increase of the population of the world [1] leads to taking new and better solutions in agriculture. In these forecasts, it is estimated that 70% more food than the food produced nowadays will have to be cultivated and manufactured by 2050. This makes agriculture become one of the key sectors of the global economy. It is necessary to achieve greater efficiency, in order to be able to supply the entire population and optimize the consumption of resources, such as irrigation water, fertilizers or pesticides.

A greater efficiency can be achieved by applying new technologies in crops. Using sensors, farmers obtain information on different parameters related to their crops and help them in making decisions [2]. The application of these new technologies in crops brings with it a significant reduction in production costs and an increase in the quality of the products. In addition, farmers may need to spend less time physically present in the crop fields, being able to obtain the crucial information that will allow them to perform data analysis in real time. This will ultimately improve the quality of life of people and the productivity of their businesses. Initially, the tendency is that, due to the need for a return on investment, the products that reach a higher price in the market will be the ones that will be subject to a greater investment in technology.

The IoT technology has a fundamental role. Its application in multiple areas makes it possible to adopt the most appropriate solutions to different problems. There are a lot of studies on the application of IoT in different environments. For example, the authors [3] presented a study of the most used IoT technologies in Smart Cities. Agriculture is one of the areas in which this technology is increasingly implemented. For example, if environmental and crop health parameters are controlled, the use of both water resources and pesticides can be avoided, which will reduce the impact on the environment. This is what we usually call precision agriculture.

The transmission of the data obtained by the sensors located in the crop fields, is usually done using wireless technologies, such as IEEE 802.11, Bluetooth, ZigBee, LoRa, 3G, 4G or 5G. Devices usually have a low energy consumption which usually has as a characteristic a low transmission range associated with it. That is partially due to the difficulty in being able to provide a constant energy supply, except if it is done by battery systems that are usually recharged by means of green technologies, such as solar panels.

In the space of IoT applied to agriculture, we can highlight for its novelty the studies presented in the IoUT. In this case, IoT devices are partially or totally buried for monitoring and detection in real time. In its application to agriculture, underground sensors are used, which control different systems, both irrigation and machinery, to help farmers and agronomists in making decisions. By using buried sensors, we can control crop parameters, such as soil temperature and humidity, more efficiently than with the parameters that are only estimated on surface. Furthermore, due to the underground location of the nodes, there are major problems when working with machinery in their environment, because they can be unused or destroyed.

Our proposal presents the study of the transmission between underground and above ground ESP8622 nodes. The study is carried out due to the lack of previous studies related to IoUT regarding its location in crops. We have studied the signal in a low-vegetation area surrounded by citrus fields. We have buried several nodes at different depths, and we have observed the degradation of the signal

 ISBN: 978-1-61208-758-0

as a function of the separation of the emitting and receiving nodes, both in distance and in depth.

The rest of the paper is organized as follows. Section 2 presents the related work. The proposed architecture is presented in Section 3. The testbed description is depicted in Section 4. The results are discussed in Section 5. Section 6 depicts the mathematical model. Finally, the conclusion and future work is presented in Section 7.

II. RELATED WORK

The IoUT is quite the recent concept, thus few papers exist on this topic. Several of them are surveys, such as the survey on the state of the art on the Internet of Underground Things performed by Vuran et al. [4]. The authors determined the different components of an IoUT architecture as Underground Things for sensors and embedded systems deployed underground, mobile sinks that gather the data from underground things, base stations that act as a gateway and cloud services that provide storage and data processing. The communication among the elements of a IoUT architecture can be between underground things or between underground and above ground things. Soil moisture and texture and variations in distance and depth influence on the quality of the communications. Furthermore, Leles et al. [5] presented a summary of the challenges of IoUT for railways networks. The authors performed a coverage test in a tunnel where signal intensities of -55 dB were reached for 100 m of distance. The considered challenges are the environmental requirements, such as power supply, electromagnetic compatibility, and the mechanical and thermal requirements, the mobility, the use of an independent frequency network that should provide enough bandwidth for the transmitted data, the QoS, the safety of the network and the energy efficiency.

Salam et al. [6] performed several studies were different depths and soil types were considered. The effects of soil type and moisture on the multi-carrier modulation were analyzed. The authors analyzed the channel frequency response and the empirical antenna return loss for sandy soil, silt loam and silty clay loam with varied moisture levels. Results showed that for distances up to 12m, 124 Mbps were reached. Furthermore, 362 Mbps were reached for shorter distances and low moisture. Moreover, the authors concluded that capacity gains between 56% and 136% were reached with sub-carrier bandwidth adaptation based on the type and moisture of the soil. Moreover, a real-time permittivity and soil moisture monitoring for wireless underground communication called Di-Sense was presented in [7]. In order to do so, the propagation path loss and the velocity of wave propagation were utilized. Experiments were performed in a greenhouse with burial depths of 10, 20, 30 and 40 cm, a frequency ranges between 100 and 500 MHz and slit loam, silty clay loam and sandy soils. Results showed high accuracy for depths up to 40 cm and distances ranging from 1 to 15 meters. Lastly, a study on the performance of varied modulation schemes in underground communications was performed in [8]. Multiple antennas were utilized to exploit the direct, lateral and reflected components of the wireless underground channel. Results showed bit errors rates (BER) of 10^{-3} for delay spreads below 0.05. Results showed that equalization impacts the performance of the IoUT communication with the 8-Tap Decision-Feedback Equalizer as the best one. Furthermore, DBPSK and DPSK presented better performance for channels without adaptive equalizations. Lastly, the authors presented two new receiver designs for IoUT communications named Lateral-Direct-Reflected and 3W-Rake. The three antenna LDR design achieved a BER of 10^{-5}.

Magnetic induction has been considered as well to perform wireless underground communication. Saeed et al. [9] presented a study on the localization in magnetic induction for IoUT for gas and oil reservoirs. The authors propose a three-dimensional MI-based location procedure based on the Cramer Rao Lower Bound (CRLB) that considers channel parameters. The considered depth is 1.8 Km. Simulation results showed that the accuracy of the localization procedure is affected by the noise variance, the frequency, the number of anchors and the number of underground things.

Considering the need of more extensive studies of the underground environment for IoT communications, especially for agricultural environments, in this paper we perform a coverage study for IoUT wireless communication performed by ESP 8266 IoT nodes.

III. ARCHITECTURE

In this section, we present the proposed architecture for an IoUT solution for agriculture. Figure 1 shows the different levels of the proposed architecture. It is formed by four levels: Nodes and Sensors, Wireless Network, Internet, Data Center and Artificial Intelligence.

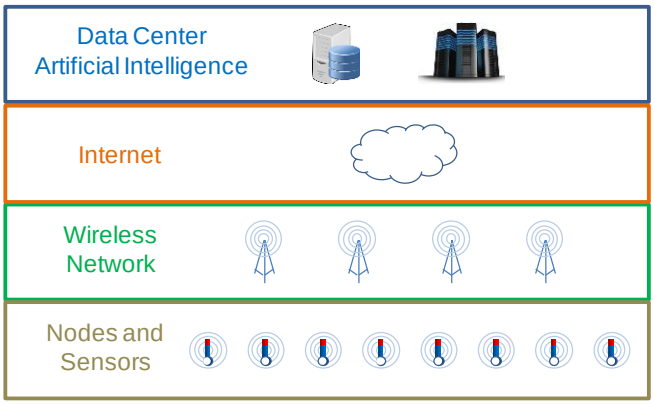

Figure 1. Proposed architecture

The nodes are located in the lower level with the sensors connected to them. These sensors will obtain all the necessary information of the crops for a later decision-making process, in which Artificial Intelligence is used in order to perform smart agriculture. The level above the first one is the level of the wireless network. At this level, the transmission of data, obtained in the fields of agriculture through the sensors by using a wireless network, is performed. At this level, the access points (AP) are located,

 ISBN: 978-1-61208-758-0

which collect the signals sent by the nodes and transmit them until they reach a gateway device. The gateway allows the connection through the Internet to a remote location. The next level is the Internet, where the obtained data is transmitted using an Internet Provider connection to the location where they are stored. This connection can be achieved using different technologies, such as DSL, wireless technology and 3G / 4G mobile data. We select the one that fits our requirements with the lowest costs depending on the location of the crops. Finally, in the upper layer, we locate our Data Processing Center that employs Artificial Intelligence. At this level, the information storage and treatment systems are located. In this location, the data will be stored so that it can be retrieved at any time and then be processed. With this data, the farmers and engineers can obtain relevant information for decision making.

IV. TESTBED DESCRIPTION

In this section, the design of the testbed is going to be described.

To perform this test, four nodes were programmed to measure the Received Signal Strength Indicator (RSSI) and one node was programmed as an AP. The utilized node was the Mini D1 ESP 8266 node for both the AP and the RSSI-meter. The Mini D1 presents 11 digital input/output pins and has an operating voltage of 3.3 V. The specifications of the ESP8266 chip and the antenna can be found in [10].

The nodes that measured the RSSI were placed on 80x80x36 mm sized protective boxes and the AP node was placed inside a 155X105X62 mm protective box that included the power supply. The power supply was a DC 5V-1000mA power bank with a capacity of 2000mAh. The ESP8266 nodes were placed inside the box with the antenna placed upwards. The nodes were taped in order to avoid any movement of the node inside the box at the time they were buried. A cable that connected the node to a laptop went through a hole of the box that was sealed afterwards so as to avoid the soil getting to the node. The data on the RSSI was gathered through the serial port of the node using the Arduino IDE.

As Vuran [4] described, IoUT may be comprised of underground and above ground elements. In this study, we test the signal strength between an underground and an above ground ESP 8266 node so as to determine the possible use of low-cost Wi-Fi nodes for IoUT purposes. As it can be seen in Figure 2, four RSSI-meter nodes were buried underground at distances 10 cm, 20 cm, 30 cm and 40 cm deep into the ground. They were placed in the same hole one on top of the other and adding the necessary soil between each protective box so as to reach the required depth. Then, the AP was placed at a height of 50 cm for each of the measures. The starting point for the measures was 1 meter. Each measure is then performed in increments of 1 meter until the connection is lost. The orientation of the antennas and the position of the nodes was always the same
for all the measures. The images of how the nodes were placed on the field are presented in Figure 3. When the RSSI-meter nodes were buried, the soil was slightly

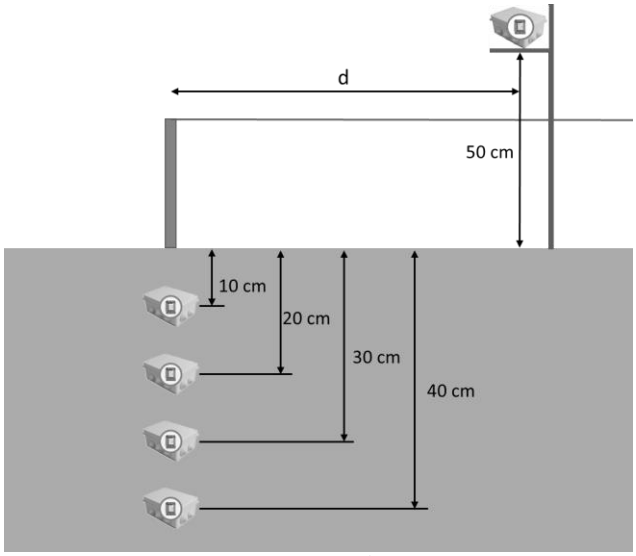

Fig. 2. Description of the testbed.

compacted, and the soil of the surrounding areas was not disrupted.

The test was performed in a Mediterranean area in a field were a citrus plot used to be. The satellite image of the field can be seen in Figure 4. As it can be seen, the area is used for agriculture and several citrus fields surround the field were the tests were performed. That area of the field was selected due to the lack of thicker and other types of vegetation. The soil was a predominantly sandy soil and has the appropriate qualities for citrus plantations. There is no presence of housing in the area and the use of IoT systems for agriculture was unknown. Therefore, a preliminary test was performed to confirm the absence of any other signal from other networks in the area.

V. RESULTS

This section presents the results of the experiment. We show the gathered RSSI at different distances. Then, the attenuation effect of the soil is described.

First, the values of RSSI are presented for each set of data (10, 20, 30 and 40 cm of buried depth.). The mean, maximum, and minimum of the RSSI gathered at different distances are shown. This step is necessary in order to evaluate the variance of the data. Figure 5 presents the data of the RSSI gathered by the node buried at 10cm. Even though we can expect to have a uniform decrease in the signal as no vegetation or building are in the studied area, the soil itself can cause multipath effect. The soil is not uniform and it can have different densities in different points which can cause those constructive and destructive interferences. In the first measured point, at 1m of the node in horizontal distance, the mean RSSI was -66dBm. The RSSI decreased quickly and uniformly to -84 when the node was placed at 3 m from the AP. This signal is considered as a poor or unstable signal, and the communication between both devices might have further problems. From this point, 3m,

 ISBN: 978-1-61208-758-0

Fig. 3. Nodes placed on the field

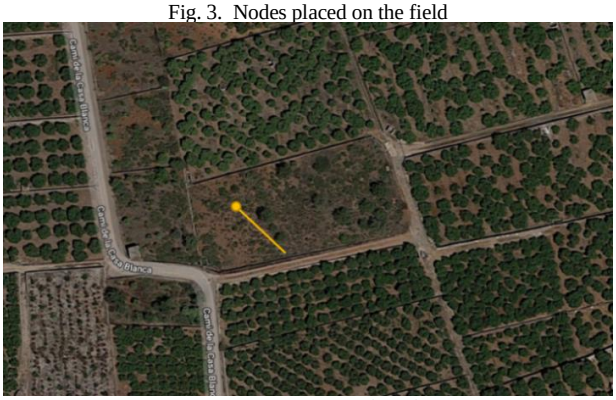

Fig. 4. Satellite image of the field.

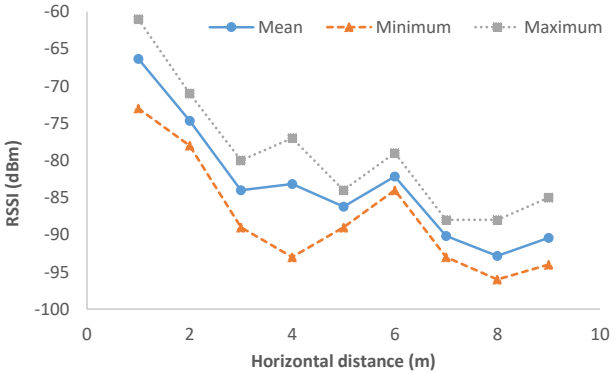

Fig. 5. RSSI with node buried at a depth of 10 cm.

the signal is affected by multipath effect and the attenuation is not uniform. In some points, 4, 6 and 9 m the RSSI increases. It is important to note that some points as 1 or 4m have a big difference between the maximum and the minimum RSSI values, with a standard deviation higher than 4 in both cases. The mean standard deviation of this set of data is 3.21. At distances 10 and 11m the connection between the node and the AP was lost.

Figure 6 details the data gathered with the node buried at a depth of 20cm. In this case the signal attenuation is more uniform than in the previous case. The RSSI in the first measured point is -61dBm (with minimum of -62 and maximum of -60dBm). The last measured point where the node is connected to the AP is 8m with a RSSI of -90dBm. In this case, no clear evidences of multipath effect are found. We suspect that, as in the precious case, there where different densities in the soil which might cause it. Nonetheless, the data (mean, maximum and minimum) follows a uniform attenuation. The standard deviation of this data is 1.67. Apparently in this case, the standard deviation increases with the distance.

The data of RSSI from the node burried at 30cm can be seen in Figure 7. In this case, the attenuation follows almost a lineal realtionship. There is one measured distance, 5m, where the RSSI increases, but in the rest of the cases it decreases with the distance. The mean RSSI at 1m is 71dBm (minimum and maximum are -68dBm and -74dBm). The last measured point where the node was connected to the AP was at 7m, with a mean RSSI of -95dBm. The mean standard deviation of this data is 1.75, which is simmilar to the standard deviation with the node buried at depth of 20 cm.

Figure 8 presents the data gathered with the node buried at a depth of 40cm. The mean RSSI at 1m was -72dBm, the minimum was -73dBm and the maximum -71dBm. The RSSI indicates a signal attenuation with the distance following a uniform behavior. Besides, at 4m, the RSSI increases because a possible multipath effect could be causing a constructive interference. The signal of the AP was lost after 6m. The last measured RSSI was -92dBm. The standard deviation of the data gathered at a depth of 40cm was 1.57. This data has almost the same standard deviation as the data from the nodes buried at a depth of 20cm and 30cm.

Finally, we can use the data shown in Figures 5 to 8 to create a visual model by interpolating this data. The model can be seen in Figure 9. The points where the signal was lost are entered as -110dB to generate this model. Even though we can expect the best results with the shallowest node, the node buried at 20cm seems to have better signal in the first 8m. Although, the node which has coverage at further distances is the node buried at 10cm, we must consider not only the link existence but also the coverage in terms of RSSI. The values of RSSI lower than -70dBm are considered as fair, lower than -80dBm are considered as unstable signal, and lower than 90 are considered as very unstable connection. Thus, although the node buried at 10cm has coverage until 9m, we should only consider the values higher than 90dBm. Therefore, the node which has higher coverage is the node buried at 20cm. The explanation is that, probably the signal of the node buried at 10 cm is highly affected by the air-soil interface.

VI. Mathematical Model

In this section, the mathematical model of the received power is presented. The received power is obtained utilizing the power balance formula [11-12] provided in (1).

$$P_{rx} = P_{tx-1m} - n * 10 * \log d - L_{humidity} - L_{soil} \quad (1)$$

Where P_{rx} is the received power expressed in dBm, $P_{tx\text{-}1m}$ is the transmitted power at 1 meter in dBm which is -59,857 dBm for the ESP8266 nodes, n is the attenuation variation index which is 2 for air, d is the distance between transmitter and receiver expressed in meters, $L_{humidity}$ is the losses due to humidity for the two main hydrometric areas of Spain, areas H and K, which is 0.0026 dB [13] and L_{soil} are the losses due to the underground propagation of the

signal. The theoretical received power at 1 meter is obtained with (2).

$$P_{tx-1m} = 20\ \log_{10} d + 20 \log_{10}(f) + 20 \log_{10}\left(\frac{4\pi}{c_0}\right) \quad (2)$$

Where c_0 is $3*10^8$ m/s and f is the operational frequency in Hz. Furthermore, the 100 mW power commonly used for WiFi transmissions should be considered. The losses due to soil, L_{soil}, are presented in (3) [14].

$$L_{soil} = L_m + L_\alpha \quad (3)$$

Where L_m is the attenuation caused by the variation in wavelengths and L_α corresponds to the losses due to the attenuation constant. Each of them is presented in (4) and (5) respectively.

$$L_m = 20 \log\left(\frac{\lambda_0}{\lambda}\right) = 20 \log\left(\frac{\frac{c_0}{f}}{\frac{c}{f}}\right) = 20 \log(\sqrt{\mu_r \varepsilon_r}) \quad (4)$$

$$L_\alpha = 8.69 \alpha d_{soil} \quad (5)$$

The attenuation constant is given by (6).

$$\alpha = \frac{1}{5.31*10^{-3}*\frac{\sqrt{\varepsilon'}}{\sigma}} \quad (6)$$

Obtained from the expressions of penetration depth d=1/α and the expression simplified expression for mediums where μ=1 as soil [15], expressed as $d = 5.31 * 10 - 3(\sqrt{\varepsilon'}/\sigma)$. The real part of the permittivity for a sandy soil ε' is 6.53 (TDR), the imaginary part of the permittivity ε' is 1.88 (TDR) and the conductivity σ is 2.32 (mS/m).

The results of the model for a depth of 10 cm are presented in Figure 10. As it can be seen, the results are very similar to the real measures obtaining a determination coefficient r^2 of 0.8256. The results of the model for a depth of 20 cm are presented in Figure 11. The r^2 for this depth is 0.8259. Figure 12 presents the results of the model for the depth of 30 cm. The obtained determination coefficient r^2 for this depth is 0.6084. Lastly, the results of the model for the depth of 40 cm are presented in Figure 13. The r^2 of this depth is 0.0158. This is the depth were the model is the least approximated, however, it is still useful for an estimation. The heterogeneity of the soil and possible stones or other materials that change the dielectric characteristics of the soil may introduce further losses that do not affect the other depths.

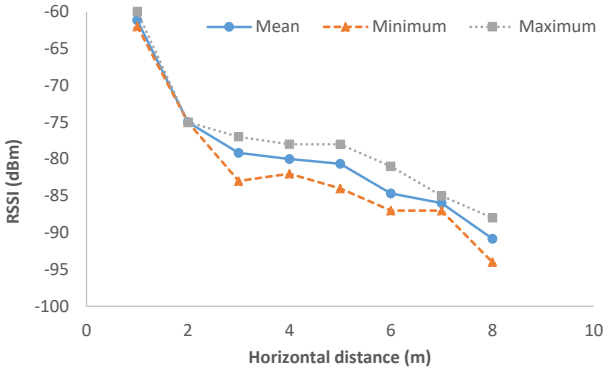

Fig. 6. RSSI with node buried at a depth of 20 cm.

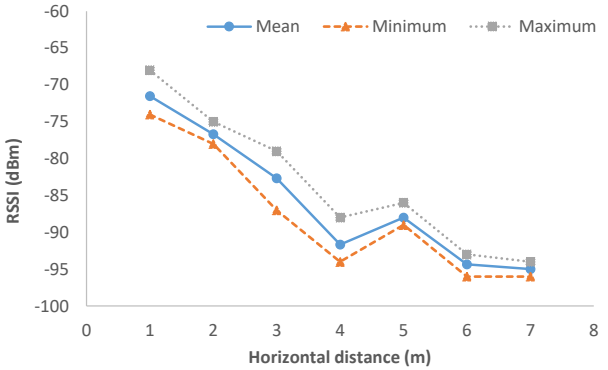

Fig. 7. RSSI with node buried at a depth of 30 cm

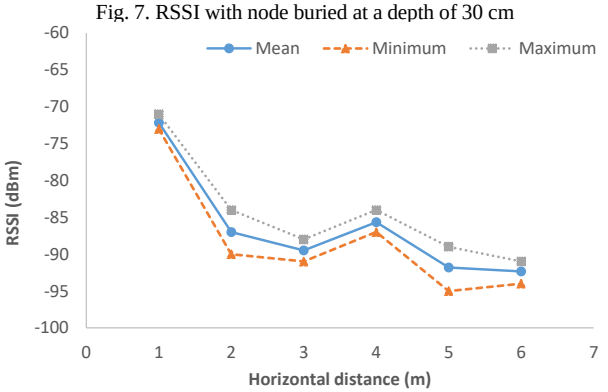

Fig. 8. RSSI with node buried at a depth of 40 cm

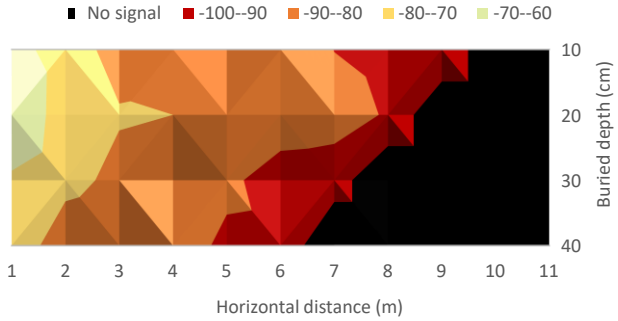

Fig. 9. Visual model of the RSSI at different depths.

VII. Conclusions

In this study, we evaluate the effects in the connectivity of different nodes buried at different depths connected to an AP that was located at 0.5m over the soil. The RSSI was measured at each depth and the AP was moved from 1m to 11m from the nodes. An Architecture for an IoUT system was proposed and a mathematical model to determine the received power between underground and above ground nodes was presented.

As it is expected, the deeper the node, the lower the coverage. The coverage with the shallowest node reaches 9m, while the coverage of the deepest mode only reaches 5m. Nevertheless, if we consider the quality of the link as the value of RSSI, we can conclude that the coverage is better when the node is buried at 20cm. The standard deviation of the RSSI is maximum when the node is located closer to the surface, with a mean value of 3.21. Once the nodes are buried at higher depths, up to 20cm, the standard deviation decreases to 1.6 approximately. It might be caused by the air-soil interface which affects the node buried at 10cm greatly.

The future works will be aimed to evaluate the effect of the change the height of the AP and to evaluate the effect of having the AP on the soil and inside the soil. Moreover, we

 ISBN: 978-1-61208-758-0

want to repeat this test bench with other IoT devices and different types of soil. Furthermore, we will perform these tests with other wireless technologies, such as ZigBee and LoRa.

ACKNOWLEDGMENT

This work has been partially supported by the European Union through the ERANETMED (Euromediterranean Cooperation through ERANET joint activities and beyond) project ERANETMED3-227 SMARTWATIR and by the European Union with the "Fondo Europeo Agrícola de Desarrollo Rural (FEADER) – Europa invierte en zonas rurales", the MAPAMA, and Comunidad de Madrid with the IMIDRA, under the mark of the PDR-CM 2014-2020" project number PDR18-XEROCESPED.

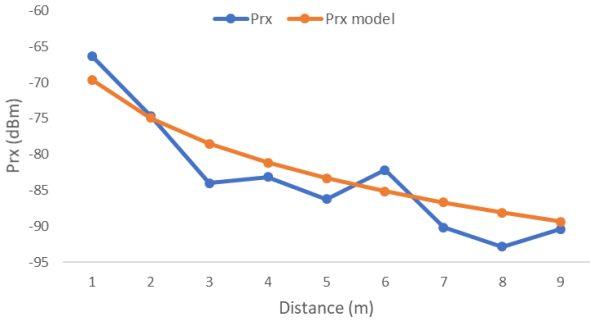

Fig. 10. Results for the model at a depth of 10 cm.

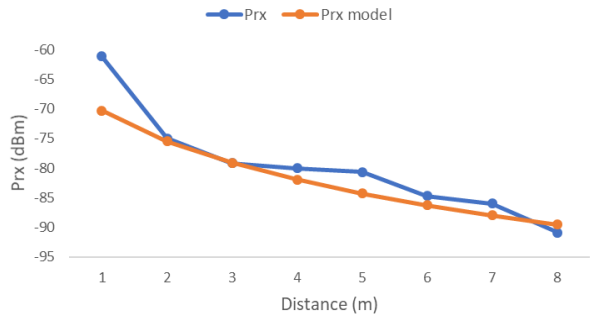

Fig. 11. Results for the model at a depth of 20 cm.

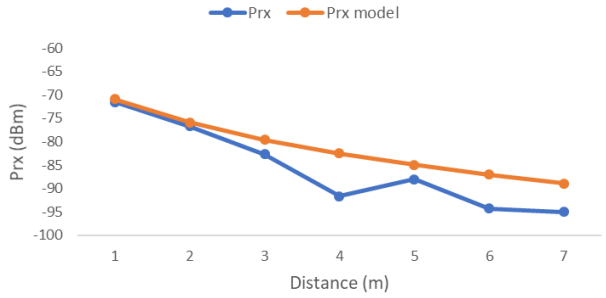

Fig. 12. Results for the model at a depth of 30 cm.

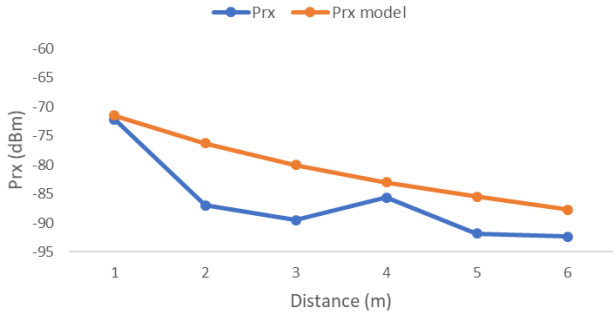

Fig. 13. Results for the model at a depth of 40 cm.

REFERENCES

[1] World Population Prospects 2017. UNITED NATIONS. DESA / POPULATION DIVISION. Available online: https://population.un.org/wpp/ (Last access October 25, 2019).

[2] L. García, L. Parra, J. M. Jimenez, J. Lloret and P. Lorenz, "Practical Design of a WSN to Monitor the Crop and Its Irrigation System", Network Protocols and Algorithms, Vol. 10, No. 4, pp. 35-52, 2018.

[3] L. Garcia, J. M. Jimenez, M. T. Abdullah and J. Lloret, "Wireless Technologies for IoT in Smart Cities", Network Protocols and Algorithms. Vol. 10, No. 1, pp. 23-64, 2018.

[4] M. C. Vuran, A. Salam, R. Wong and S. Imark, "Internet of Underground Things: Sensing and Communications on the Field for Precision Agriculture", IEEE 4th World Forum on the Internet of Things, Singapore, Singapore, 5-8 February 2018, pp. 586-591.

[5] R. de C. D. Leles, J. J. P. C. Rodeigues, I. Woungang, R. A. L. Rabêlo and V. Furtado, "Railways Networks – Challenges for IoT Underground Wireless Communications", IEEE 10th Latin-American Conference on Communications, Guadalajara, Mexico, 14-16 November 2018, pp. 1-6.

[6] A. Salam and M. C. Vuran, "Impacts of Soil Type and Moisture on the Capacity of Multi-Carrier Modulation in Internet of Underground Things", 25th International Conference on Computer Communication and Networks, Waikoloa, HI, USA, 1-4 August 2016, pp. 1-9.

[7] A. Salam, M. C. Vuran and S. Irmak, "Di-Sense: In situ real-time permittivity estimation and soil moisture sensing using wireless underground communications", Computer Networks, Vol. 151, pp. 31-41, 2019.

[8] A. Salam and M. C. Vuran, "Wireless Underground Channel Diversity Reception With Multiple Antennas for Internet of Underground Things", IEEE ICC 2017 Mobile and Wireless Networking, Paris, France, 21-25 May 2017, pp. 1-7.

[9] N. Saeed, M. Alouini and T. Y. Al-Naffouri, "On Achievable Accuracy of Location in Magnetic Induction-Based Internet of Underground Things for Oil and Gas Reservoirs", arXiv preprint arXiv:1901.09556, 2019.

[10] Specifications of the ESP8266. Available online: https://www.elecrow.com/download/ESP-12F.pdf [Last access October 25 2019]

[11] J. Lloret, I. Bosch, S. Sendra and A. Serrano, "A Wireless Sensor Network for Vineyard Monitoring That Uses Image Processing", Sensors, Vol. 11, pp. 6165-6169, 2011.

[12] J. Lloret, J. J. López, C. Turró and S. Flores, "A Fast Design Model for Indoor Radio Coverage in the 2.4 GHz Wireless LAN", 1st - international Symposium on Wireless Communication Systems, Mauritius, 20-22 September 2004, pp. 408-412.

[13] Recommendation UIT-R PN.837-5. Characteristics of Precipitation for Propagation Modeling. Online: http://www.itu.int/md/R07-WP3J-C-0014/en (Last access October 25, 2019)

[14] L. Li, M. C. Vuran and I. F. Akyildiz, "Characteristics of Underground Channel for Wireless Underground Sensor Networks", The sixth Annual Mediterranean Ad Hoc Networking Workshop, Corfu, Greece, 12-15 June 2007, 92-99.

[15] A. M. Sadeghioon, D. N. Chapman, N. Metje and C. J. Anthony, "A New Approach to Estimating the Path Loss in Underground Wireless Sensor Networks", Journal of Sensor and Actuator Networks, Vol. 6, No. 18, pp. 1-11, 2007.

 ISBN: 978-1-61208-758-0

Practical Study of the Temperature Effect in Soil Moisture Measurements

José Luis García-Navas[1], Mar Parra[1], Lorena Parra[1], Javier Rocher[1], Sandra Sendra[1,2], Jaime Lloret[1]
[1] Instituto de Investigación para la Gestión Integrada de zonas Costeras.
Universitat Politècnica de València Valencia, Spain
[2]Dept. of Signal Theory, Telematics and Communications Department (TSTC).
Universidad de Granada, Granada, Spain
Email: jogarna3@teleco.upv.es, marparbo@hotmail.es, loparbo@doctor.upv.es, jarocmo@doctor.upv.es, ssendra@ugr.es, jlloret@dcom.upv.es

***Abstract*—Precision agriculture is a current tendency whose goal is to increase the crop production while reducing the water and fertilization use. The use of low cost sensors and Wireless Sensor Networks (WSNs) are frequently used to implement complex systems to control the irrigation process in crops. Taking into account the importance of developing these low cost systems, in this paper we present a practical study that compares a commercial soil moisture sensor with the prototype of our inductive soil moisture sensor, which is based on two solenoid coils. Additionally, we measure its performance as a function of the soil temperature to quantify the effect of this parameter in the sensor measurements. The results show that the temperature greatly affects the sensors measurements and, although our sensor could be used to measure the soil moisture as a function of the temperature, the configuration of two solenoids is not the most suitable to perform this kind of measurements.**

Keywords-Inductive sensor; temperature; moisture sensor; wireless sensor networks (WSNs); inductive sensors; water consumption saving.

I. INTRODUCTION

In the last years, the use of sensors in agriculture has experienced a very important growth. Its use has allowed to develop more efficient and precise methods of cultivating. Precision Agriculture is related to the use of technologies (remote sensing, sensors, irrigation strategies, etc.) to enhance the production of the crops and reduce the use of water and fertilizers [1].

The reduction of water usage in agriculture is an important challenge to ensure food security and water resource in the future. Currently, it is estimated that 70% of the water extracted in the world is intended for agriculture. Nowadays, there are different investigations related to the development of water saving techniques since it is foreseeable that the Global Warming will reduce the available water. For this reason, future irrigation systems should be based on the use of moisture sensors and the development of new and more efficient irrigation strategies. Irrigation strategies consist of an improvement in irrigation systems, i.e., the use of drip irrigation instead of flood or sprinkler. It is also interesting to reduce the amount of water in the soil to avoid percolation losses. These are not unique. Any technique and method to control the use of water will help to increase the production of crops. An example of applying new irrigation techniques can be found in the strawberry crop where the application of an irrigation threshold of about -10 kPa, inside the range from -8 kPa to -35 kPa seems to have better results in production and benefits while reducing the water usage [2].

The irrigation strategies are complemented by using different sensors. Many authors propose the use of moisture sensors for controlling the irrigation. An interesting idea to combat the problems in irrigation is to combine the values of soil moisture with environmental parameters such as rain, wind, light or photographic analysis, among others, for calculating the evapotranspiration or detecting disease in plants. For example, Parra et al. [3] propose the use of sensors to monitor water quality, soil moisture, and meteorology. Their system estimates the irrigation needs of citrus plots considering the status of soil and the historic data of measurements.

In regards to soil moisture sensors, we can mainly find two different models, i.e., sensors based on Capacity, Frequency Domain Reflectometry (FDR) and Time Domain Reflectometry (TDR). FDR sensors are based on the measurement of the working frequency of an oscillating circuit. TDR sensors are based on the echo measurement of an electrical signal sent through a material with water. FDR sensors are cheaper than TDR sensors. However, TDRs do not need new calibrations for different soils and it is more precise.

Another method to measure the soil moisture is the use of inductive sensors [4], which have the advantage of not being in contact with the soil, compared to the traditional ones, such as FDR and TDR sensors that must be completely in contact with the ground. The contact of metallic parts of sensors with the ground usually generates problems of corrosion and wrong reading of sensor measurements. The inductive sensors are based on a primary coil that generates a magnetic field which induces a current in the secondary coil. One of the main gaps of this type of sensor is that they are not widely developed. The effects of the temperature, the type of salts or other parameters have not been studied.

This paper presents a practical study to quantify the effect of the temperature in the inductive sensors for monitoring the soil moisture. We test your own prototype based on two coils compared to a commercial sensor. To measure the soil moisture, we measure the induced current

 ISBN: 978-1-61208-758-0

which depends on the environment where it is. Finally, the results are related to the soil temperature.

The rest of the paper is structured as follows. Section 2 shows different papers related to our work. The proposed system is detailed in Section 3. Section 4 describes the communication protocol used to transmit the data between nodes and the algorithm that controls the message exchanges. The obtained results are presented in Section 6. Finally, Section 7 summarizes the conclusion and future work.

II. RELATED WORKS

This section analyzes different papers related to the use of moisture sensors for irrigation crops and gardens.

Haley and Dukes [5] study the water usage in controllers of gardens in four different scenarios, i.e., (1) soil moisture sensor with an automatic controller that does not initiate the irrigation if the volume of water in the soil is over 10%, (2) rain sensor and educational materials with an automatic timer, (3) rain sensor with automatic timer, which stops the system after 6 mm of rainfall, and (4) automatic timer only, which is typical for the region under study. Their results show that the system that reduces the water usage is the moisture sensor with the automatic timer irrigation (scenario 1). In addition, the use of education material (scenario 3) initially reduces the use of water. However, the water consumption increases as a function of the time.

Buttaro et al. [6] study the effect of the irrigation in tomatoes and cucumbers in the cycles of fall-winter and spring-summer. Author use tensiometers to assign the values of water in the soil and analyze two set points, tomatoes in -100 hPa and -400 hPa and Cucumber in -100 hPa and -300 hPa. In the fall-winter cycle, the tomatoes are not affected by the low irrigation while cucumber present a reduction of 8% in the production. In the spring-summer cycle, the cucumbers do not present difference between the two points. However, the tomatoes present a reduction of 40% of production. So, the use of tensiometers with the knowledge of the effect of poor irrigation could be used to reduce the use of water without affecting production.

Kizito et al. [7] study the use of capacity sensors for measuring the moisture and electrical conductivity of soil. To perform the experiments, authors use the ECH2O sensor in the working frequency range from 5 MHz to 150 MHz. Results show that the sensor, working at 70 MHz, could be used in different mineral soils independently to the soil conductivity. However, it is required a specific calibration to measure the conductivity while temperature has low effect on the values of conductivity and moisture thanks to the internal sensor compensation.

Nevertheless, Varble and Chávez [8] compare three sensors (CS616/625, TDT, and 5TE) to measure the permeability of an environment for monitoring the water content. The results show big fluctuations due to temperature, soil texture and conductivity. Moreover, Mittelbach et al. [9] compare three low cost moisture sensors (two of them based on FDR sensors and a capacitive sensor) and a high-accuracy moisture sensor (based on TDR sensor) to see the effect of temperature and the drift over the measurements. The results show that the low cost sensors require a correction to compensate the temperature effect and specific calibration that the TDR sensor does not need.

Nolz et al. [10] compare the use of moisture soil sensor with the soil matrix potential sensors in a vineyard. According to the authors' conclusions, the moisture soil sensor presents faster response to the water evolution and it does not require calibration. Meanwhile, the matrix potential sensor shows the contrary behavior. However, the matrix potential sensors present absolute values. Authors propose the use of the two sensors for obtaining better results during the irrigation monitoring.

Cardell-Oliver et al. [11] describe a wireless sensor network for measuring the soil moisture with a reactive and more robust network. They used Decagon Echo-20 dielectric sensors to measure the soil moisture and a Decagon Echo rain to detect the rain. The objective of this paper is to calculate the evolution of soil moisture. For this reason, the time between measurements changes according to the detected rainfall by the rain sensor. In dry weather, the evolution of water in the soil does not present big variation. With this system, the hydraulic recharge of aquifers and water transport in a field can be estimated the hydraulic recharge of aquifers and water transport in a field

Now, the moisture sensors have an important paper in the reduction of water use in agriculture. The sensors based on capacitive or FDR are the less expensive devices than the TDR ones. Nonetheless, capacitive and FDR sensors are affected by temperature. Therefore, they need to be corrected with a temperature sensor for the correct monitoring of soil moisture. Moreover, they need to be calibrated for the different sort of soil. On the other hand, the TDR are more robust and do not need specific calibration. However, TDR is more expensive than FDR and capacitive sensors. The matrix water sensors are another alternative. However, this type of sensor has high costs and do not provide a rapid response to changes in soil moisture. The sensor presented in this work is cheap and the effect of temperature in the measures is low. This allows the reduction of costs in the deployment of the system in great extensions.

III. SYSTEM DESCRIPTIONS

This section presents the scenario and the architecture proposed in this work. This work is developed in a natural environment where elements like vegetation and orography can influence communications between sensors and all nodes included in the architecture. This architecture will combine sensing devices, communication nodes, and a gateway.

The architecture must be able to collect all data provided by the sensors, to communicate it in a reliable way and to connect to the Internet. Data must be sent from the different sensing devices along the network to reach a Base Station (BS) that works as a Gateway and will be connected to the internet via Ethernet. The Base Station will upload all the data received to a database located on the Internet. The information stored on the Data Base (DB) will be studied and used to extract conclusions about the use of this type of sensors.

 ISBN: 978-1-61208-758-0

Figure 1 shows the architecture of the proposal. It is a Wi-Fi network composed of different Internet of Things (IoT) networks, each one connected to a single BS. On each IoT Network several sensing devices will communicate all his information to a Network Head (NH) that will communicate with the BS. The BS will upload the information to a DB located on the Internet. The information will be uploaded to the DB depending on where the information arrived from.

The sensor modules are divided into two parts, the humidity sensor and the communication module. The humidity sensor is underground, and the communication module is outdoors. Both parts are connected by a wire in order to send the information from the sensor to de communication module. The communication module is an Arduino Wi-Fi module. This module will be programmed in order to read the sensor value and send it to the NH with an Id that relates the sensor value with the sensor that took the value. That Id will permit separate the information to upload it to the DB. Figure 2 is an example of how the sensor is used.

As explained before, sensing devices communicate with an NH and it communicates with the BS. This organization results in a star network where the hub is the BS-Gateway. Using this type of network has the advantage that if some Wi-Fi module stops working it will not affect the entire network. All the information will pass across the BS so it must be enough robust to not stop working. The entire network depends on it. Arduino Wi-Fi modules are programmed to establish a Wi-Fi communication with the nearest NH. Once communication is established, the module will be responsible for generating a package for each value that arrives from the sensor. The package will contain a sensor ID, the sensor value and a time stamp. The time stamp is not going to be used in our study but will help to find out if the sensor stopped working at some point. Each package will be sent to the NH.

The Network Head will be located strategically to take advantage of the low Wi-Fi range. NH will be as near as possible to each sensor and also to the BS to ensure good communication. In cases where the distance or the orography can affect to the Wi-Fi range communication, could be possible the necessity to add one more hop to reach the BS. Talking about the function of HN, it only has to receive every package and transmit them. In this proposal, there are not priorities and the most important aspect is not to lose packages so NH will have enough memory to store a large number of packages queued to be sent.

As shown in Figure 3, the proposal implements the BS by using a Raspberry Pi module gateway. The Raspberry Pi must support Wi-Fi and Ethernet. The BS must be able to receive all the information from different NH using Wi-Fi communication. Once the BS has received the information, it must read it and obtain which sensor the information belongs and depending on that the BS will upload the data on the corresponding table of the DB located on the Internet. The Raspberry Pi will be programmed using SQL sentences in order to upload the DB.

In order to obtain enough and different data to be compared and to extract conclusions about how useful our prototype is, different types of sensors will be used in this architecture, the sensor prototype presented in this paper and also different commercial sensors. In addition, they will be located in different types of soil. This variety of sensors and locations where sensors will be makes the amount of data uncertain. It is also possible that the time between measurements could change from each sensor to others depending on the placement of the sensor.

For all these reasons, the BS must be programmed to be able to process a great amount of data. Moreover, in cases when the BS cannot process all the information and upload it to the Internet, it must have an algorithm that when there is an overflow of information not to lose always the information of the same sensors. That will permit to obtain a regular amount of data of all the sensors.

In order to ensure that no information is lost in wired communication, the data will be sent using the TCP protocol. The ACK confirmation will permit to resend lost packets. The database, which has been mentioned throughout the document, will store all the data obtained for each detection device. For each sensor, there will be a different table on the DB in order to save the information separately and to have it easily accessible. The information stored in that DB will be used in next section to analyze it.

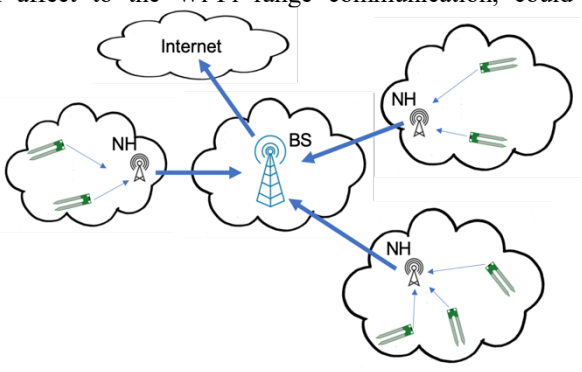

Figure 1. Proposed architecture.

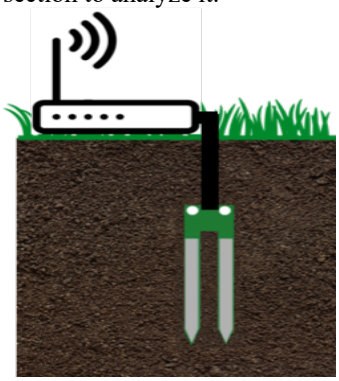

Figure 2. Sensor and Arduino Wi-Fi module

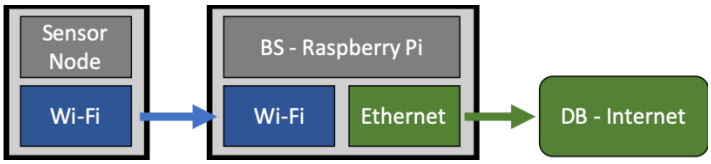

Figure 3. Base Station as Gateway supporting Wi-Fi and Ethernet

IV. PROTOCOL DESCRIPTION

When a new sensor joins the network, it sends a Hello message informing that he wants to join the network. Due to the importance of knowing which sensor is sending the information, all sensors will be programmed with a different ID from the rest, before joining the network. The sensor will include its own ID in the Hello message.

All Network Heads who receive this message will forward it to the BS. When BS receives this message, it will verify if it is the first time this sensor joins the network and, in that case, the BS will create an entry in the DB. BS will respond to the NH with a Hello ACK and the NH will forward it to the sensor.

BS will respond all received Hello messages, even if they are not the first (only one DB entry will be created) due to the possibility of different communication channels. It is the sensor who will finally set the path. The sensor will only accept the first Hello ACK received, learning what NH should communicate. The sensor will send a keep-alive message to this NH and it will forward it to the BS. Now BS also knows what path the sensor will use. The sensor will discard the rest of Hello ACK messages. Once the communication is established, the information exchange is only from sensor to BS. For each data received, the BS updates the DB on the Internet. Figure 4 illustrates how the protocol works.

After the first keepalive message, every data message will also actuate as a keepalive message. In case no data is received in BS for a long time, BS will delete information about path, but not DB information. Because DB information is not deleted, when a sensor wants to join the network for the second time, BS could check that this sensor has already an entry in the DB.

V. ALGORITHM

When sensing devices join the network, they send a Hello Message in order to initiate the connection with the BS. Once the path is set, they begin sending messages. In case of NH, their operation mode consists of forwarding packets between sensing devices and BS, and vice versa. Finally, BS-Gateway operation mode is more complex than other entities operation mode. In this section, we are going to explain the operation algorithm applied in the BS.

After the system starts, it will be receiving messages all the time. Messages can be Hello messages or Data messages. Depending on the type of received message, the BS will actuate in a different way.

When the BS receives a Hello message, it will look at the DB in order to know if it is the first time that the incoming Sensing Device joins the network. The BS will check if this Sensing Device has an entry on the DB. In case of not having an entry, it means that it is the first time that the sensor joins the network, and the BS will create a new table on the DB to store the information of this sensor. BS will always respond to a Hello Message sending a Hello ACK to the sensor through the same path that it arrived from.

In case BS receives a Data Message it will carry out an overflow prevention protocol. Overflow emergency will start with 85% of store occupation. BS keeps track of the number of messages of each sensor that are waiting to be processed. Based on the number of messages the base station will organize the sensors from high to low number of messages waiting to be processed.

In case of an overflow emergency, if the message arrives from a sensor that belongs to the half of the sensors that have more packets waiting, the message will be discarded. If there is no overflow emergency or the message arrives from a sensor that belongs to the half of the sensors that have less packets waiting, BS will put the message in the buffer and will update the count of the number of messages coming from that sensor.

Figure 5 shows the operation algorithm applied when a message arrives to the BS. Once there are packets to be processed, the BS takes the message that first arrived. BS will obtain the Sensor ID from the message and will upload the sensor value to the corresponding table of the DB.

VI. RESULTS

In this section, the results of the aforementioned tests are presented. In order to better understand them, this section is divided into two subsections. The first deals with the results from the first type of soil, the one with 95 % of sand. The results from the soil with 90 % of sand are presented in the second subsection.

A. Results from the first soil

After cooling the soil, with the sensors inside, it reached 1.2 ºC. The soil absorbs heat slower than the air, therefore that temperature is highly probable during the coldest months of the year. Data was collected every 0.1 ºC until the temperature of the soil reached 20 ºC.

 ISBN: 978-1-61208-758-0

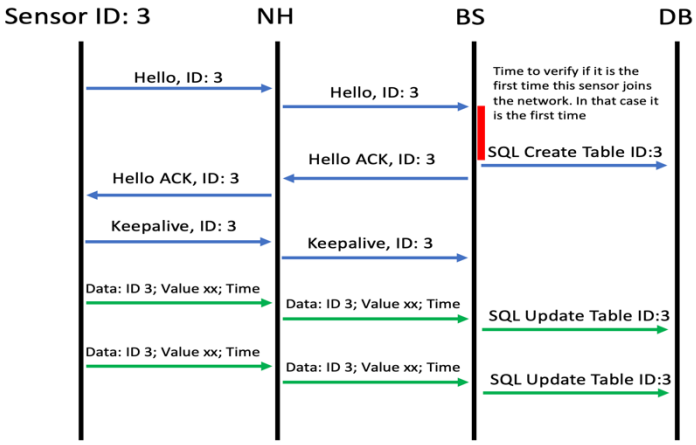

Figure 4. Communication protocol

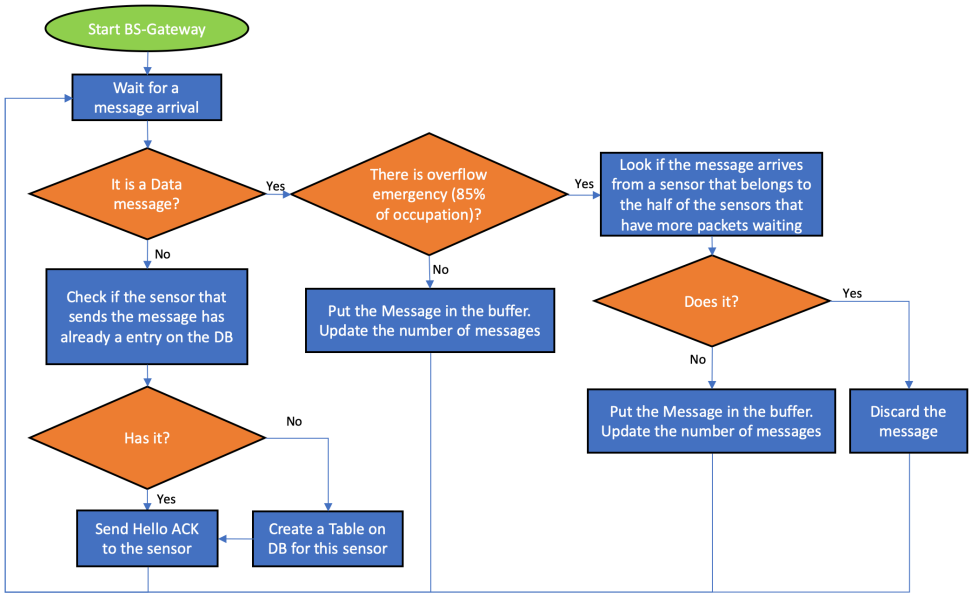

Figure 5. Operation algorithm applied in the BS when a message arrival

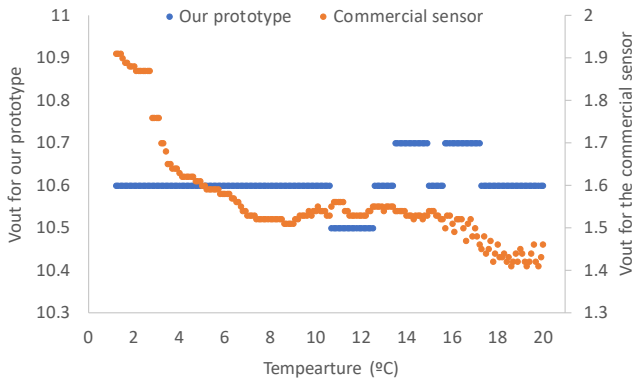

Figure 6. *V*out of both sensors for the first soil form 1.2 ºC to 20 ºC.

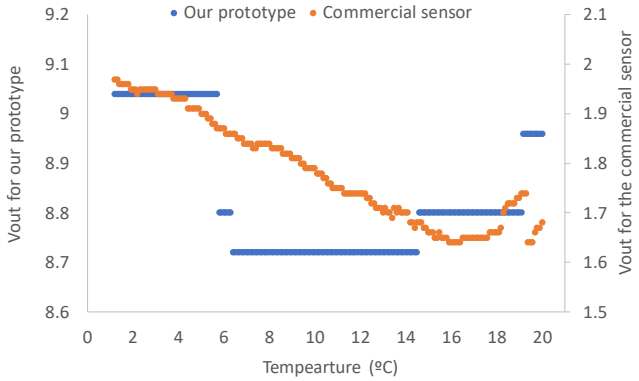

Figure 7. *V*out of both sensors for the second soil form 1.2 ºC to 20 ºC.

The first soil is composed mostly of sand (95%) and has about 45% of soil moisture. For our prototype, the frequency used to measure the Vout is 770 kHz, which is close to the peak frequency. We compare it to the Vout of the commercial sensor.

 ISBN: 978-1-61208-758-0

The results from both can be seen in Figure 6. In order to compare the variation of each sensor, two axes have been developed. Both of them are divided every 0.1 V in their correspondent Vout range.

As we can see in Figure 6, the difference between the readings of our prototype is 0.1 V and the value of 10.6 is almost constant through all the heating process. The amplitude of the data ranges from 10.7 V to 10.5 V, changing barely 0.2 V. Moreover, most of the readings are the same, 10.6 V. The sensitivity of the device used to measure the Vout, in this case, is 0.1 V, thus explaining the variation between the data. Nevertheless, we can affirm that our prototype gives consistent outputs.

When analyzing the data from the commercial sensor it is obvious that the Vout decreases as the temperature increases. We observe that the changes between each temperature are not as extreme as the ones from our prototype, as seen in Figure 6. Nevertheless, this is probably due to the sensibility of the oscilloscope, as mentioned in the previous paragraph. The amplitude of the data goes from 1.9 V to 1.41 V, changing almost 0.5 V. This variation, as well as the inconsistency of the readings makes, the commercial sensors a poor choice for cultures exposed to temperature changes. First, the readings from the commercial sensor increase and decrease with changes of 0.01 V. Later on, when the temperature of the pot reaches 15 ºC, the changes get bigger and they start to increase and decrease with more frequency than they did before.

Seeing the readings from this type of soil, the commercial sensor is not very promising. The changes from the temperature could very easily interfere with the changes from soil moisture and give false readings. On the contrary, our prototype shows a constant value for the Vout, which only changes 0.1 V on some occasions. Depending on the calibration of the sensor this variation could affect in a greater or smaller way. Nevertheless, most of the readings, including both extremes, gave the same output. A total of 139 out of 188 readings gave as Vout 10.6, which is a 73.94 % of the readings.

B. Results from the second soil

As in the experiment done on the first soil, the lowest temperature achieved for this soil was 1.2 ºC. Moreover, it was heated up to 20 ºC as well. This soil, as the first one, is composed mostly of sand. Nevertheless, the percentage of soil composed by said component is 90 %, different from the 95 % of the first soil. It presents a 47% soil moisture, slightly higher than the first soil. The frequency chosen for our prototype is 755 kHz, close to the peak frequency. The readings from our prototype are compared to the readings of the commercial sensor in Figure 7.

We can observe the data represented with a double axis. The axis on the left is for the Vout of the commercial sensor whereas the axis on the right is for the Vout of our prototype. Both show divisions of 0.1 V in the range of each sensor. Our prototype presents bigger differences for this soil. The highest Vout is 9.04 V and the lowest is 8.72 V. The change is of 0.32 V, too big to consider our prototype to be unaffected by the temperature. Moreover, the data shows no consistency in the Vout readings. Both 8.72 V and 8.80 V are the most frequent data with 82 and 52 readings each. They account for 43.61 % and 27.66 % of the readings respectively. Nevertheless, the last data suggest another increase, as seen in Figure 7.

The data from the commercial prototype can be seen in Figure 7. It shows a decrease in the Vout as the temperature increases. Unlike the behavior showed for the first soil, the changes do not get bigger and more frequent after 15 ºC. They do, however, start increasing after 16.5 ºC. At 19.4 ºC the data decreases drastically and starts increasing again. The highest Vout reading for this sensor is 1.97 V and the lowest is 1.64 V. The difference between these readings is of 0.33 V, only 0.01 V bigger than the difference for our sensor. The irregular behavior at higher temperatures makes impossible the modeling of and adjusting equation for the Vout based on the temperature. It is also noted that the sensitivity of the oscilloscope used to measure the Vout of our sensors is of 0.08 V for Vout readings between 1 V and 10 V, which explain the differences between the readings.

VII. CONCLUSION AND FUTURE WORK

Water consumption for agriculture must be efficiently controlled to avoid wasting without reducing the productivity of a crop. To do this, researchers usually use soil moisture sensors. However, their measurements are sometimes affected due to the effect of temperature. Therefore, in this paper, we have performed a practical study to quantify the effect of temperature on soil moisture measurements with inductive sensors. The results have shown that the temperature effect over the soil moisture measurements is quite important and taking into account this data, none of the sensors used for this experiment would be the ideal model for this kind of soil. Nevertheless, it should be noted that a difference of 0.3 V on readings around 9 V is not the same as a difference of 0.3 V on readings around 1.8 V. This change would affect in a greater manner the readings from the commercial sensor.

As future work, we will extend our research by adding group of sensors mechanisms [12] or using clustering techniques [13].

ACKNOWLEDGMENT

This work has been partially supported by the European Union through the ERANETMED (Euromediterranean Cooperation through ERANET joint activities and beyond) project ERANETMED3-227 SMARTWATIR by the “Ministerio de Educación, Cultura y Deporte”, through the “Ayudas para contratacion predoctoral de Formación del Profesorado Universitario FPU (Convocatoria 2016)”. Grant number FPU16/05540.

REFERENCES

[1] R. Gebbers and V. I. Adamchuk, “Precision Agriculture and Food Security,” Science, vol. 327, no. 5967, pp. 828–831, 2010.

[2] L. Gendron et al., “Real-time irrigation: Cost-effectiveness and benefits for water use and productivity of strawberries,” Scientia Horticulturae, vol. 240, pp. 468–477, 2018.

 ISBN: 978-1-61208-758-0

[3] L. Parra et al., “Design of a WSN for smart irrigation in citrus plots with fault-tolerance and energy-saving algorithms,” Network Protocols and Algorithms, vol. 10, no. 2, p. 95, 2018.

[4] N. I. Huth and P. L. Poulton, “An electromagnetic induction method for monitoring variation in soil moisture in agroforestry systems,” Soil Research, vol. 45, no. 1, pp. 63, 2007.

[5] M. B. Haley and M. D. Dukes, “Validation of Landscape Irrigation Reduction with Soil Moisture Sensor Irrigation Controllers,” Journal of Irrigation and Drainage Engineering, vol. 138, no. 2, pp. 135–144, 2012.

[6] D. Buttaro et al., “Irrigation Management of Greenhouse Tomato and Cucumber Using Tensiometer: Effects on Yield, Quality and Water Use,” Agriculture and Agricultural Science Procedia, vol. 4, pp. 440–444, 2015.

[7] F. Kizito et al., “Frequency, electrical conductivity and temperature analysis of a low-cost capacitance soil moisture sensor,” Journal of Hydrology, vol. 352, no. 3–4, pp. 367–378, 2008.

[8] J. L. Varble and J. L. Chávez, “Performance evaluation and calibration of soil water content and potential sensors for agricultural soils in eastern Colorado,” Agricultural Water Management, vol. 101, no. 1, pp. 93–106, 2011.

[9] H. Mittelbach, I. Lehner, and S. I. Seneviratne, “Comparison of four soil moisture sensor types under field conditions in Switzerland,” Journal of Hydrology, vol. 430–431, pp. 39–49, 2012.

[10] R. Nolz, P. Cepuder, J. Balas, and W. Loiskandl, “Soil water monitoring in a vineyard and assessment of unsaturated hydraulic parameters as thresholds for irrigation management,” Agricultural Water Management, vol. 164, pp. 235–242, 2016.

[11] R. Cardell-Oliver, M. Kranz, K. Smettem, and K. Mayer, “A Reactive Soil Moisture Sensor Network: Design and Field Evaluation,” International Journal of Distributed Sensor Networks, vol. 1, no. 2, pp. 149–162, 2005.

[12] J. Lloret, M. Garcia, J. Tomás, and F. Boronat, “GBP-WAHSN: a group-based protocol for large wireless ad hoc and sensor networks,” Journal of Computer Science and Technology, vol. 23, no. 3, pp. 461-480, 2008.

[13] A. Mehmood, J. L. Mauri, M. Noman, and H. Song, “Improvement of the wireless sensor network lifetime using LEACH with vice-cluster head,” Ad Hoc & Sensor Wireless Networks, vol. 28, no. 1-2, pp. 1-17, 2015.

 ISBN: 978-1-61208-758-0

Quantifying the Production of Fruit-Bearing Trees Using Image Processing Techniques

Laura Garcia[(1,2)], Lorena Parra[(1)], Daniel A. Basterrechea[(1)], Jose M. Jimenez[(1,2)], Javier Rocher[(1)], Mar Parra[(1)], José Luis García-Navas[(1)], Sandra Sendra[(3)], Jaime Lloret[(1)], Pascal Lorenz[(2)], Jesus Tomás[(1)], Abdelhafid Abouaissa[(2)], Miguel Rodilla[(1)], Silvia Falco[(1)], María Teresa Sebastiá[(1)], Jesus Mengual[(1)], Juan Andrés González[(1)], Bernat Roig[(1)]

[(1)] Instituto de Investigación para la Gestión Integrada de Zonas Costeras, Universitat Politècnica de València. C/ Paranimf nº 1, Grao de Gandía – Gandía, Valencia (Spain)

[(2)] Network and Telecommunication Research Group, University of Haute Alsace, 34 rue du Grillenbreit, 68008, Colmar, France

[(3)]Dept. of Signal Theory, Telematics and Communications Department (TSTC). Universidad de Granada, Granada, Spain

E-mail: - laugarg2@teleco.upv.es, loparbo@doctor.upv.es, dabasche@epsg.upv.es, jojiher@dcom.upv.es, jarocmo@doctor.upv.es, maparbo@epsg.upv.es, jogarna3@teleco.upv.es, ssendra@ugr.es, jlloret@dcom.upv.es, lorenz@ieee.org, jtomas@upv.es, abdelhafid.abouaissa@uha.fr, mrodilla@hma.upv.es, sfalcog@hma.upv.es, mtsebastia@hma.upv.es, jemencu@hma.upv.es, juagonr1@hma.upv.es, bernat@upv.es

***Abstract*—In recent years, the growth rate of world agricultural production and crop yields have decreased. Crop irrigation becomes essential in very dry areas and where rainfall is scarce, as in Egypt. Persimmon needs low humidity to obtain an optimal crop. This article proposes the monitoring of its performance, in order to regulate the amount of water needed for each tree at any time. In our work we present a technique that consists of obtaining images of some of the trees with fruit, which are subsequently treated, to obtain reliable harvest data. This technique allows us to have control and predictions of the harvest. Also, we present the results obtained in a first trial, through which we demonstrate the feasibility of using the system to meet the objectives set. We use 5 different trees in our experiment. Their fruit production is different (between 20 and 47kg of fruit). The correlation coefficient of the obtained regression model is 0.97.**

Keywords-Persimmon; fruit; image processing; RGB bands, histogram.

I. INTRODUCTION

Agriculture is the main way of obtaining food nowadays. More or less, the 95% of the consumed food is produced directly or indirectly in the soil. This consume is so large that the Food and Agriculture Organization (FAO) had made a project of world crops demand between the years 2015-2030. FAO concluded that is expected by 2030, the demand for life consumption will be large and it needs more agriculture production, expecting that last year an increase of 67 million people. In recent years, the growth rate of agriculture production and crop yield have declined. This has raised fears that the world will not be able to sufficiently increase the production of food and other products to ensure adequate food for the future population [1].

The decline in the production can be explained by a lot of causes like intensive agriculture, which causes degradation in the soil, losing most of the nutrients in this process [2]. Among these nutrients are: Magnesium (Mg), Potassium (K), Phosphorus (P), Nitrogen (N), Sulfur (S), Calcium (Ca) and Iron (Fe), where nitrogen plays an important role, maintaining an optimal ratio with C:N which allows bacteria to provide nutrients to crops[3]. Other causes could be the abrupt changes produced by time due to climate. These sudden changes can cause crop losses in the harvest, due to the rise in temperature, hailstorm, scarcity in water, etc. [4]. This problem intensifies in countries like Egypt where the weather is very dry and the rains are scarce [5]. Because of this, water is a precious resource and implementations are made to improve crop irrigation.

One of the agricultural crops in this area is persimmon, which needs low humidity to obtain an optimal crop. This makes Egypt a place with suitable conditions for the cultivation of this fruit. Due to this factor, the monitoring of the amount of fruit in the tree has been necessary to be able to control the evolution of the crop and regulate irrigation[6]. By monitoring the quantity and quality of the yields of this fruit, it can be regulated the amount of water needed for each tree in each moment, with the advantage of doing the best use of the country's water resources. On the other hand, this agricultural product has caused a lot of controversy among farmers and buyers of this fruit. The technique applied in this paper will help to reduce this problem by providing data of great relevance and improving the capacity of the area to increase the production.

In this paper, we propose a system will consist of the treatment techniques of images, with which to be able to quantify the amount of fruit (in this case of persimmons) relating the pixels to the weight, of each tree and in this way to be able to obtain reliable data of the harvest, being able to take control over these. In this article, a first essay has been carried out, in which the images have been taken with a mobile device. In the future, this method will be carried out by using a drone, allowing measurements of a larger area.

The rest of the paper is structured as follows. Section II presents related works about the techniques of processing images and methods for monitoring irrigation water by other authors. A proposal of the technic is going to be proposed in

 ISBN: 978-1-61208-758-0

Section III. Moreover, Section IV shows the results of the used method. Finally, Section V presents the conclusion and future works

II. RELATED WORK

In this section, we are going to compare other systems that used image processing techniques in farming. The image processing is an important issue for agriculture. Therefore, many scientists have been work on their identification based on pictures.

Other techniques are also analyzed, which is of great importance for agricultural development.

Parra et al. [7] showed the use of image processing techniques to detect the presence of undesired grass species. They utilize a drone with an Arduino module to take pictures. The obtained images are used to determine the best option to detect the presence of weeds. Their results pointed out that the combination of different layers of a single image can be used for detecting the presence of undesired plants.

Ulzii-OrshikhDorj et al. [8] proved the utility of a computer vision algorithm to detect and count citrus on the tree using processing techniques. Their system was able to estimate the yield and comparate the yield estimation results obtained through several methods. They collected 84 images from 21 trees.

Marín et al. [9] showed how the Information and Communication Technology (ICT) offers the possibility of monitoring the grass state to adjust the irrigation regime. They used a drone to take pictures with different vegetation coverage and can obtain results processing this information.

Mello [10] created a system, which includes an aerial platform including a spectral imaging device, a position sensor, an orientation sensor and includes a ground-based sensor platform including at least one soil sensor.

Hutchinson et al. [11] presented a technique for monitoring vegetation changes and dynamics using satellite image time series analysis. The BFAST time series decomposition method was applied, to a ten-year MODIS NDVI time series dataset for the Fort Riley military installation and Konza Prairie Biological Station (KPBS) in northeastern Kansas. Their results had shown that the generated indicators are useful for different uses in land management.

In other cases, different sensors are used for monitoring the requirements of the plants, including irrigation needs. In [12], Achouak et al. showed the use of a wireless network composed of sensors and actuators for controlling the requirements of crops in a greenhouse. Finally, Rocher et al.in [13] presented a sensor for monitoring the fertigation in smart irrigation systems for fruit-bearing trees which can be used jointly with our system.

Our technique has advantages over the others, (i) it is easier to apply only being necessary a front photo of the tree, and (ii) we use a combination of the RGB bands (Red, Green, and Blue). Thus, we obtain an image in which the persimmons are observed correctly and it is possible to apply different equations to predict the harvest quantity.

III. DESCRIPTION OF THE PROPOSAL

In this section, we are going to present the description of the system that we have used, through which we have achieved results that support our initial proposal, as shown in Section IV.

As this is a preliminary test, to minimize the use of resources, the pictures will be taken in the horizontal plane using a camera. In the future, the pictures will be taken in the vertical plane with a drone. To carry out our proposal it has been necessary to use a "curtain" of an opaque material. It allows us to hide the trees behind the tree to be studied. Furthermore, a mobile device has been used from which the images are obtained, which will then be treated.

As we take pictures in different fields and the distances between trees might are not always the same, the distance between the camera and the trees is not constant in all the cases. To solve this problem, we propose to use a reference object. Using this reference object we will be able to correct the distance effect, which may appear when acquiring the images. Figure 1 shows how a tree image is captured.

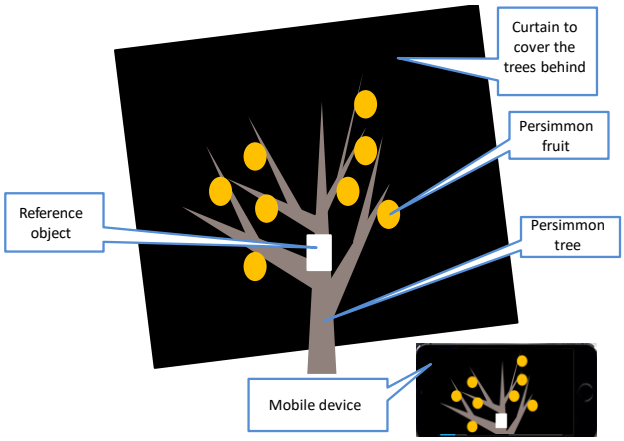

Figure 1. Scenario description

Our experiment is based on the fact that these fruit trees, when the fruit is collected, has lost its leaves. Due to this phenomenon, it is possible to recognize and differentiate the fruits from the rest of the objects that may appear in the images. Therefore the possible effects of overlapping structures are minimized. The branches are the sole overlapping structure and, since they are thinner than the fruits, their possible influence in the prediction model can be despised. Moreover, as the trees are similar in shape and height, the possible underestimation is a constant value. Therefore, it will not affect our prediction model.

As shown in Section IV, once the images were obtained, they have been processed. Decomposing them in the basic colors R, G and B layers (or rasters). The RGB images are to be combined using mathematical operations to obtain new rasters. Then, the histograms of these new rasters are obtained. In this way, it will be possible to detect the region of the histogram that represents the fruit and does not represent the soil.

 ISBN: 978-1-61208-758-0

Subsequently, the histogram is normalized by the surface of the reference object. Finally, the histograms of the difference images are compared with the real kilograms of fruit that were harvested from the tree. A regression model is used to relate the histogram and fruit production.

The data obtained can be used by the farmer as a tool, because he can estimate the harvest he is going to obtain. In addition, as it is already stated in Section 1, this system allows the irrigation to be adjusted according to the observations made.

IV. RESULTS

In this section, we show the obtained pictures and the processing techniques used to quantify the fruit production. First, the combination of bands to find the best composition for fruit detection is presented. Following the correction of the effect of distance is described. Finally, we show the correlation between the number of pixels and production.

A. *Evaluation of best band combination*

The first step is to evaluate which band or bands of the image can be used for fruit detection. The coloration of Persimmon in the moment of yield is between orange and red, therefore we expect to find high pixel-values in the band of red, intermediate values in the green band and low values in the blue band. In Figure 2, the RGB composition and the representation of single bands are presented. The representation of a single band is shown as a color ramp from black (when the pixel value is low) to white (when the pixel value is high). As expected, the fruits have been clearly identified in the red band. Nonetheless, the color of clouds and soil is similar to the color of fruits. The spectral signature is a well-known term, used in remote sensing, which is used to identify different surfaces by comparing the data of two or more bands. It has been used to identify fruits [14].

Therefore, it is necessary to combine the red band with a second band (green or blue). In order to evaluate which is the best band composition, it is necessary to represent and compare the different options. In this paper, and with the purpose of maintaining the system operation as simple as possible, we are going to evaluate the combination of only two bands and using the mathematical operators of addition, subtraction, multiplication, and division.

Figure 3 summarizes the different combinations of R and G or B band in greyscale. The fruits can be distinguished in five out of ten combinations. From those combinations where fruits can be distinguished, in two of them the differences between fruits and soil are higher (R - B and R - G). The highest difference between value of fruit pixels and soil pixels is observed in R - G combination. Moreover, in Figure 3, we can observe the effect of the curtain, and how the curtain is more effective in some band combinations (R+G or R-G) than in others (R/G or G/R).

B. *Correction of the distance effect*

Following, it is necessary to consider the effect of distance from the camera to the tree. Since our units of surface are the pixel and the distance from the camera to the object affects the relation of surface in the picture ($pixel^2$) to surface in reality (cm^2), the effect of different distances must be included in our method. During the picture collection, a reference was included in all the pictures. The reference was attached to the trunk of the tree.

Then, the surface of the reference object in pixels is calculated. The size of the reference in each picture is shown in Table 1. The value in pixels of the reference object will be used to normalize the values of the histogram. Other relevant data for future subsections, such as code of crop field and fruit weight are included. The field number is used as picture ID and the weight is used for the correlation of histograms and fruit production.

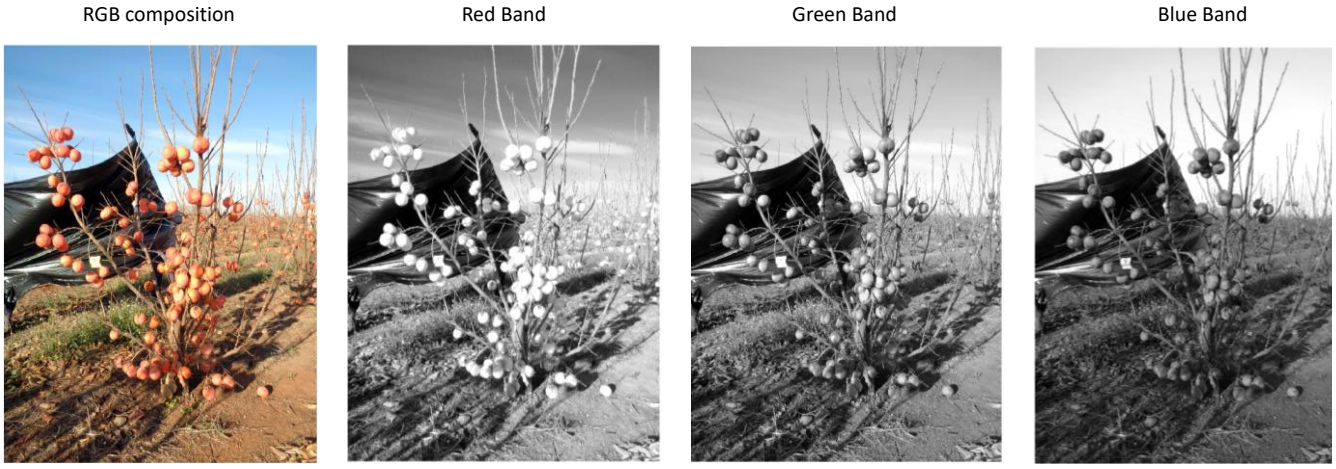

Figure 2. System description.

 ISBN: 978-1-61208-758-0

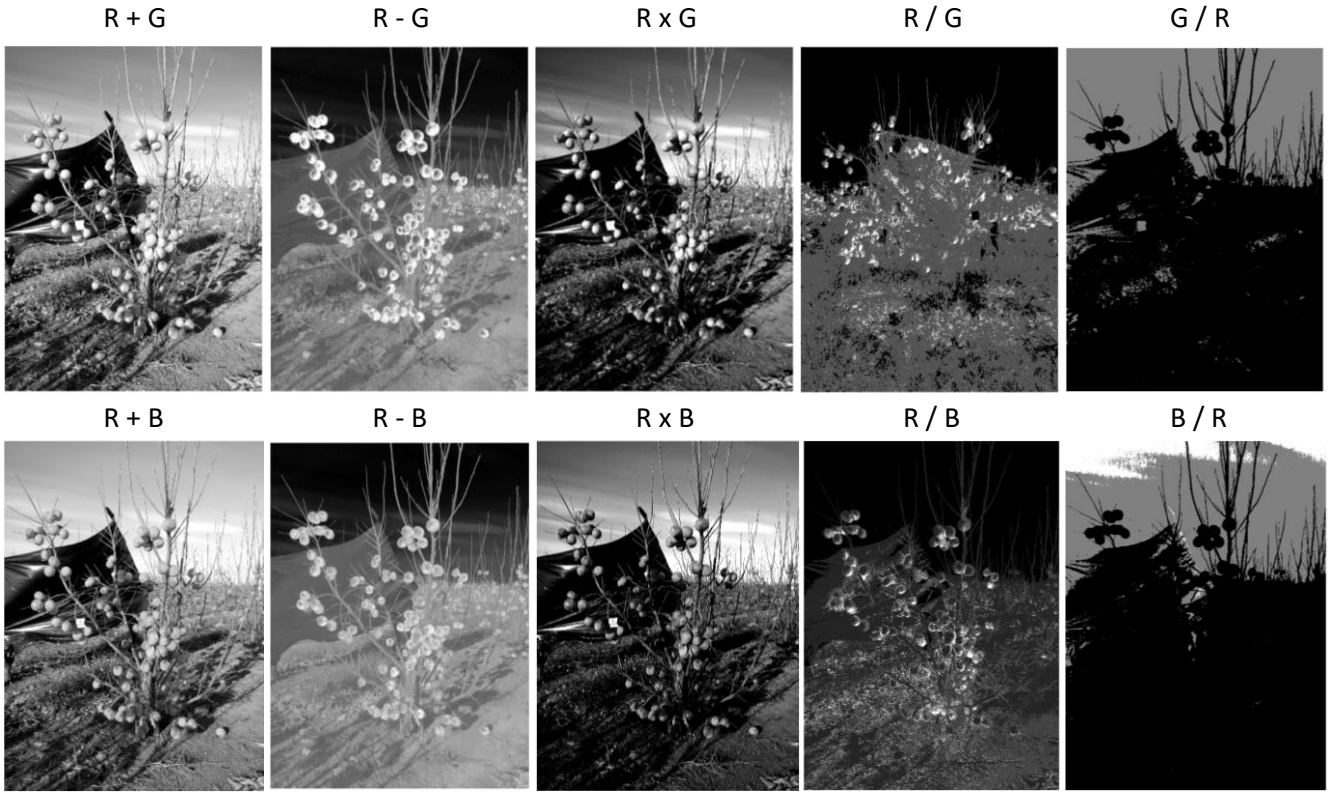

Figure 3. Combination fo R band with G or B band to maximize the fruit detection

TABLE I. REFERENCE OBJECT IN THE USED PICTURES

Image n°	**1**	**2**	**3**	**4**	**5**
Reference surface (pixels^2)	17192	6299	8771	6299	8273
Field number	2446	2696	3230	1535	1541
Fruit weight (kg)	37	35	20	47	43

C. Analysis of histogram data

The next step is to obtain the histogram of the picture, it can be done using different options. In our case, we use the code described in [10] to obtain the data of the histogram using Matlab. Then the obtained histogram is represented, see Figure 4. In this graphic, the comparison of different histograms can be observed. The histogram represents the number of pixels in the image that have a certain value. In the original raster (RGB rasters) the value of pixels is between 0 and 255. Besides, in the newly generated raster, the pixels can have values from -255 to 255. In Figure 4, the different pictures are numbered according to the fruit weight in kg. Before analyzing the differences in the histograms of different pictures, it is necessary to normalize the data. Therefore, we are going to consider the surface of the reference object as 1UA (1 unit of area). Thus, the results of the histograms can be comparable even if the pictures have different sizes and are taken at different distances. The corrected histograms are presented in Figure 5. It is possible to see that the histogram shape has changed. In Figures 4 and 5, the different pixel values represent different surfaces. In our case, the persimmon, according to Figure 3, will be represented by the highest values. Therefore, the last part of the histograms is where the data about the fruit is contained.

 ISBN: 978-1-61208-758-0

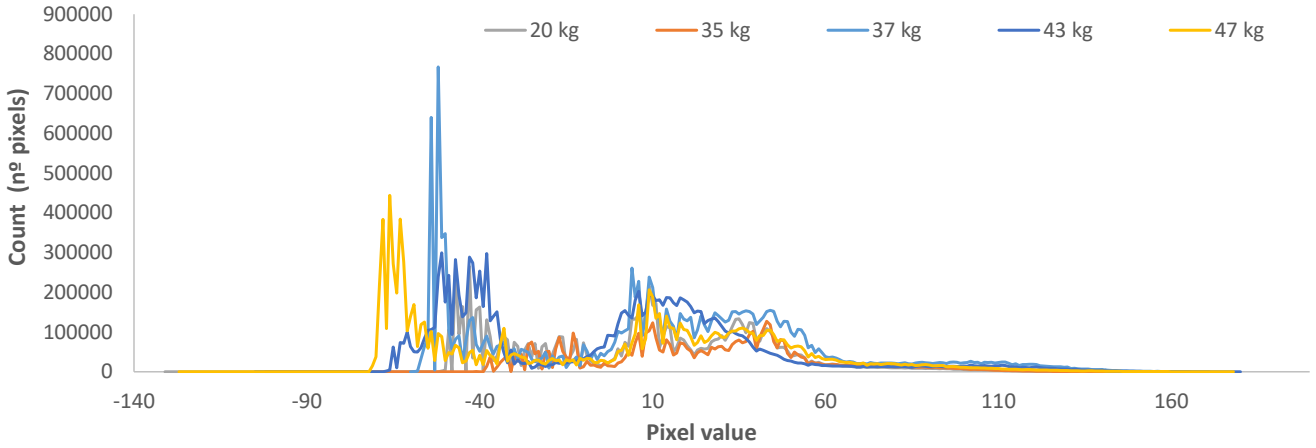

Figure 4. Histogram of studied images

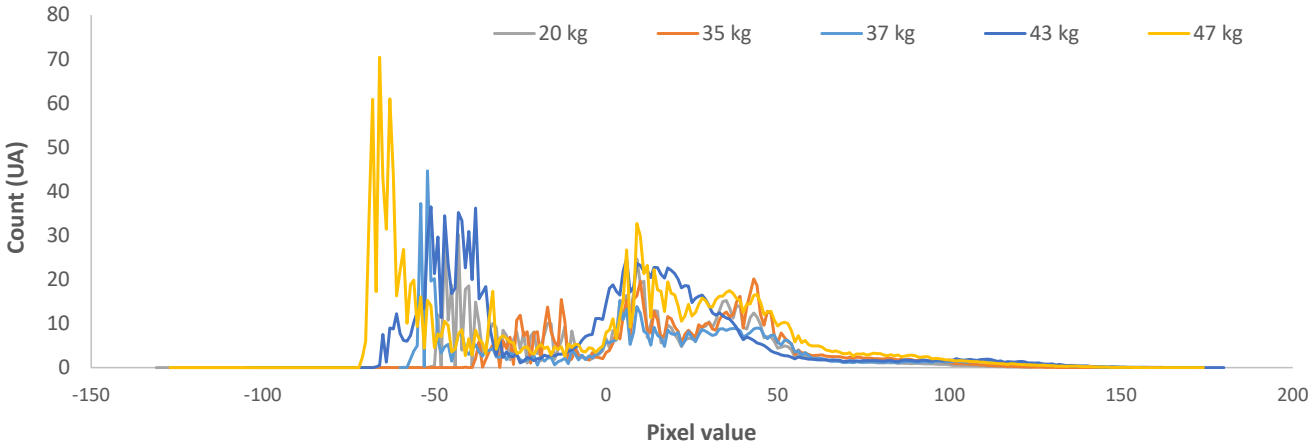

Figure 5. Corrected histogram of studied images considering the effect of distance

As different parts of the fruit might have different colorations, which correspond to different pixel values, several pixel-values will be used in the correlation. First of all, we check the values of pixels in the generated rasters. The observed values of pixels in persimmon fruits go from 72to 171. The representation of histograms in this range is displayed in Figure 6. In this graphic, the images of trees with more fruits have higher values in the Count (UA). The distributions of values along the range (72 to 171) is related to the fruit coloration. In images 4 (47 kg), 2, (35 kg) and 3 (20 kg) the peak of pixels associated with fruit is found around 73 to 75 pixel-value. Meanwhile, in other images, this peak is found at 102 pixel-value. This is caused by the differences in fruit maturity or fruit quality. The fruits of the images with a peak located at the highest pixel-value have a better coloration (uniform red color).

Finally, the correlation between the summation of pixels with pixel values between 72 and 171 and fruit production is presented in Figure 7. The mathematical model can be expressed as shows the Eq. (1). The correlation coefficient of the mathematical model is 0.97. The correlation coefficient offers information about the goodness of the correlation. It can take a value between 0 and 1, the closer to 1 the better the model.

$$\frac{\sum_{72}^{171} Counts\ (UA) - 19.44}{2.61} = Fruit\ weight\ (kg) \qquad (1)$$

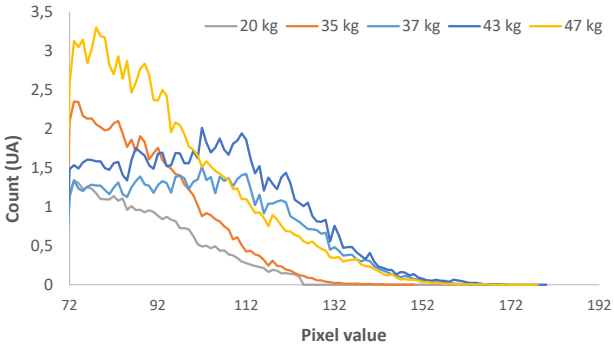

Figure 6. Detail of the corrected histograms

 ISBN: 978-1-61208-758-0

V. CONCLUSION

We propose a system to quantify the amount of fruit, based on image processing techniques.

We use pictures of the trees and data of their harvested fruit in kg. We decompose the original RGB image into single bands colors. The fruit of Persimmon usually is orange or red. The fruits have been clearly identified in the red band. But, it is necessary to combine the red band with a second band (green or blue), to differentiate the fruits to the color of the soil. The highest difference is observed in the R - G combination.

For our system, it is necessary to consider the effect of distance from the camera to the tree. We include a reference object in the original picture collection to normalize the data of the histograms. Finally, we used the normalized histograms for the correlation with fruit production.

For future work, we will perform a new study using a drone to capture the pictures. We expect that taking the images from the drone will be easier to carry out the process of identifying the fruit. Therefore we can better adjust the regression model for estimating productivity. Moreover, we will evaluate the option of using a camera that allows having a thermal image. The use of non-visible bands, such as infrared or ultraviolet, can increase the performance of our model.

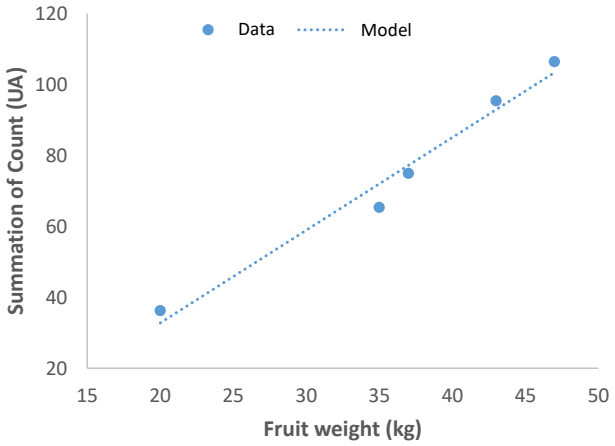

Figure 7. Correlation between the summation of pixels and fruit weight

ACKNOWLEDGMENT

This work has been partially supported by European Union through the ERANETMED (Euromediterranean Cooperation through ERANET joint activities and beyond) project ERANETMED3-227 SMARTWATIR by the Conselleria de Educación, Cultura y Deporte with the Subvenciones para la contratación de personal investigador en fase postdoctoral, grant number APOSTD/2019/04, and by the Cooperativa Agrícola "Sant Bernat" Coop.V.

REFERENCES

[1] J. J. Bruinsma, "World agriculture: towards 2015/2030", Routledge, 2017, pp. 29-36.

[2] M. A. Tsiafouli et al. "Intensive agriculture reduces soil biodiversity across Europe", Global change biology, 2014, vol. 21, no. 2, pp. 973-985.

[3] M. Satoh and S. Aboulroos, "Irrigated Agriculture in Egypt: Past, present and future", Springer, Switzerland, 2017, pp. 1-9.

[4] J. Simon, M. Dannenmann, R. Pena, A. Gessler, and H. Rennenberg, "Nitrogen nutrition of beech forests in a changing climate: importance of plant-soil-microbe water, carbon, and nitrogen interactions", Plant and Soil, 2017, vol.418, no 1-2, pp.89-114.

[5] S. Ali et al. "Climate Change and Its Impact on the Yield of Major Food Crops: Evidence from Pakistan" Foods,2017, vol. 6, p. 39.

[6] G. Llácer and M. L. Badenes, "Persimmon Production and Market", Options Méditerranéennes, Serie A, 2002, no. 51, pp. 9-21.

[7] L. Parra, V. Torices, J. Marín, P. V. Mauri, and J. Lloret, "The Use of Image Processing Techniques for Detection of Weed in Lawns", The Fourteenth International Conference on Systems (ICONS 2019), Valencia, Spain, 24 – 28 March 2019, pp. 50-55

[8] D. Ulzii-Orshikh, M. Lee, and S. Yun, "An yield estimation in citrus orchards via fruit detection and counting using image processing", Computers and Electronics in Agriculture, August 2017, vol. 140, pp. 103-112.

[9] M. P. Mello, "System and method for monitoring crops.",U.S. Patent Application No. 15/871,758.

[10] J. Marín et al. "Urban Lawn Monitoring in Smart City Environments" Journal of Sensors, vol. 2018, pp. 1-16.

[11] J. M. S. Hutchinson, A. Jacquin, S. L. Hutchinson and J. Verbesselt, " Monitoring vegetation change and dynamics on U.S Army training lands using satellite image time series analysis", Journal of environmental management, vol 150, 2015, pp. 355-366.

[12] T. Achouak, B. Khelifa, L. García, L. Parra, J. Lloret, and B. Fateh, "Sensor Network Proposal for Greenhouse Automation placed at the South of Algeria", Network Protocols & Algorithms, vol10, no 4, 2018, pp. 53-69.

[13] J. Rocher, D. A. Basterrechea, L. Parra and J. Lloret, "A New Conductivity Sensor for Monitoring the Fertigation in Smart Irrigation Systems", In 10th International Symposium on Ambient Intelligence, Ávila, Spain, 26- 28 Jun 2019, pp. 136-144.

[14] Herold, Bernd. 3.2 Monitoring and Mapping of Fresh Fruits and Vegetables Using Vis Spectroscopy. Optical Monitoring of Fresh and Processed Agricultural Crops, 2008, p. 157.

 ISBN: 978-1-61208-758-0

Ceratophyllum demersum L. as Phytoindicator and Potential Phytoremediator of Lead Under Hydroponic Conditions

Manal Fawzy [1], Ahmed. El-Khatib [2], Nadia Badr [1], Amany Abo-El-Kasem[2], Javier Rocher[3], Daniel A. Basterrechea[3]

[1] Environmental Sciences Dept., Faculty of Science.
Alexandria University,
Alexandria ,Egypt [2]
Botany Dept, Faculty of
Science Sohag
University, Sohag, Egypt
[3]Instituto de Investigación para la Gestión Integrada de zonas Costeras.
Universitat Politècnica de València Valencia, Spain

Email: dm_fawzy@yahoo.com, elkhatib@yahoo.com, nadiaelsayed1965@gmaill.com, aaboelkassem@yahoo.com
jarocmo@doctor.upv.es, dabasche@epsg.upv.es

***Abstract*— The contamination of water by heavy metals like Pb is a huge problem for the environment. In this paper, we test *Ceratophyllum demersum L.* plants as phytoindicator. These were exposed to different concentrations of Pb for 1–21 days, under hydroponic conditions, where they exhibited both adsorption and absorption efficiency. These efficiencies influenced in concentration and duration in a dependent manner. For the three initial treatments 0.125, 0.250, 0.500 µg/ml, the values of regression coefficients described the occurred variance on the rapid decrease in the Pb concentration in the hydroponic media, reflecting highest removal efficiency by *C. demersum*. *Significant variation (*P< 0.05) was recorded between the concentration of Pb accumulated in *C. demersum* at 0.125 and 0.250 µg/ml, while a highly significant value (P< 0.01) was recorded between them at 0.500 µg/ml. The regression coefficient denotes the pronounced impact of treatment concentration on the accumulation rate (R^2 = 0.9987). The adsorption efficiency of *C. demersum* appeared to be influenced by the Pb hydroponic media concentration, where after 21 days, the higher Pb adsorption was recorded at 0.125 µg/ml and the lowest one was obtained at 0.500 µg/ml. Results suggest that plants responded positively to the increase of Pb concentrations and they accumulated a high amount of metal. Due to metal removal coupled with detoxification potential, the plant appears to have potential for its use as phytoremediator species in aquatic environments.**

Keywords-lead; Biomonitoring; Bioremoval; biosorption; macrophytes;

I. INTRODUCTION

Pb is a very persistent element, which has been used in the past and is still used nowadays. This is the cause that is one of the most frequent inorganic contaminants in water [1]. It is potentially toxic even at low concentrations and above 15 µg/ L in drinking water, is considered as a risk for human health [2]. Many industries, such as the petrochemical, painting and coating, newsprint, smelting, metal electroplating, mining, plumbing and battery industries, discharge lead (Pb) into the environment without adequate purification in some cases [3].

The presence of lead in wastewater is dangerous for the aquatic flora and fauna even in relatively low concentration and stringent environmental regulations attract the attention of chemists and environmental engineers for its control [4]. While the focus has turned towards remediation with regards to preventing human exposure, much is still needed in the way of determining appropriate measures to monitor and protect the aquatic environment, particularly with regards to point source pollution [5].

Macrophytes (Aquatic plants) confirm very well too many of the criteria listed for an "ideal" biomonitor organism: they are sedentary, visible to the naked eye, easy to collect, simple to handle and easy to identify in the field. Also, they concentrate metals and nutrients in their tissues and reflect the environmental contamination [6]. Some species have the expressive ability of bioconcentration, and therefore, increased accumulation, of nutrients and heavy metals [7]. Further, the high concentration of some elements in plant tissues may be the result of the substantial availability of those elements in the surrounding environment. In this way, macrophytes can be used as bioindicators. Some of those species can also be used to remove, degrade or transform harmful hazardous materials, present in the aquatic environment. This application of plants, as phytoremediators, highly depends on factors, which define the absorption, accumulation and organic production of each taxon. In the case of *Ceratophyllum demersum*, *it grows* in water heavily polluted either by domestic sewage or by agricultural wastes [8]. It is known that the high accumulation of heavy metals like Cd, Cu, Cr, Pb, and Hg, are very usual in this kind of wastes [9][10].

Recently, substantial accumulation and high tolerance of Pb has been reported in *C. demersum* [11] when it is exposed to various concentrations of Pb, exhibited both phytotoxic and tolerance responses. Accordingly, the aim of this research was to determine the Pb removal efficiency by *C. demersum*, through investigating its absorption and

 ISBN: 978-1-61208-758-0

adsorption capability, under hydroponic conditions.

The rest of the paper is structured as follows. Section II presents the materials and methods that were used in the study. Section III the results of our experiment are presented. In section IV the discussion is shown. Finally, In Section V the conclusions and future works are explained.

II. MATERIAL AND METHODS

In this section, we explain the material used in the experiment and the methods. In the first section, we present the apparatus used, in section b present the grown condition, sequently we show the preparation of lead as a heavy metal contaminant, and finally, we present the protocol of the experiment.

A. Experimental apparatus

Ceratophyllum demersum L. was grown in a growth chamber equipped with holding tanks, lighting systems, aeration system, and temperature- monitoring system. Hold tanks used in this design have consisted of three boxes, each box for each pollutant concentration. Each box (25 x 100 x 30 cm) was divided into four compartments: one compartment was used as a control, while the others received the different pollutant concentrations. Moreover, each compartment (25 x 25 x 30 cm) was filled with 10 L of Hoagland nutrient solution; where it was previously used to improve cucumber grow [12]. The light intensity of 1950 lux provided by the artificial lighting system was used to be similar to that of natural lighting required for aquatic plants. Also, an aeration unit was installed for each compartment to provide oxygen for aquatic plants.

The air flows from the main laboratory supply to a manifold with four outlets. Each outlet was connected to the aerator which was located in each compartment. Further, the dissolved oxygen daily monitored and was ranged between 7-7.5 mg/l. The water and the ambient air temperature were monitored during the experimental period. Besides, the thermometer was used to measure the ambient air temperature above the water surface in each box and also to measure the water temperature in each compartment.

B. Plant material and growth conditions

Ceratophyllum demersum L. (Coontail or hornwort, family Ceratophyllaceae) is a submerged macrophyte of broad geographical distribution and is widely used in wastewater treatments. It is selected because it grows quickly, has high biomass, and has been found to accumulate metals in its leaves and stem. It is a completely submersed plant and commonly seen in ponds, lakes, ditches, and quiet streams with moderate to high nutrient levels [13]. It does not produce roots, instead, it absorbs all the nutrients it requires from the surrounding water. Also, it grows rapidly in shallow, muddy, quiescent water bodies at low light intensities. If it is growing near the lake bottom, it will form modified leaves, which it uses to anchor to the sediment. However, it can float free in the water column and sometimes forms dense mats just below the surface. The plant reproduces by fragments breaking from the parent plant.

Samples were taken from plants growing in the mainstream of the River Nile bank at Sohag Governorate, south Egypt. The plants were grown in a growth chamber, where they were grown hydroponically. Before the start of the experiment, whole plants of *Ceratophyllum* were thoroughly cleaned under running tap water to remove debris and other foreign particles and then rinsed in redistilled water. The plants were transferred to the system and kept for 2 weeks in Hoagland nutrient solution (Cleland and Briggs Formulation) to acclimatize before starting the experiment and adding the contaminant. The nutrient solution was aerated continuously to achieve constant stirring and buffered to pH 5.8 with NaOH or HCL.

C. Preparation of lead as a heavy metal contaminant

Three concentrations of lead were investigated in this study (125, 250, and 500 µg/l). The lead element was used as Lead nitrate Pb $(NO_3)^2$. All the concentrations were calculated based on the individual element versus their compound form. The reagents were dissolved in bidistilled water to achieve the appropriate contamination level. After the adaptation period, the contaminants were added to the three compartments receiving three treatments.

D. Experimental protocol

One box (four compartments) was used for each treatment. Each compartment received 10 L of water and the recommended amount of nutrient solution. About 100 g healthy fresh weight of *C. demersum* was placed in each of the four compartments in the holding tank assigned for the different treatments: A control in each box, with modified Hoagland nutrient solution and three Pb treatments: 125, 250, and 500 µg/l of Pb. Each treatment was replicated three times. A constant volume of water was maintained in the aquaria by the addition of redistilled water. Moreover, the lighting system was turned on and was controlled with a timer, which was adjusted to achieve 11 h light and 13 h dark.

The plants were left for 2 weeks to adapt to the new environment. After the acclimatization period, the desired amounts of lead were added to the treatment compartment of each holding tank. Temperature readings were recorded every day in order to monitor the change in the water ($21 \pm 2\ ^0C$ during the light period and $20 \pm 2\ ^0C$ during dark periods) and the ambient air temperatures ($25 \pm 2\ ^0C$) during the experimental period. The growth of the individual plant was also observed on a daily basis. The entire experiment was reported. The plants were treated under the above-mentioned laboratory conditions for a period of 21 days.

E. Sampling and analysis

Water samples of 15 ml were collected from all compartments at 1, 10, and 21 days intervals for lead analyses. A polarography and voltammetry 797 VA Computrace Ω Metrohm Ltd CH-9101 Herisau, Switzerland was used for Pb analyses. Lead concentration values are expressed as µg / L (Ppp). Batch adsorption experiments

 ISBN: 978-1-61208-758-0

were performed for all compartments at 1, 10, and 21 days intervals for lead analyses by using 0.2 g F.W of plant material (leaves or stems) with 10 ml of freshly prepared solution of $MgCl^2$ containing 100g/L was added.

The container flasks were caped and shaken at 200 rpm at room temperature for one hour. After thorough mixing the solution was centrifuged at 4000 rpm for 5 min, Supernatant was collected for Pb concentration analyses. Plant samples (5 g each) were collected at the start, at 10 days, and at the end of the experiment and analyzed for the presence of lead. Harvested plants were thoroughly washed in distilled water and then separated among stems and leaves. The plant samples were dried in a convection oven for 24 h at 48 ^{o}C to determine the accumulation of contaminants. After drying, the plants were ground to a fine powder.

For analysis, dry plant material was digested according to the wet digestion procedure involving concentrated nitric acid [14]. 10 ml concentrated nitric acid (HNO_3) and 0.5 ml hydrofluoric acid (HF) were added to 0.5 g of dry plant sample in a closed Teflon vessel, was designed for the purpose, at a temperature of 130 ^{o}C for 24h. Digestion in solution continues until clear. The resultant liquid was diluted up to 25 ml with distilled water then stored for analysis. Then the Pb was determined by Perkin–Elmer 2380 atomic absorption spectrophotometer.

III. RESULTS

In this section we presented he results. The different data were analyzed statistically by ANOVA and regression investigated using the basic statistic module of Statistical software (StatSoft Inc., '99 edition, kernel release 5.5 A). Homogeneity of variances and normality of variables tests were performed

A. Lead removal from nutrient media

Results revealed an increasing trend of Pb removal with time in all the experimental sets. The changes in Pb concentration in the nutrient medium over the duration of the experiment are shown in Figure 1. Removal of lead at its low initial treatment 0.125 µg/ml over time is shown in Figure 1, it reduced to 0.0833µg/ml within the 1st day. The Pb removal continued over the remaining days of the experiment and decreased to 0.056 µg/ml after 10 days and to 0.0437 µg/ml by the end of the experiment. The decrease of Pb concentration in the nutrient medium with an initial value of 0.250 µg/ml is shown in Figure 1. the concentration of Pb was sharply decreased to 0.1848 µg/ml after the 1st day of the experiment. Meanwhile, the concentration of Pb was reduced to 0.1277 µg/ml and 0.1099 µg/ml after 10 and 21 days, respectively. The removal of lead at its high initial value of 0.500 µg/ml is shown in Figure 1. It appears that there is an increasing trend in lead removal all over the experimental period. Where, Pb concentration decreased to 0.4108, 0.3211, and 0.2102 µg/ml after 1, 10, 21 days, respectively.

The highest removal was recorded on the last day in all the experimental sets. For all the three initial treatment 0.125, 0.250, 0.500 µg/ml, the values of regression coefficients using exponential model are R^2:0.8475, 0.8342 and 0.9696. This described the occurred variance of the rapid decrease in the Pb concentration. The exponential model is represented in the equation 1, 2 and 3 for the treatment of 0.125, 0.250, 0.500 µg/ml respectively.

All treatments achieved the highest removal efficiency (Table 1) at the end of the experiment, while the lowest treatment 0.125 µg/ml recorded the highest removal efficiency (65%) than the others.

$$Concentration\ (\tfrac{\mu g}{ml}) = 0.1006e^{-0.043*time\ (days)} \quad (1)$$

$$Concentration\ (\tfrac{\mu g}{ml}) = 0.2106e^{-0.035*time\ (days)} \quad (2)$$

$$Concentration\ (\tfrac{\mu g}{ml}) = 0.4639e^{-0.038*time\ (days)} \quad (3)$$

TABLE I. THE REMOVAL EFFICIENCY OF LEAD BY *C. DEMERSUM* GREW IN DIFFERENT LEAD TREATMENTS THROUGHOUT THE EXPERIMENT.

Pb concentration in the nutrient media (µg/mL)	**Days**		
	1st day (%)	***10 days (%)***	***21 days (%)***
0.125	33.36	55.20	65.04
0.250	26.08	48.92	56.04
0.500	17.84	35.78	57.96

B. Lead absorption

An increase in lead absorption by *C. demersum* was detected with the different applied treatments Figure 2. The initial concentration of Pb in the plant biomass was 1.0704 µg/g at 0.125 µg/ml. After one day, the lead content increased up to 1.5442 µg/g. With an increase in duration, a sharp increase in metal accumulation rate was recorded, since lead content was 4.4224 µg/g after 10 days and 8.5289 µg/g after 21 days. The same trend in accumulation pattern was recorded for the applied initial treatments 0.250 µg/ml Figure 2. Where the initial concentration of Pb was 1.3766 µg/g. After one day treatment, the concentration reached 3.1625 µg/g but after 10 days the accumulation increased up to 9.3569 µg/g. By the end of the experiment, it was 13.5341 µg/g. The initial concentration of Pb in the higher treatment (0.500 µg/ml of Pb) was 0.6647 µg/g then increased to 3.4918 µg/g after the 1st day and 13.0933 µg/g after 10days. By the end of the experiment, the amount of Pb absorbed by *C. demersum* reached up to 21.5744 µg/g. The experiment showed that the lead uptake by *C. demersum* occurs very rapidly over time with different types of treatments. The values of R^2 were 0.9987, 0.9649, and 0.9831 respectively (with a linear model). The linear model is represented for equation 4, 5 and 6 for the treatment of 0.125, 0.250, 0.500 µg/ml respectively.

$$Concentration\left(\tfrac{\mu g}{ml}\right) = 0.3509 * time(day) + 1.0846 \quad (4)$$

$$Concentration\left(\tfrac{\mu g}{ml}\right) = 0.5647 * time(day) + 2.3399 \quad (5)$$

 ISBN: 978-1-61208-758-0

$$Concentration\left(\frac{\mu g}{ml}\right) = 0.9682 * time(day) + 1.9608 \quad (6)$$

Significant variation (P< 0.05) was recorded between the concentration of Pb accumulated in *C. demersum* growing at 0.125 and 0.250 µg/ml, while a highly significant value (P< 0.01) was recorded between them at 0.500µg/ml. The concentration of Pb at the end of the experiment (after 21 days of treatment) demonstrated that the uptake of Pb by C. *demersum* increased with increasing metal concentration.

After 21 days, the higher Pb accumulation was recorded at 0.500 µg/ml treatment and the lowest with those of 0.125 µg/ml. The regression coefficient denotes the pronounced impact of treatment concentration on the accumulation rate (R = 99.8%).

C. Lead adsorption (exchangeable fraction)

The effect of contact time on the extent of adsorption of lead on *C. demersum* over the duration of the experiment is illustrated in Figure 3. The initial concentration of Pb, in the lower treatment (0.125 µg/ml), adsorbed on the tested plant was 0.3099 µg/g and it reached up to 0.331 µg/g after one day, 1.6574 µg/g after 10 days and 1.6792 µg/g at the end of the experiment. At 0.250 µg/ml Pb treatment, the concentration of the adsorbed Pb increased from 0.443 µg/g to 0.7429 µg/g within one day and reached up to 1.8806 µg/g after 10 days.

At the end of the experiment (after 21 days), the adsorption of lead on *C. demersum* was diminished to 1.4157 µg/g. The initial concentration of Pb adsorbed on the plant was 0.4876 µg/g at 0.500 µg/ml. After one day the adsorbed Pb fraction was 1.3084 µg/g and 3.0178 µg/g after 10 days. With an increase in duration, a sharp decrease in metal adsorption rate was recorded, where the adsorbed Pb fraction was 0.897 µg/g after 21 days. For all the three initial treatment 0.125, 0.250, 0.500 µg/ml, the values of R are 0.9784, 0.9974 and 0.9909, respectively. The polynomic model of 2 degrees is represented in equations 7, 8 and 9.

$$Concentration\left(\frac{\mu g}{ml}\right) = -0.0065 * time(day)^2 + 0.2067 * time(day) + 0.2273 \quad (7)$$

$$Concentration\left(\frac{\mu g}{ml}\right) = -0.0088 * time(day)^2 + 0.2284 * time(day) + 0.4801 \quad (8)$$

$$Concentration\left(\frac{\mu g}{ml}\right) = -0.0207 * time(day)^2 + 0.4461 * time(day) + 0.6701 \quad (9)$$

The final adsorption of lead on *C. demersum* after 21 days treatment is shown in Figure 3. The adsorption of Pb by *C. demersum* decreased with increasing metal concentration. After 21 days, the higher Pb adsorption was recorded at 0.125 µg/ml treatment and the lowest one was recorded with 0.500 µg/ml, the regression coefficient denotes the important impact of treatment concentration on the adsorption rate.

IV. DISCUSSION

The results obtained from the experiment indicated that *C. demersum* can accumulate and adsorb a high amount of Pb in concentration and duration dependent manner. With an increase in duration, metal accumulation increased while adsorption decreases after 10 days. The maximum rate of metal accumulation was found after 21 days when about (21.57µg/ g at 0.500 µg/ml) of the total metal was taken up by the plant. Being without roots and having forked leaves with thin cuticle, *C. demersum* can efficiently uptake metals from aquatic bodies through its large surface area with no complication of root– shoot metal partitioning. These features thus contributed to adequate Pb accumulation observed in this study.

A comparison between initial and final metal concentrations within the plant had shown that the final concentrations were more than 7, 12, 21 folds of the initial metal concentration, in the nutrient media, at 0.125, 0.250, and 0.500 µg/ml, respectively. Biosorption is the first stage of metal accumulation. It involved adsorption of metal onto the cell wall of microorganisms, algae, and aquatic macrophytes, independently of metabolism [15]. Adsorption processes on the biosurface involve the release of hydrogen ions or the other cations and the adsorption or surface complexing of metal ions. Adsorption fraction represents very loosely bound elements and may regulate and/or reflect the composition of surface water [16].

From the work presented here, *C. demersum* could be an effective biosorbent for lead under dilute metal conditions. This plant adsorbed an appreciable amount of Pb from the water up to 1.3 Fold at 0.125, 1.4 fold at 0.250, and 2.6 fold at 0.500µg/ml after 10 days. However, the adsorbed fraction increased after the 10^{th} day. This suggests saturation of a finite number of binding sites on the plant cell surface after exposure to Pb, and possibly the advent of metabolism dependent transport of metal to the inner cell mass [17], [18]. This decrease in the rate of adsorption could also be explained by the decrease of Pb concentration in the water, which causes a reduced concentration gradient.

According to Guilizzoni [19] and Keskinkan [20], there is, however, scarce research about heavy metal uptake by submerged aquatic plants. The use of submerged aquatic macrophytes for wastewater treatment is therefore still at an experimental stage, with species like *Potamogeton* spp. [21],[22],[23], *Ceratophyllum demersum* [7] and *Myriophyllum spicatum* [20] being tested. Bader and Fawzy [24], reported that *C. demersum* proved to be an effective biosorbent and bioaccumulator for Pb rending the species of interest for use in phytoremediation and bio-monitoring of polluted waters.

The rootless submerged plant *C. demersum* was found capable of removing comparatively higher amounts of Pb from pond water. This agrees with the earlier report [25] that submerged plants had higher metal uptake ability due to more surface/biomass ratio.

 ISBN: 978-1-61208-758-0

V. CONCLUSIONS

In the course of this study, it was concluded that: *C. demersum* proved to be an effective biosorbent and bio-accumulator for Pb. This plant was found to accumulate 7, 12, 21 folds of the initial metal concentration, in the nutrient media, at 0.125, 0.250, and 0.500 µg/ml, respectively after 21 days. Also, it can absorb an appreciable amount of Pb from the water up to 1.3 Fold at 0.125, 1.4 fold at 0.250, and 2.6 fold at 0.500µg/ml after 10 days. Being widely distributed and fast-growing submerged plants, *C. demersum* can be utilized as a safe and cost-effective tool for the removal of Pb from low to medium strength wastewater.

The use of submerged aquatic macrophytes for wastewater treatment is still at an experimental stage. Studies with regard to aquatic macrophytes combinations to be used in treatment ponds and the period of macrophyte replacement should be seriously undertaken for developing a more efficient, natural and economic integrated macrophyte based system, most advantageous for heavy metal removal.

In future works the performance of *C. demersum* and other aquatic plants will be investigated using multi-elements solution instead of mono-element one to test their potentials to remediate polluted waste water containing various toxic metals

ACKNOWLEDGMENT

This work has been partially supported by the European Union through the ERANETMED (Euromediterranean Cooperation through ERANET joint activities and beyond) project ERANETMED3-227 SMARTWATIR by the “Ministerio de Educación, Cultura y Deporte”, through the “Ayudas para contratacion predoctoral de Formación del Profesorado Universitario FPU (Convocatoria 2016)”. Grant number FPU16/05540.

REFERENCES

[1] Z. Sun, J. Chen, X. Wang, and C. Lv, “Heavy metal accumulation in native plants at a metallurgy waste site in rural areas of Northern China,” Ecological Engineering, vol. 86, pp. 60–68, Jan. 2016.

[2] Environmental Protection Agency., National recommended water quality criteria. Washington, Dc: Office Of Water, 2006.

[3] X.-M. Zhan and X. Zhao, “Mechanism of lead adsorption from aqueous solutions using an adsorbent synthesized from natural condensed tannin,” Water Research, vol. 37, no. 16, pp. 3905–3912, Sep. 2003.

[4] C. K. Singh, et al. “Studies on the removal of Pb(II) from wastewater by activated carbon developed from Tamarind wood activated with sulphuric acid,” Journal of Hazardous Materials, vol. 153, no. 1–2, pp. 221–228, May 2008.

[5] E. M. Mager, H. Wintz, C. D. Vulpe, K. V. Brix, and M. Grosell, “Toxicogenomics of water chemistry influence on chronic lead exposure to the fathead minnow (Pimephales promelas),” Aquatic Toxicology, vol. 87, no. 3, pp. 200–209, May 2008.

[6] X. Sun, Y. Xu, Q. Zhang, X. Li, and Z. Yan, “Combined effect of water inundation and heavy metals on the photosynthesis and physiology of Spartina alterniflora,” Ecotoxicology and Environmental Safety, vol. 153, pp. 248–258, May 2018.

[7] A. A. El-Khatib, A. K. Hegazy, and A. M. Abo-El-Kassem, “Bioaccumulation Potential and Physiological Responses of Aquatic Macrophytes to Pb Pollution,” International Journal of Phytoremediation, vol. 16, no. 1, pp. 29–45, Sep. 2013.

[8] M. Chen, L.-L. Zhang, J. Li, X.-J. He, and J.-C. Cai, “Bioaccumulation and tolerance characteristics of a submerged plant (Ceratophyllum demersum L.) exposed to toxic metal lead,” Ecotoxicology and Environmental Safety, vol. 122, pp. 313–321, Dec. 2015.

[9] P. Aravind and M. N. V. Prasad, “Cadmium-Zinc interactions in a hydroponic system using Ceratophyllum demersum L.: adaptive ecophysiology, biochemistry, and molecular toxicology,” Brazilian Journal of Plant Physiology, vol. 17, no. 1, pp. 3–20, Mar. 2005.

[10] M. A. Fawzy, N. E. Badr, A. El-Khatib, and A. Abo-El-Kassem, “Heavy metal biomonitoring and phytoremediation potentialities of aquatic macrophytes in River Nile,” Environmental Monitoring and Assessment, vol. 184, no. 3, pp. 1753–1771, Mar. 2012.

[11] S. Mishra, et al. “Lead detoxification by coontail (Ceratophyllum demersum L.) involves induction of phytochelatins and antioxidant system in response to its accumulation,” Chemosphere, vol. 65, no. 6, pp. 1027–1039, Nov. 2006.

[12] H. Li and Z. Cheng, “Hoagland nutrient solution promotes the growth of cucumber seedlings under light-emitting diode light,” Acta Agriculturae Scandinavica, Section B — Soil & Plant Science, vol. 65, no. 1, pp. 74–82, Oct. 2014.

[13] D. Johnson, T. Goward, and D. H. Vitt, Plants of the western boreal forest & aspen parkland. Edmonton, Alta., Canada ; Redmond, Wash., USA: Lone Pine, 1995.

[14] Y. P. Kalra and Soil And Plant Analysis Council, Handbook of reference methods for plant analysis. Boca Raton: Crc Press, 1998.

[15] S. Mishra, G. Wellenreuther, J. Mattusch, H.-J. Stärk, and H. Küpper, “Speciation and Distribution of Arsenic in the Nonhyperaccumulator Macrophyte Ceratophyllum demersum,” Plant Physiology, vol. 163, no. 3, pp. 1396–1408, Sep. 2013.

[16] M. A. H. Saad, M. A. Abdel-Moati, and N. B. Badr, “suspended matter and particulate copper speciation in the polluted Abu-Kir Bay, Egypt,” Fresenius Environmental Bulletin, vol. 11, no. 9A, pp. 542–552, 2002.

[17] H. N. Christensen, “The Living cell as a metal-binding agent,” Federation of American Societies for Experimental Biology, vol. 20, no. 187–90, 1961.

[18] D. T. Swift and D. Forciniti, “Accumulation of lead by Anabaena cylindrica : Mathematical modeling and an energy dispersive X-ray study,” Biotechnology and Bioengineering, vol. 55, no. 2, pp. 408–418, Jul. 1997.

[19] P. Guilizzoni, “The role of heavy metals and toxic materials in the physiological ecology of submersed macrophytes,” Aquatic Botany, vol. 41, no. 1–3, pp. 87–109, Jan. 1991.

[20] O. Keskinkan, M. Z. L. Goksu, A. Yuceer, M. Basibuyuk, and C. F. Forster, “Heavy metal adsorption characteristics of a submerged aquatic plant (Myriophyllum spicatum),” Process Biochemistry, vol. 39, no. 2, pp. 179–183, Oct. 2003.

[21] R. R. Goulet et al., “Phytoremediation of effluents from aluminum smelters: A study of Al retention in mesocosms containing aquatic plants,” Water Research, vol. 39, no. 11, pp. 2291–2300, Jun. 2005.

[22] Å. Fritioff and M. Greger, “Uptake and distribution of Zn, Cu, Cd, and Pb in an aquatic plant Potamogeton natans,” Chemosphere, vol. 63, no. 2, pp. 220–227, Apr. 2006.

 ISBN: 978-1-61208-758-0

[23] A. O. Bello, B. S. Tawabini, A. B. Khalil, C. R. Boland, and T. A. Saleh, "Phytoremediation of cadmium-, lead- and nickel-contaminated water by Phragmites australis in hydroponic systems," Ecological Engineering, vol. 120, pp. 126–133, Sep. 2018.

[24] K. Peng, C. Luo, L. Lou, X. Li, and Z. Shen, "Bioaccumulation of heavy metals by the aquatic plants Potamogeton pectinatus L. and Potamogeton malaianus Miq. and their potential use for contamination indicators and in wastewater treatment," Science of The Total Environment, vol. 392, no. 1, pp. 22–29, Mar. 2008.

[25] Z. Wang, L. Yao, G. Liu, and W. Liu, "Heavy metals in water, sediments and submerged macrophytes in ponds around the Dianchi Lake, China," Ecotoxicology and Environmental Safety, vol. 107, pp. 200–206, Sep. 2014.

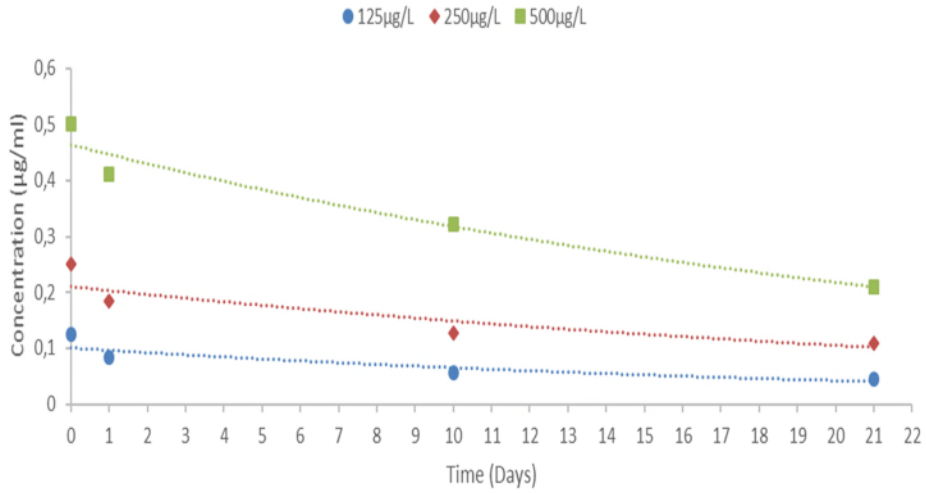

Figure 1. Average concentration of pb removal from the nutrient media at different pb treatments; 0.125; 0.250; 0.500 µg/ml.

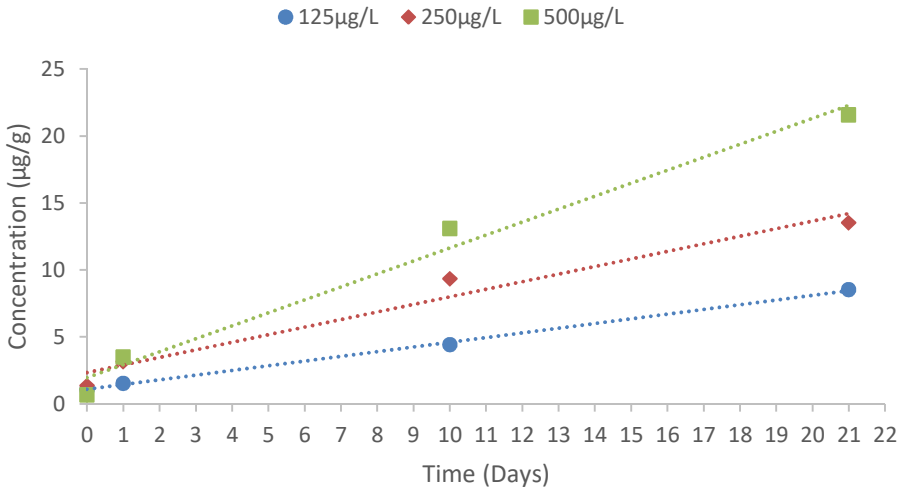

Figure 2. The average concentration of pb absorbed by c. Demersum growing in nutrient media with different pb treatments.

 ISBN: 978-1-61208-758-0

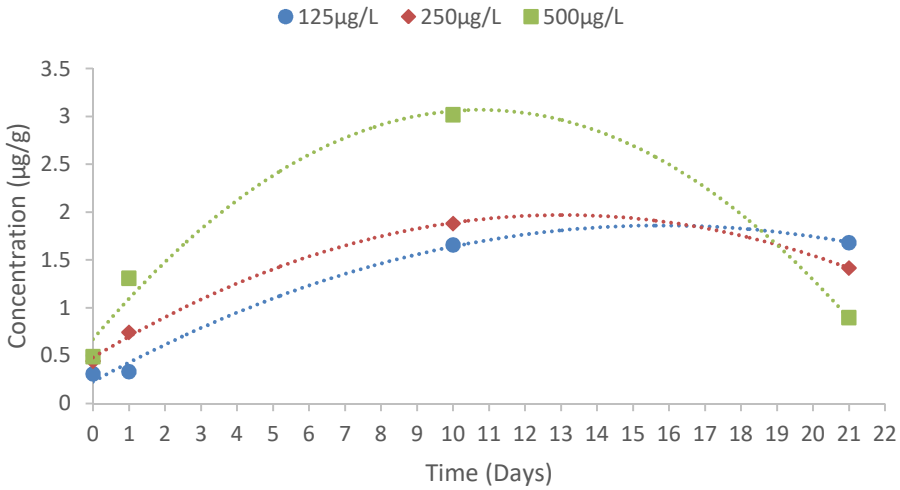

Figure 3. Average Concentration Of Pb Adsorbed (Exchangeable Fraction) on c. demersum growing in nutrient media with different pb treatments; 0.125; 0.250; 0.500 µg/ml, during the experiment duration.

 ISBN: 978-1-61208-758-0

Optimized Load Balancing Mobile Network using a Generative Adversarial Network Based Network Simulator

Load Balancing Mobile Network by GAN

Tin-Yu Wu
Department of Computer Science and Information Engineering
National Ilan University
Yilan County, Taiwan
tyw@niu.edu.tw

Yueh Wu
Department of Computer Science and Information Engineering
National Ilan University
Yilan County, Taiwan
willy821230ptr@hotmail.com.tw

Fu Jie Tey
Department of Computer Science and Information Engineering
National Ilan University
Yilan County, Taiwan
alexsword88@gmail.com
line 4: e-mail: name@xyz.com

Bo-Hong Huang
Department of Computer Science and Information Engineering
National Ilan University
Yilan County, Taiwan
b0643027@ems.niu.edu.tw

***Abstract*—With the advances of neural networks and the 5th generation mobile networks (5G), how to use Artificial Intelligence (AI) in 5G wireless networks has become a widely discussed topic while neural network is one form of artificial intelligence. Due to the complexity of 5G networks, it would be difficult to achieve load balancing. For this reason, before the 5G networks are officially launched, this study would like to investigate the processing capacity and learning capacity of neural networks over complicated problems. We combine Generative Adversarial Network (GAN) with the network simulator ns-3 and use neural networks for load-balancing simulation parameter adjustment and load balancing optimization.**

Keywords- 5G; GAN (Generative Adversarial Network); load balance; neural network

I. INTRODUCTION

When a world of 5th Generation Mobile Networks (5G) is approaching, we are expecting a complex environment interwoven with mobile network, Wi-Fi, millimeter wave and so on. Many methods have been proposed to solve the load-balancing problems for wireless networks, but most of them focus on the switch between Wi-Fi, D2D (Device to Device) and large/small base stations (BS).

On the edge of large-scale BS coverage, the signal strength is poor and the interference is significant. Additional small BSs can be deployed to fix the problem but it requires deployment cost. Therefore, considerations must be made to ensure if the existing BSs can possibly achieve load balancing. With the rise of Software-Defined Networking (SDN), the load balancing methods for wire-line networks have been extensively studied and become quite mature. However, it is inappropriate to use the methods for wire-line networks in wireless networks. In wire-line networks, nodes are connected by physical wires. According to SDN, a centralized controller gathers load balancing data and directs the data flow to the chosen destination to achieve load balancing. However, compared with wire-line networks, the transmission efficiency of wireless networks is far lower because of the path loss and interference, making the load balancing methods for wire-line networks not suitable for wireless networks. Therefore, this study attempts to make use of the neural networks to enable load balancing in wireless networks.

A network simulator is required for simulation of load balancing and it could be somebody else's design, like ns-3, or a simulator built according to one's needs. In this study, ns-3 is adopted. During the simulation, we will setup parameters, conduct the simulation, investigate the results, analyze the performance and adjust the parameters for follow-up simulations. Because such a series of steps must be repeated and requires a lot of time, we hope that by integrating neural networks with simulation systems, the parameters can be automatically adjusted and the target parameters can be figured out without substantial modifications of the overall simulation environment. We will use Generative Adversarial Network (GAN): utilizing its parameters and combining GAN with the simulation system to achieve automatic generation and parameter adjustment [11][12].

The rest of this paper is organized as follows: Section II reviews researches on load-balancing methods and background. Section III details how about system architecture and proposed method. In Section IV, we perform the experiment and simulate the parameters with our proposed models. Finally, we summarize our findings and results.

II. BACKGROUND AND RELATED WORKS

This section will introduce load-balancing methods, Generative Adversarial Network (GAN) and SeqGAN.

 ISBN: 978-1-61208-758-0

A. Load Balancing Methods

In wire-line networks, a centralized controller is responsible for monitoring computers and routers in the network, and managing the data flow to achieve load balancing.

- Standard Deviation Based

The standard deviation based load balancing algorithm depends on the centralized controller to collect load-balancing data of all routers and compute the standard deviation of each router. The standard deviation is usually used to measure the spread of the data about the mean value. For load balancing, the standard deviation is used to find out a light-loaded router so that flows of a congested path can be redirected to a light-loaded path [1].

- Weight Based

In the weight based load balancing algorithm, all routers are given assigned weights initially. According to the load-balancing status of the current BS, weights can be adjusted accordingly [2].

- Mobile Network and Wireless Network

Due to the reasons mentioned above, the load-balancing algorithms designed for wire-line networks are not suitable for wireless networks. But, many methods have been proposed to implement load balancing. Most of them propose to transfer mobile devices to the neighboring BSs to alleviate congestion [3], to use Device-to-Device (D2D) communications to offload the data traffic in the congested small cell to the neighboring small cell BSs [4], or to use an architecture based on fog computing [5]. Note that D2D communications are not allowed under all circumstances. Still some are based on Wi-Fi to determine how and when to connect with the right AP [2] [6]. Nevertheless, Wi-Fi and cellular networks are different in signal strength, interference and so on. Even earlier, some algorithms have been proposed for mobile load balancing in LTE system [7]. However, the existing simulation environment architectures are not suitable for the new 5G networks.

B. Generative Adversarial Network (GAN)

Generative Adversarial Network (GAN), first presented in 2014, combines a generative network with a discriminative network [8]. The generative network generates new data instances and the discriminative network identifies if the data is real or fake. The two fight against each other to improve throughout the training process. Take the imaging data generated by the generative network for example. When the samples get closer to real images, the discriminative network can discriminate more and more accurately. However, if the generative network's training is too fast, the discriminative network might not be able to converge. On the contrary, if the discriminative network converges too fast, the generative network will be affected also. GAN has often proved difficult to train because it is hard to converge, or the result is not as expected. To cope with this problem, parameter adjustments together with some real data are required. The development of GAN has grown rapidly and most of them focus on discriminating images, such as DCGAN [9] and WGAN [10]. In this study, we choose SeqGAN.

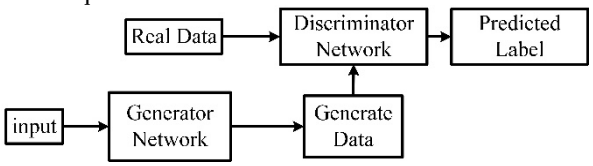

Figure 1. Generative Adversarial Network

C. SeqGAN

Proposed in 2016, Sequence GAN (SeqGAN) [11] enables GAN to process discrete outputs. GAN can differentiate sequential image data but not languages or words. To solve this differentiation problem, SeqGAN directly performs gradient policy update. The RL reward signal comes from the GAN discriminator judged on a complete sequence, and is passed back to the intermediate state-action steps using Monte Carlo search.

III. System Architecture and Proposed Method

This section introduces the design of both the proposed load-balancing environment and Generative Adversarial Network (GAN), as displayed in Figure 2. A GAN consists of two neural networks: generator and discriminator. Finally, we will describe the full process.

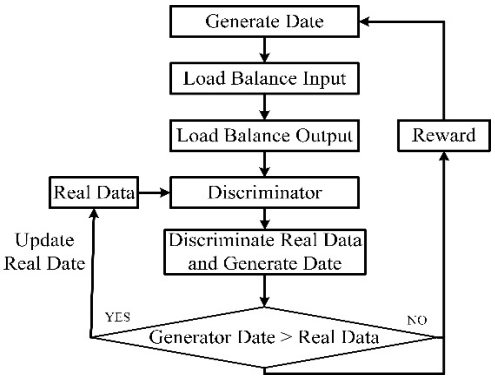

Figure 2. System Architecture

A. Load Balancing Simulation

For load balancing simulation, we first set and adjust parameters, including number of BSs, number of users, simulation time and weighting parameters defined by GAN. Simulations can be conducted using self-motivated software or specific simulators. After the simulation, we output the results for performance analysis. In this study, the result output is the load balancing test throughput.

B. Combing GAN with Load Balancing Simulation Test

To combine GAN with the load balancing simulation test, the data generated by the generator must correspond to the parameters of the network simulator. The result of the load balancing simulation will be returned to the neural network as feedback for further analysis.

- Corresponding Parameter Design

Based on SeqGAN, our proposed method generates a one-dimension array as weighted parameters for BSs in the load-balancing simulation. This study evaluates "throughput," instead of "test loss" because the test loss is defined as a percentage. It is possible that the throughput greatly varies but the test loss is similar. Therefore, the higher throughput means the better performance of the load-balancing simulation test. The result is then sent back to the neural network.

- Adjustment of SeqGAN

The generator based on SeqGAN and our proposed method is basically the same: a one-dimensional array composed by normally distributed random numbers. The discriminator then identifies if the generated data is real or fake. If the data is recognized as authentic by the discriminator, the data generated by the generator will be very close to real data. The real data of the original SeqGAN are poetry data generated by a trained RNN but its goal is different from ours. Therefore, we take the generated data of a better load balancing simulation result as the basis of real data.

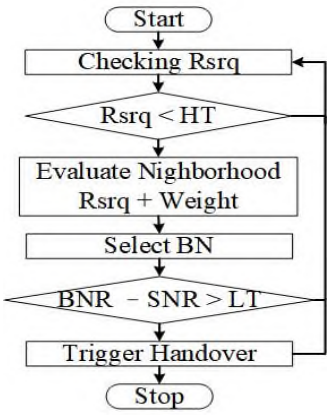

Figure 3. BN selection based on weights

- Impact of Weight Parameters on BS Selection

To investigate the impact of weight parameters on BS selection, we initially selected the BS with high weight value. However, the result could be bad if the user connects to a BS providing low signal strength. For this reason, signal strength and weight values generated by the generator are both taken into consideration while choosing the best BS. According to the flowchart shown in Figure 3, the user first checks the current Reference Signal Receiving Quality (RSRQ). If the RSRQ is smaller than High Threshold (HT), proceed to the handover evaluation, in which the Best Neighborhood (BN) is chosen according to RSRQ and weight value. To avoid edge shake, when the current Serving Neighborhood RSRQ (SNR) minus the Best Nighborhood RSRQ (BNR) is larger than the Low Threshold (LT), the handover is triggered.

IV. RESULTS AND ANALYSIS

This section will introduce the integration of Tensorflow and ns-3, analyze the Generative Adversarial Network (GAN) training process and conduct the load-balancing test to evaluate the performance of the method.

A. *Integration of Tensorflow and ns-3*

As for the neural network, this study uses TensorFlow. TensorFlow is a Python learning library while ns-3 is a simulator written in C++ that uses the waf commands to enable examples and tests. To integrate TensorFlow with ns-3, we modify the file in ns-3 using Python programming language, and ask the system to run the waf commands of ns-3. In this way, the two systems can be integrated.

B. *GAN Training Result*

This study is based on the SeqGAN of the open source machine learning TensorFlow library. Normally, we examine the test loss to check if a neural network converges. A convergent curve decreases and becomes flat. Since we modify the input, output and data type, it is necessary to evaluate the convergence. Figure 4 shows that the test loss decreases and becomes stable. It means the convergence in the training of neural networks, confirming the importance of deep learning.

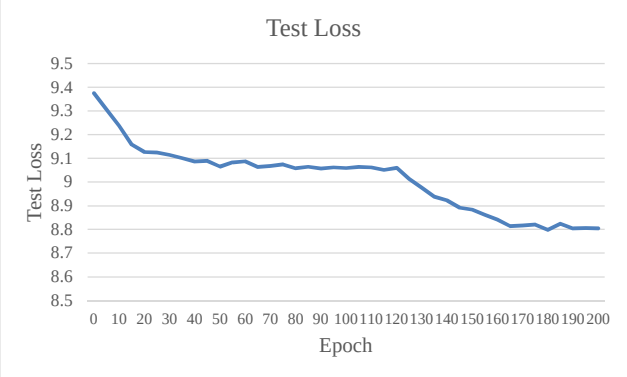

Figure 4. Test Loss

C. *Load-balancing System*

Instead of using self-motivated simulation software, we use the ns-3 simulator in this study. Although self-motivated software and GAN are easier, the design might not be perfect. Therefore, we use the widely recognized simulator to connect with GAN. Table 1 lists the basic load-balancing configuration parameters. Number of User Equipment (UE) is adjusted according to different modes. There are 7 BSs in the simulation and the simulation time is set to 10 seconds. Packet size and individual user throughput are determined according to the setting of the ns-3 simulator.

TABLE I. BASIC LOAD-BALANCING PARAMETERS

UE Amount	40
BS Amount	7
BS dBm	46
Simulation Time(second)	10

In the simulation scenario shown in Figure 5, BSs are deployed in an area of 1500m x 1500m. In the simulation,

users are randomly distributed around BSs and weights are adjusted accordingly to achieve load balancing.

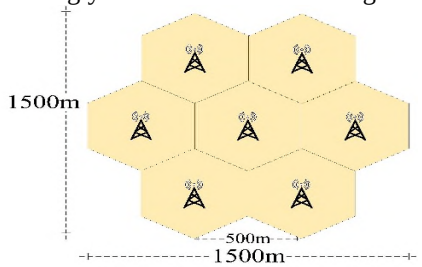

Figure 5. BS deployment in the simulation

D. *Load-Balancing Test*

In the simulation, we compare the impact of RSRQ and RSRQ Weight in which weights are generated by GAN. Figure 6 shows that RSRQ Weight obviously outperforms.

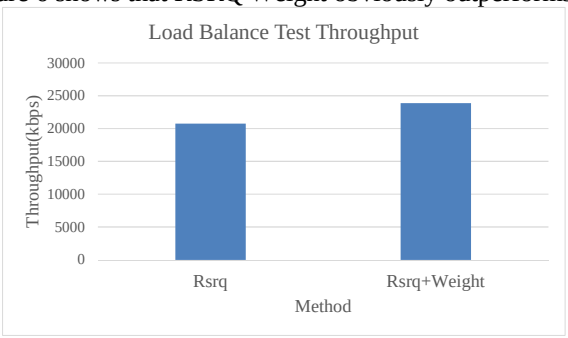

Figure 6. Throughput

V. CONCLUSION

By using a GAN based network simulator without substantial modifications, this study proposed an optimized load balancing mobile network, in which the TensorFlow learning library for Python was combined with the NS-3 simulator. The results revealed that our proposed method could reduce the packet loss rate by approximately 6% packet drop rate. Our future target is to further improve the method to build a truly competent neural network.

ACKNOWLEDGMENT

This study was supported by the National Science Council, Taiwan, under grant No. MOST 107-2221-E-197 -007 -MY3

REFERENCES

[1] Y. L. Lan, K. Wang and Y. H. Hsu, "Dynamic Load-balanced Path Optimization in SDN-based Data Center Networks," 2016 10th International Symposium on Communication Systems, Networks and Digital Signal Processing (CSNDSP), July 2016.

[2] C. Y. Lin, W. P. Tsai, M. H. Tsai and Y. Z. Cai, "Adaptive Load-balancing Scheme Through Wireless SDN-based Association Control," 2017 IEEE 31st International Conference on Advanced Information Networking and Applications(AINA), March 2017.

[3] Y. C. Wang and K. C. Chien, "A Load-aware Small-cell Management Mechanism to Support Green Communications in 5G Networks," The 27th Wireless and Optical Communications Conference (WOCC), May 2018.

[4] H. Zhang, L. Song and Y. J. Zhang, "Load Balancing for 5G Ultra-Dense Networks," IEEE Transactions on Wireless Communications, Vol.17, No. 6, pp. 4039-4050, June 2018.

[5] J. Jijin, B. C. Seet, P. H. Joo Chong and H. Jarrah, "Service Load Balancing in Fog-based 5G Radio Access Networks," IEEE 28th Annual International Symposium on Personal, Indoor, and Mobile Radio Communications (PIMRC), October 2017.

[6] K. Nahida, C. Yin and A. Zaid, "AP Load Balance Based Handover in Software Defined WiFi Systems," 2016 International Conference on Network Infrastructure and Digital Content (ICNIDC), September 2016.

[7] Y. Yang, P. Li, X. Chen and W. Wang, "A High-efficient Algorithm of Mobile Load Balancing in LTE System," 2012 IEEE Vehicular Technology Conference (VTC Fall), September 2012.

[8] R. Alec, M. Luke and C. Soumith, "Unsupervised Representations Learning With Deep Convolutional Generative Adversarial Networks," 4th International Conference on Learning Representations (ICLR 2016), May 2016.

[9] M. Arjovsky, S. Chintala and L. Bottou, "Wasserstein GAN," arXiv:1701.07875v3, December 2017.

[10] L. Yu, W. Zhang, J. Wang and Y. Yu, "SeqGAN : Sequence Generative Adversarial Nets with Policy Gradient," The Thirty-First AAAI Conference on Artificial Intelligence (AAAI 2017), February 2017.

[11] K. M. Addali, S. Younis B. Melhem, Y. Khamayseh, Z. Zhang and M. Kadoch,"Dynamic Mobility Load Balancing for 5G Small-Cell Networks Based on Utility Functions," IEEE Access, Vol. 7, pp. 126998-127011, September 2019.

[12] K. Addali and M. Kadoch,"Enhanced Mobility Load Balancing Algorithm for 5G Small Cell Networks," IEEE Canadian Conference of Electrical and Computer Engineering (CCECE2019), May 2019.

 ISBN: 978-1-61208-758-0

A Rate-distortion Optimization Approach to Omnidirectional Video Coding for VR Systems

Yufeng Zhou, Hua Chen, Mei Yu
Faculty of Information Science and Engineering, Ningbo University, Ningbo, China
yumei2@126.com

Gangyi Jiang
Faculty of Information Science and Engineering, Ningbo University, Ningbo, China
jianggangyi@126.com

***Abstract*—Virtual reality (VR) systems employ omnidirectional video to provide users with a strong sense of immersion. Compared with traditional video, omnidirectional video has the characteristics of full field of view, high resolution and immersion. However, a spherical omnidirectional video has to be projected into two-dimensional plane (e.g., common equirectangular projection (ERP) format) before encoding. This greatly limits the performance of the encoder due to the geometric distortion, content redundancy and other issues. Thus, considering the characteristics of projected omnidirectional images, an omnidirectional video coding rate-distortion optimization (RDO) method based on weighted-to-spherically-uniform structural similarity (WS-SSIM) is proposed. Specifically, according to the distortion of the internal structure similarity of the projection plane and the relationship between the spherical distortion and the projection plane distortion, the WS-SSIM is proposed to describe the distortion of the local block of the ERP image relative to the viewing sphere. Then, it is applied to the RDO process of omnidirectional video coding and adaptive selection of quantization parameters to improve vision-based coding efficiency. The experimental results show that compared with the HM16.9 test platform of HEVC standard, the proposed method can achieve significant bit rate savings under the same visual quality, which proves that the proposed method has a satisfactory effect on improving the RDO performance.**

Keywords-Omnidirectional video; rate-distortion optimization; ERP; weighted-to-spherically-uniform structure similarity.

I. INTRODUCTION

Omnidirectional video (also known as 360° video) is widely used in virtual reality (VR) and augmented reality (AR) to provide users with immersion [1]. Omnidirectional video is a video with complete field of view, high resolution, which is widely used in medical, educational, sports and museum scenes [2]. Fig. 1 shows the typical omnidirectional video communication system, includes imaging, projection, coding, transmission, reverse projection and interactive display [3]. Due to the limitations of existing encoders, spherical omnidirectional video needs to be projected as a two-dimensional plane.

Traditional video encoders, such as H.265/HEVC, etc., can be directly used to encode projected planar omnidirectional video. However, geometric distortion and content redundancy are inevitable due to the projection process, which limits the performance of the encoder. For the commonly used ERP, Hendry et al. [4] proposed an adaptive quantization parameter (QP) coding based on latitude factors. According to the latitude factors, a higher QP value is adopted to remove the redundancy in the high latitude region. However, this method only considers the relationship between QP and latitude factor, but does not consider the irrationality of distortion in the rate-distortion process. Similarly, Liu et al. [5] optimized the bit allocation process of the encoder according to the objective quality evaluation scheme S-PSNR and P-PSNR of the ERP omnidirectional video, and achieves better coding performance improvement under the corresponding evaluation method. In addition, some adaptive encoding and streaming methods for omnidirectional video were proposed to reduce the transmission bandwidth. He et al. [6] proposed a scalable coding method for omnidirectional video, in which the base layer stream contains a complete low quality view, and the enhancement layer stream contains a high quality user viewport area. However, this method requires the client to have a special SHVC decoder, which is incompatible with most of the client devices.

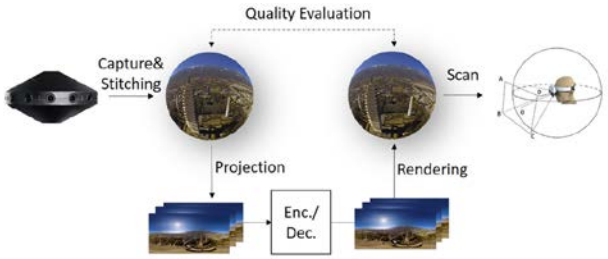

Figure 1. Omnidirectional video communication system.

By considering the shortcomings of the rate-distortion optimization model in traditional video coding, this paper proposes a rate-distortion optimized model based on weighted-to-spherically-uniform structural similarity (WS-SSIM) for ERP omnidirectional video. According to the distortion of the structure similarity of the ERP plane and the relationship between the spherical distortion and the projection plane distortion, WS-SSIM is proposed to describe the distortion of the local block of the plane omnidirectional image relative to the viewing sphere. Then, it is applied to the rate-distortion optimization process and adaptively selects quantization parameters to improve vision-based coding efficiency.

The rest of this paper is organized as follows. The proposed rate-distortion optimization coding method is

 ISBN: 978-1-61208-758-0

described in section 2. Experimental results and analysis are provided in section 3, and the conclusion in section 4.

II. PROPOSED METHOD

The purpose of rate-distortion optimization (RDO) in video coding is to select the appropriate coding mode to optimize the coding effect. However, in the RDO process of traditional video coding, the measure of distortion only considers the pixel level. Since the pixel level distortion metric has a certain difference from the human eye's perception of distortion, the structural similarity (SSIM) [7] is an efficient evaluation method. We use SSIM to describe the distortion by modifying the original RDO model. In addition, for ERP omnidirectional video, the SSIM distortion in the RDO model is optimized according to the distortion transmission from plane to sphere in different regions, so that the distortion of different regions has different weights. Based on the improved RDO model, QP is adjusted accordingly to increase the coding effect.

A. Rate-distortion optimization based on WS-SSIM

RDO model calculates the rate-distortion cost of different coding modes, and selects the mode with the lowest rate-distortion cost as the optimal coding mode. The rate distortion cost is calculated as

$$\min\{J = D + \lambda \times R\} \tag{1}$$

where J is the cost, D and R represent the distortion generated by the current coding mode and the consumed bits, respectively. In addition, λ is a Lagrangian factor used to weight the relationship between bit rate and distortion. In HEVC coding, distortion D often uses pixel level sum of square error (SSE), which is different from human perception of distortion. As an objective quality evaluation model, SSIM combines brightness, contrast and structure comparison to measure image distortion, and defined as (2):

$$\mathrm{SSIM} = \left(\frac{2\mu_x\mu_y + c_1}{\mu_x^2 + \mu_y^2 + c_1}\right)\left(\frac{2\sigma_{xy} + c_2}{\sigma_x^2 + \sigma_y^2 + c_2}\right) \tag{2}$$

where μ_x and μ_y represent the mean of the reference image block and the distorted image block, respectively, σ_x^2 and σ_y^2 represent the variance, σ_{xy} represents the covariance, c_1 and c_2 are constants.

Let x be the original block and y be the reconstructed block of x, assuming that the error caused by the code is linear, i.e., $y=x+e$, where e is the error caused by the coding, and its mean and variance are 0 and σ_e^2, respectively. Then, the mean square error (MSE) can be calculated by:

$$\mathrm{MSE} = \frac{1}{M}\sum_{i=1}^{M}(y_i - x_i)^2 = \frac{1}{M}\sum_{i=1}^{M} e_i^2 \tag{3}$$

where M represents the number of pixels in the current block. From the law of large numbers, as M gets large, $\mathrm{MSE} \to \sigma_e^2$.

It is easily verified that under the high-resolution quantization approximation: $u_x \approx u_y$, $\sigma_y^2 \approx \sigma_x^2 + \sigma_e^2$, $\sigma_{xy} \approx \sigma_x^2$. Substitute this relationship into (2):

$$\mathrm{SSIM} = \frac{2\sigma_x^2 + c_2}{2\sigma_x^2 + \sigma_e^2 + c_2} \tag{4}$$

Since 0<SSIM<1, and the larger the SSIM value, the higher the similarity between the reconstructed image and the original image. Define the SSIM-based distortion metric dSSIM according to Eq. (5):

$$\mathrm{dSSIM} = \frac{1}{\mathrm{SSIM}} = 1 + \frac{\sigma_e^2}{2\sigma_x^2 + c_2} \approx 1 + \frac{\mathrm{MSE}}{2\sigma_x^2 + c_2} \tag{5}$$

where dSSIM>0, and the larger the dSSIM is, the larger the SSIM distortion of the reconstructed image is. Eq. (5) shows the relationship between dSSIM and MSE, which can define a new rate-distortion model for coding blocks:

$$\begin{aligned} J &= M \times \mathrm{dSSIM} + \lambda \times R \approx M\left(1 + \frac{\mathrm{MSE}}{2\sigma_x^2 + c_2}\right) + \lambda \times R \\ &= M + \frac{1}{2\sigma_x^2 + c_2} \times (D_{SSE} + (2\sigma_x^2 + c_2) \times \lambda \times R) \end{aligned} \tag{6}$$

where D_{SSE} represents the SSE distortion in the current coding mode. Similarly, the rate-distortion cost of each code block is defined as follows

$$J = D_{SSE} + (2\sigma_x^2 + c_2) \times \lambda \times R \tag{7}$$

By multiplying λ with the coefficient related to the variance of the local block, the distortion metric of the rate-distortion model is transformed from SSE to dSSIM, so that the structural information of the image is considered in the process of RDO. To keep the bit rate of the entire frame [8], the dSSIM-based λ of the i-th coding block is obtained by

$$\lambda_{SSIMi} = w_{SSIMi} \times \lambda = \frac{2\sigma_{xi}^2 + c_2}{\exp\left(\frac{1}{S}\sum_{j=1}^{S}\log(2\sigma_{xj}^2 + c_2)\right)} \times \lambda \tag{8}$$

where λ is the original Lagrangian factor, S is the number of blocks in the current frame, σ_{xi}^2 and σ_{xj}^2 are the variance of the i-th and j-th original blocks, respectively.

The omnidirectional video system converts the spherical omnidirectional video into planar omnidirectional video through projection, and returns the spherical by inverse projection on the client side. Exactly, different areas of planar omnidirectional video have different weights, resulting in a nonlinear relationship between plane distortion and spherical distortion. Taking ERP as an example, there are more pixels redundancy in the high latitude area. Most of those pixels in the inverse projection are down sampled, which are invisible to the user. Therefore, the distortion transmission rate of these areas relative to the sphere is lower, and more distortion can be tolerated in coding. According to the area ratio of different regions of ERP in inverse projection [9], the distortion weights of different regions are introduced:

$$w(u,v) = \cos\left(\left(v - \frac{H}{2} + \frac{1}{2}\right) \times \frac{\pi}{H}\right) \tag{9}$$

where u and v represent the horizontal and vertical coordinates in the frame, in which the current pixel is located, and H represents the height of the frame.

 ISBN: 978-1-61208-758-0

The weight $w(u,v)$ gradually decreases with the increase of latitude, and reaches the minimum in the polar region. The distortion weight of the inverse projection is introduced into the rate-distortion cost, and the RDO model based on WS-SSIM is established in Eq. (10):

$$\min\{J = D_{SSE} \times w_{ci} + w_{SSIMi} \times \lambda \times R = D_{SSE} + \lambda_i \times R = D_{SSE} + \frac{w_{SSIMi}}{w_{ci}} \times \lambda \times R\} \quad (10)$$

where w_{ci} (the distortion weight of the current block center pixel) is used to represent the distortion weight of the block. And λ_i based on WS-SSIM is calculated by

$$\lambda_i = \frac{w_{SSIMi}}{w_{ci}} \times \lambda = \frac{2\sigma_{xi}^2 + c_2}{\exp(\frac{1}{S}\sum_{j=1}^{S}\log(2\sigma_{xj}^2 + c_2)) \times w_{ci}} \times \lambda \quad (11)$$

B. Quantitative parameter adjustment based on WS-SSIM

In the encoding process, there is a relationship between λ and QP. QP is one of the keys to determine the quality of the coding, so it is necessary to adjust the QP according to the RDO model. In HEVC coding, the original λ has the following relationship with QP:

$$\lambda = \beta \times 2^{(QP-12)/3} \quad (12)$$

where β is a constant independent of QP. According to the change of λ based on WS-SSIM rate-distortion optimization, Eq. (13) is obtained by

$$QP_{offseti} = QP_i - \overline{QP_i} = 3 \times \mathrm{lb}(w_{SSIMi} / w_{ci}) \quad (13)$$

where $\overline{QP_i}$ is the original QP of the i-th block, QP_i represents the new QP obtained based on the WS-SSIM RDO model, $QP_{offseti}$ is the adjusted QP and calculated by

$$QP_{offseti} = QP_i - \overline{QP_i} = 3 \times (P_i - \frac{1}{S}\sum_{j=1}^{S} P_j) - 3 \times \mathrm{lb}(w_{ci}) \quad (14)$$

$$P_i = \mathrm{lb}(2\sigma_{xi}^2 + c_2) \quad (15)$$

Eq. (15) shows that the WS-SSIM RDO process guides the quantization adjustment parameters of each block. In the encoding process, in order to reduce the computational complexity, the calculation is performed with coding tree unit (CTU).

III. Experimental Results

In order to verify the effectiveness of the proposed omnidirectional video coding RDO method based on WS-SSIM, the proposed method is implemented in the HM16.9 test platform of HEVC coding standard. The omnidirectional video test sequence used in the experiment comes from Nokia [10] and Letin VR [11], including scene movement and fixation, as shown in Fig. 2.

The coding configuration uses typical Low-delay P (LDP), and QP is set to 22, 27, 32 and 37, respectively. The objective quality evaluation method uses WS-PSNR [9], and the previously proposed WS-SSIM [12] which is verified to have more accurate evaluation accuracy. The comparison between the proposed method and the original HM16.9 test platform is shown in Table Ⅰ.

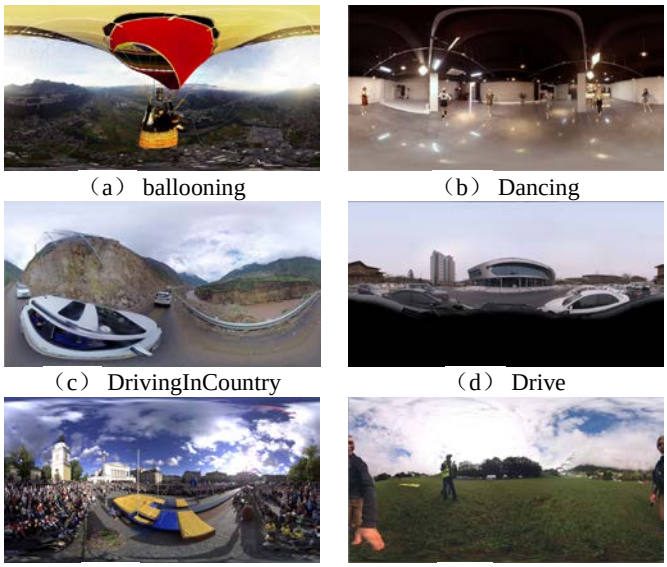

（a） ballooning （b） Dancing

（c） DrivingInCountry （d） Drive

（e） PoleVault （f） training

Figure 2. Omnidirectional video test sequence

TABLE I. Comparison of the proposed method with the original HM16.9 platform coding results

Sequence	WS-PSNR		WS-SSIM	
	BD-WS-PSNR(dB)	BD-Rate(%)	BD-WS-SSIM	BD-Rate(%)
Balloning	0.84	-26.50	0.0085	-40.16
Dancing	0.60	-14.97	0.0032	-27.26
DrivingIn Country	0.41	-14.73	0.0101	-24.10
Drive	0.44	-10.79	0.0025	-19.34
PoleVault	0.31	-10.99	0.0052	-21.13
Training	0.10	-3.65	0.0036	-14.90
Average	0.45	-13.61	0.0055	-24.48

As can be seen from Table Ⅰ, whether WS-PSNR or WS-SSIM, the proposed method achieves better coding results. It should be noticed that the WS-SSIM evaluation method not only takes into account the characteristics of ERP omnidirectional video, but also combines the SSIM evaluation model, which is a more reasonable objective quality model than WS-PSNR, and is more suitable for evaluating the performance of the proposed method.

TABLE II. Comparison between the proposed method and the adaptive QP method

Sequence	BD-WS-SSIM	BD-Rate(%)
Balloning	0.0021	-8.87
Dancing	0.0026	-21.49
DrivingInCountry	0.0018	-4.38
Drive	0.0010	-8.31
PoleVault	0.0017	-6.33
Training	0.0024	-7.60
Average	0.0019	-9.50

 ISBN: 978-1-61208-758-0

In addition, we compare the proposed method with the adaptive QP method [4] to further illustrate the effectiveness of the proposed method. The results of the comparison between the proposed method and the adaptive QP method under the WS-SSIM evaluation method are shown Table Ⅱ.

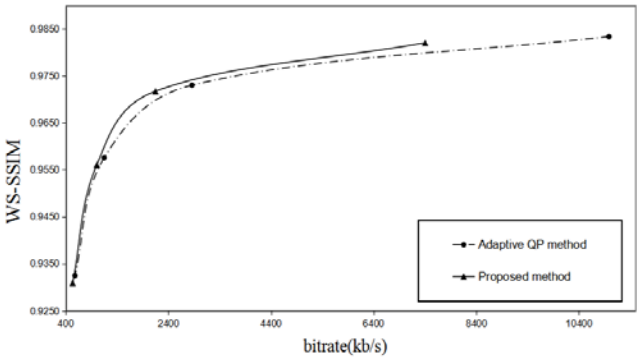

Figure 3. Rate-distortion performance of the proposed method and adaptive QP method in Balloning sequences

As can be seen from Table Ⅱ, the proposed method achieves better coding results than the adaptive QP method. Specifically, for the Dancing sequence, the adaptive QP method has a poor effect. The reason is that there are many smooth areas and the cameras are fixed. The coding modes of these regions are almost Skip mode, resulting in little bit and independent of QP. The proposed method allocates a larger QP to low latitude non-skip regions (texture complex, motion with better masking), achieving more bit savings under the same perceptual quality. In addition, Fig. 3 shows the rate-distortion performance of the Balloning sequence under different coding methods. It can be seen from Fig. 3 that the proposed method has better rate-distortion performance than the adaptive QP method.

IV. CONCLUSION

In view of the distortion of ERP structure similarity and the relationship between spherical distortion and projection plane distortion, this paper proposed an omnidirectional video coding RDO method based on weighted-to-spherically-uniform structural similarity (WS-SSIM). The WS-SSIM is used to describe the distortion of the local block of the plane omnidirectional image relative to the viewing sphere, which is applied to the RDO process of omnidirectional video coding and adaptively selects QP to improve the vision-based coding efficiency. The experimental results show that the proposed method can improve the encoding effect of omnidirectional video and achieve bit rate savings, significantly. In the future work, we are planning to consider the impact of user's viewport on encoding to improve the encoding efficiency of omnidirectional video.

ACKNOWLEDGMENTS

The work was partly supported by the Natural Science Foundation of China (61671258,61871247).

REFERENCES

[1] F. Duanmu, Y. Mao, S. Liu, S. Srinivasan and Y. Wang, “A Subjective Study of Viewer Navigation Behaviors When Watching 360-Degree Videos on Computers,” IEEE Int. Conf. on Multimedia and Expo, San Diego, CA, USA, 2018, pp. 1-6.

[2] A. Mahzari, A. Taghavi Nasrabadi, A. Samiei and R. Prakash, “FoV-Aware Edge Caching for Adaptive 360° Video Streaming,” ACM Multimedia Conference on Multimedia Conference. Seoul, Korea, 2018, pp. 173-181.

[3] Z. Chen, Y. Li and Y. Zhang, “Recent advances in omnidirectional video coding for virtual reality: Projection and evaluation,” Signal Processing, 2018, pp. 66-78.

[4] F. Hendry, M. Coban, G. V. Der Auwera and M. Karczewica, “AHG8: adaptive QP for 360º video ERP projection,” JVET of ITU-T SG16 WP3 and ISO//IECJTC1/SC29/WG11 JVET-F0049, March 31-April 7, 2017, Hobart, Australia.

[5] Y. Liu, L. Yang, M. Mai and Z. Wang, “Rate control schemes for panoramic video coding,” Journal of Visual Communication and Image Representation, 2018, pp. 76-85.

[6] G. He, J. Hu, H. Jiang and Y. Li, “Scalable video coding based on user’s view for real-time virtual reality applications,” IEEE Communications Letters, 2017, pp. 25-28.

[7] Z. Wang, A. C. Bovik, H. R. Sheikh and E. P. Simoncelli, “Image quality assessment: from error visibility to structural similarity,” IEEE Transactions on Image Processing, 2004, pp. 600-612.

[8] C. Yeo, H. Tan and Y. Tan, “On rate distortion optimization using SSIM,” IEEE Transactions on Circuits and Systems for Video Technology, 2013, pp. 1170-1181.

[9] Y. Sun, A. Lu and L. Yu, “Weighted-to-spherically-uniform quality evaluation for omnidirectional video,” IEEE signal processing letters, 2017, pp. 1408-1412.

[10] S. Schwarz, A. Aminlou, M. M. Hannuksela, E. Aksu, “AHG8: tampere pole vaulting sequence for virtual reality video coding,” Joint Video Exploration Team (JVET) of ITU-T SG 16 WP 3 and ISO/IEC JTC 1/SC 29/WG 11. JVET-D0143, October 15-21, 2016, Chengdu, China.

[11] W. Sun, R. Guo and X. Men, “AHG8: test sequences for virtual reality video coding from LetinVR,” JVET of ITU-T SG 16 WP 3 and ISO/IEC JTC 1/SC 29/WG 11. JVET-D0179, October 15-21, 2016, Chengdu, China.

[12] Y. Zhou, M. Yu, H. Ma, H. Shao and G. Jiang, “Weighted-to-Spherically-Uniform SSIM Objective Quality Evaluation for Panoramic Video,” IEEE International Conference on Signal Processing (ICSP), Beijing, China, 2018, pp. 54-57.

 ISBN: 978-1-61208-758-0

Broadband as a Public Good

The Pros and Cons

Karikoga Gorejena
Information Systems. North West University
NWU
Mafikeng, South Africa
Email: kogagorejena@gmail.com

Olebogeng H. Nojila
Computer Science. University of Limpopo
UL
Limpopo, South Africa
Email: olebogenghellennojila@gmail.com

***Abstract*— from its inception in the 90's broadband has continued to capture and influence economic and social variables globally at astronomic rate. In making a case for public policy on broadband, many studies have sought to identify and measure broadband economic benefits. The everyday benefits of broadband include the medical fraternity remote and complex surgical operations carried out by robots via satellites, executives are empowered to make decisions and access new opportunities through online information and the list is endless. In an increasingly integrated global economy, broadband is central in providing economic growth and competitiveness to any organization, country or region. Few studies however have focused on the complexities and inherent repercussions associated with the deployment of broadband. Much few scholars have zoomed in at broadband as a socially constructed artefact, exuding its relationship and sharing space with societal norms and values. This paper displays the tenets of broadband as a public good, highlighting its value, complexities, demystifying its benefits and applications, attributes, and activities it enables. Finally, the data gathered from thirteen nations of the Sub-Saharan Africa, the Southern African Development Community (SADC) was analyzed in relation to inherent repercussion associated with broadband deployment and its social construction. Some policy suggestions to curb the challenges that come with broadband access are deduced from data including those for the socio-technical relationships.**

Keywords-broadband; public good; deployment; complexities.

I. INTRODUCTION

The context and scope of this research is SADC, which comprise thirteen countries at the time of the research. Therefore, primary data was gathered from these countries. According to [18], mobile penetration in Africa by 2013 was at 63%, leaving broadband as a private good for the select few. There are number of factors that affect broadband penetration and part of them are the inherent attributes and repercussions of cyber space itself [19]. Education, both generically and in matters concerning cyber space is among the main causes of low broadband uptake [2]. Hence, the focus of this paper is to explain the ramifications, intricacies and value of broadband. The question of what determines the other between society and technology in the context of broadband was explored. This aspect was necessary to address the possibility of conflict between cultural beliefs and technology, which could pose a factor of broadband penetration. The primary research question of this paper is how to provide broadband as a public good? The secondary questions are; what are the values, complexities and ramifications of broadband, how can they be ameliorated and how does broadband relate with society?

In section II the sample size, data gathering methods, scope of research and the tools that were used to analyze data are discussed. In section III, the concept of broadband was introduced. Its values, complexities, benefits, application and attributes are differentiated. In section IV, the repercussions of a socio-technical environment are highlighted and the results with regard to these repercussions are discussed. Policy interventions as a means to mitigate the repercussions discussed in section IV are discussed in sections IV (A) and the results concerning these interventions are tabled in the same section. Section V looks at the relationship that ought to exist between society and technology in light of what the participants suggested. Finally, section VI gives conclusions and recommendations for future work.

II. SAMPLE SIZE AND DATA GATHERING

This research used a survey questionnaire and interviews to gather data. The survey questionnaire used consisted of two sections. The first section comprised close-ended questions designed according to [1] reliability standards that enables it to elicit consistent responses. The second section was open-ended question allowing for more insights that are detailed. University students from thirteen SADC countries were used to answer the questionnaires and seven experts were interviewed for completeness of in-depth knowledge on the subject. More than 550 participants responded to the survey questionnaires. This data was collected in 2017. Figure 1 below shows the distribution of participants by country.

 ISBN: 978-1-61208-758-0

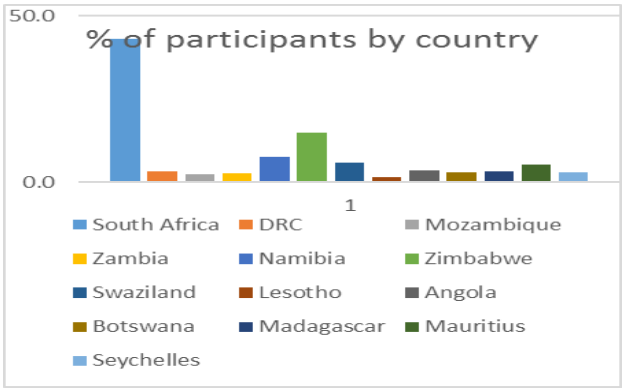

Fig 1. Participation by country

Analysis of the qualitative part from Atlas.ti is not shown in this paper. However, the results shown in Table 1 and Table 2 incorporate those from Atlas.ti. This paper is part of a bigger research that used mixed method approach. The quantitative part of the survey was analyzed using Analysis of a Moment Structures (AMOS) in Software Package for the Social Sciences (SPSS) and that part is not covered in this paper. Only a part of this big research is presented in this paper.

The following section defines broadband and introduces it as a public good.

III. BROADBAND

This research uses as a working definition of broadband as "the provision of telecommunications infrastructure that enables information traffic in a continuous and uninterrupted manner, with sufficient capacity to provide access to data, voice and video applications that are common or locially relevant to users as determined by the" SADC "from time to time" [2].

The following section looks at attributes of broadband in terms of its value, complexities and some of its areas of applications.

A. *Broadband as a public good*

In some developed and developing nations, the government runs broadband or state controlled agencies until late 20th century [3]. In congruent with these two, the move to have telecommunication controlled by the state was necessitated among other things by the need to protect those aspects of telecommunications that are of public interest. Today, even though many telecommunications markets have been privatized and liberalized, government regulatory agencies are still responsible for ensuring that public good issues are provided for. These issues are security, prevention of interference while transmitting and client safety. Two things distinguish public goods from all others and these things are: Non-excludability, which means any member consuming a public good cannot be denied it by another member enjoying the same public good [3]. The second characteristic is that a public good is non-rivalry in consumption [3]. This means therefore that the government to guarantee non-rivalry in the market should provide for public goods. In some developed countries, broadband forms part of Universal Service Obligation (USO), meaning that it is the citizens' right, to have access to it and governments should provide for it. In most countries, however telecommunications is just a universal service and not necessarily an obligation on the part of government. It is in the potential benefits of broadband and a common thrust to bridge the digital divide which gives broadband its public good character.

B. *Value and complexities of broadband*

According to [4], broadband is a tool for the development of economies that are based on knowledge. Many studies corroborate that enhanced broadband penetration has desirable effects on the growth of any economy, improved access and delivery of social services apart from bridging the digital divide. All these impacts of broadband result in high quality way of living and economic index of countries. According to [5], broadband is at the center of organizations' improved efficiency, faster connectivity, and access to operation-specific applications which usher in new ways of doing business and give birth to new business models.

In considering the value of broadband, research has concentrated on benefits of it singly without taking into account the problems that inherently comes with these benefits. There are quite some complex issues that tend to hinder proper of the benefits of broadband. One such issue is the confusion that literature has had between benefits of broadband and its applications, attributes of broadband and the activities that these attributes enable. "Applications include video on demand, gaming, streamed video, and voice over the internet. Attributes include greater speed, always on and the capacity for Local Area Networks (LANs). The activities that these attributes enable include teleworking, e-gaming, e-gambling, e-learning, e-health, e-commerce, and e-government" [6]. Publications of repute and which have contributed immensely to broadband research but which made this ontological error include International Telecommunications Union (ITU) on their briefing paper on broadband promotion according to [7].

The other one is that confusing benefits with activities gives the notion that it is gross outcome rather net that counts. In so much as broadband-enabled activities bring benefits, they also have negative outcomes which include increased worker isolation and less mentoring in the case of teleworking, financial problems (e-gambling), and displacement of conventional social contacts in general [8].

Another complexity is that of cost, if the cost of broadband excludes multiple voices in favor of a monopoly then there is need for constitutional and social considerations [5]. From the above given arguments, it is clear that a high broadband penetration does not equally mean high broadband benefits. Furthermore according to [9],

 ISBN: 978-1-61208-758-0

calculated revenues expected to be coming from broadband related enterprises do not reflect an adequate measure of benefits of broadband. Lastly, owing to poor planning and veiled understanding of broadband scenarios, the ways by which governments sometimes attempt to use to grow broadband may disrupt the economic and social dynamics [10].

Notwithstanding the highlighted complexities associated with accurately identifying the benefits and hence the value of broadband, the following section explains the broadband benefits in five main areas:

1) Edducation: According to [5], where e-learning is asynchronous, meaning where there is no need for real time interaction between student and instructor, narrowband is sufficient. However when synchronous and collaborative learning in real time takes place, broadband is needed. Where multiple students access the web simultaneously, even for asynchronous e-learning, broadband is needed. Broadband therefore has the ability to provide educational platform which transcends geographical and financial challenges [4]

2) Health: Broadband applications that are health specific and services are significantly improving health and medical outcomes around the world, particularly for patients in remote areas and those with limited mobility, through e-health and m-health initiatives [11]. In view of the fact that in 2012 there were "fewer than 27 million doctors and nurses for the more than 6 billion people in the world and only 1.2 million doctors and nurses in the lowest-income countries", using mobile technologies is a valuable tool for enabling health care practitioners to reach patients [12]. In spite of the fact that voice and data connections can be useful in improving medical care, broadband connectivity is necessary if full potential of e-health services that include telemedicine, which enables real-time audio and video communications between patients and doctors as well as between health care providers, broadband connection is required. Online medical procedures need high processing power, huge storage capacity, much bandwidth and protection of personal data of patients [13]..

3) E-Governance: E-government refers to a wide range of applications that transform government processes and the ways in which governments connect and interact with businesses and citizens. This facilitates citizens participation in national issues and society, improves accountability, effectiveness and efficiency in governments' day today business. Broadband is an essential component of e-government, since it provides the foundation for public administration networks that allow smooth flow of processes. E-government can in return be a catalyst for increased demand for broadband as basic services are made available online, consultations with citizens on issues of policy and online multimedia as two way exchange technology. Tax returns, debate forums, applications and registrations are all made easily available by e-government as enabled by broadband. Republic of Korea, the United States, and Canada are in the top three places with regard to the number of online government services available. However, countries have made significant progress over the last two years, including Bahrain, Chile, Colombia, and Singapore. In addition, the use of mobile phones for e-government services, such as alert messages, applications, and fee payments, is almost as popular in developing countries as it is in developed countries [14].

4) Gross Domestic Product: A study by the World Bank cited by many researchers found out that for low to middle income countries "about a 1.38 percentage point increase in GDP for each 10 percent increase in broadband penetration" between the years 2000 and 2006 [15]. The same study further revealed that broadband impact was more in developing economies than in developed countries which "enjoyed a 1.21 percentage point increase in per capita Gross Domestic Product (GDP) growth" for each 10 percent increase in broadband penetration. This study also evidenced that broadband has a potentially larger growth effect than other Information Communication Technologie (ICTs), including wireline telephony, mobile telephony, and the Internet. There are other studies that confirm the findings of the World Bank such as Management consulting firm McKinsey and Company which estimated that "a 10 percent increase in broadband household penetration delivers a boost to a country's GDP that ranges from 0.1 percent to 1.4 percent" [16]. It therefore, follows that broadband can increase the economy of a country by e-commerce, creating new jobs, developing and attracting new industries and by providing access to local, regional and global markets.

5) Cloud Computing: Cloud computing generally allows storage, processing and instant access to applications and data remotely via broadband connectivity [17]. This translates into reduced costs of IT infrastructure including hardware, software and technical support. The point to note here is that the benefits of cloud computing are directly the benefits of broadband because without broadband cloud computing as we know it today would not be possible. According to [17], cloud computing has the following other potential benefits: reduced need for up-front investment, since cloud computing is typically based on a pay-as-you-go pricing model, lower operating costs, since the service provider does not need the provision capacities according to the peak load, easy access through a variety of broadband-enabled devices and lower business risks and maintenance expenses, since business risks (such as hardware failures) and maintenance costs are shifted to infrastructure providers, which often have better expertise and are better equipped to manage these risks. There are many other benefits of broadband such as leisure, entertainment, social

 ISBN: 978-1-61208-758-0

relations, gaming, green computing, aviation and much more. Governments across the globe have set out ambitious targets for broadband growth and penetration due to the unquestionable value of broadband as discussed above. Notwithstanding the benefits of broadband, these come with some side effects. The following section discusses the challenges associated with broadband growth and penetration.

IV. THE RAMIFICATIONS OF BROADBAND

A question was posed to participants to the effect of identifying the repercussions that are caused by broadband penetration. The chart below gives the most significant phrases in answering this question:
Digitization and computerization of services has social repercussion among workers and customers. Which are some of these repercussions in your opinion? The responses to this question are illustrated in Figure 2. In the figure, the size of the shapes indicates the percentage of participants that gave similar answers. This question's responses were integrated with responses from experts to reach a more robust conclusion in answering the objective of social repercussions. Figure 2 was further refined and integrated with expert responses resulting in the following Table 1.

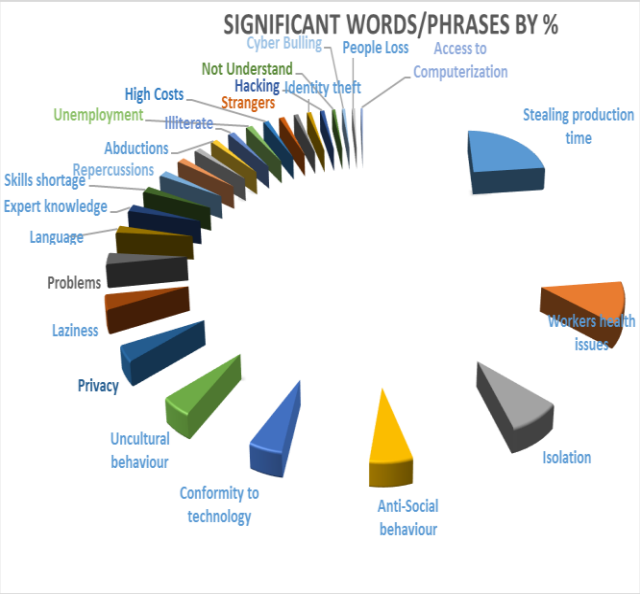

Fig 2. Cyber space ramifications

TABLE I. BROADBAND REPERCUSSIONS

Social repercussions							
Cyber bullying	Data confidentiality	Health issues	Isolation	Unemployment	E-Gambling	Indecent content	Abductions
Data Integrity	Data Availability	Indirect effects	Anti-social behavior	Uncultured behavior	Profiteering	Unproductivity	Theft

A. *Policy intervations*

The following quotations are extracted from the primary documents of responses given by some experts to various interview questions. In response to the question of negative social effects of broadband and the possible solution to that, the expert said the following:

"There are supposed to be rules in using technology. Some use ICT do illegal or immoral things like online divorce, cyber bullying, isolation, kids and parents don't know each other anymore. Educate people also about the bad side of technology."

In this response, the expert called for a balance between the implementation of broadband and an equally important implementation of the educational programs on correct and incorrect use of it. Here, the experts indicate that the gains intended to be achieved by such technological developments can be reversed by lack of education about the same development. Education has been the preeminent solution to many attributes. Targeted education to address the ills of misuse of broadband is needed from the expert's point of view. Table 2 below summarizes some of the policy solutions given by experts with regarding the broadband ramifications. Given below is just a subset of all the responses.

TABLE II. POLICY INTERVENTIONS

Social Repercussions			
Data integrity	Anti-social behavior	Unproductivity	Identity theft
Policies for social repercussions			
Encryption	Education	Targets	Secure networks
White hat hackers	Mentorship	Incentives	Best practices
	Team work	Performance management	

The interventions highlighted by the experts manifest themselves in various ways but their themes remain the same. These results are useful to decision makers at different levels of management in curbing the negative effect of cyber space. The following section deals with question of the relationship that should exist between technology such as broadband and the society in which it is used.

V. SOCIETY AND TECHNOLOGY

On the question of reciprocal shaping between technology and society, one expert had this to say:

"I don't know if I agree with reciprocal shaping. According to me, society balances itself out. Unsuitable inventions or technology will naturally be damped. To policy that can be counter development. Regulation should be after the fact to guard fundamental human rights."

According to this expert, there need not be any regulation on technological development beforehand but rather after the event. Regulation of inventions before they are done is counterproductive, the expert said. This is a remarkable contribution by this expert. The researcher concludes that even regulation that is done after the event will still affect new events therefore the effect is the same expect in areas where regulation does not yet exist.

"It depends on the type of technology. Society has requirements and manufacturers tend to take these requirements in their products. Manufacturers do their research and do production without consulting but society accepts it. Others can be refuted due to societal beliefs and values eg, abortion, genetic manipulation, human being cloning. There is no one way fits all. The two need to be in a reciprocal shaping because technology is meant to serve people and not people technology, to maintain a balance of values."

The researcher acknowledges the above response as striking as it gives balance between control and liberalism. Indeed not all technologies are the same and broadband based technologies are vast and different. Steve Jobs once said "A lot of times, people don't know what they want until it is shown to them." This concurs with the expert's response on society accepting new products made without market research. At the same time, the expert is acknowledging the need for consultation pointing that it depends on the type of technology involved. The pivotal point the expert makes is that technology should serve people and not the other way round. The two should be in reciprocal shaping relationship.

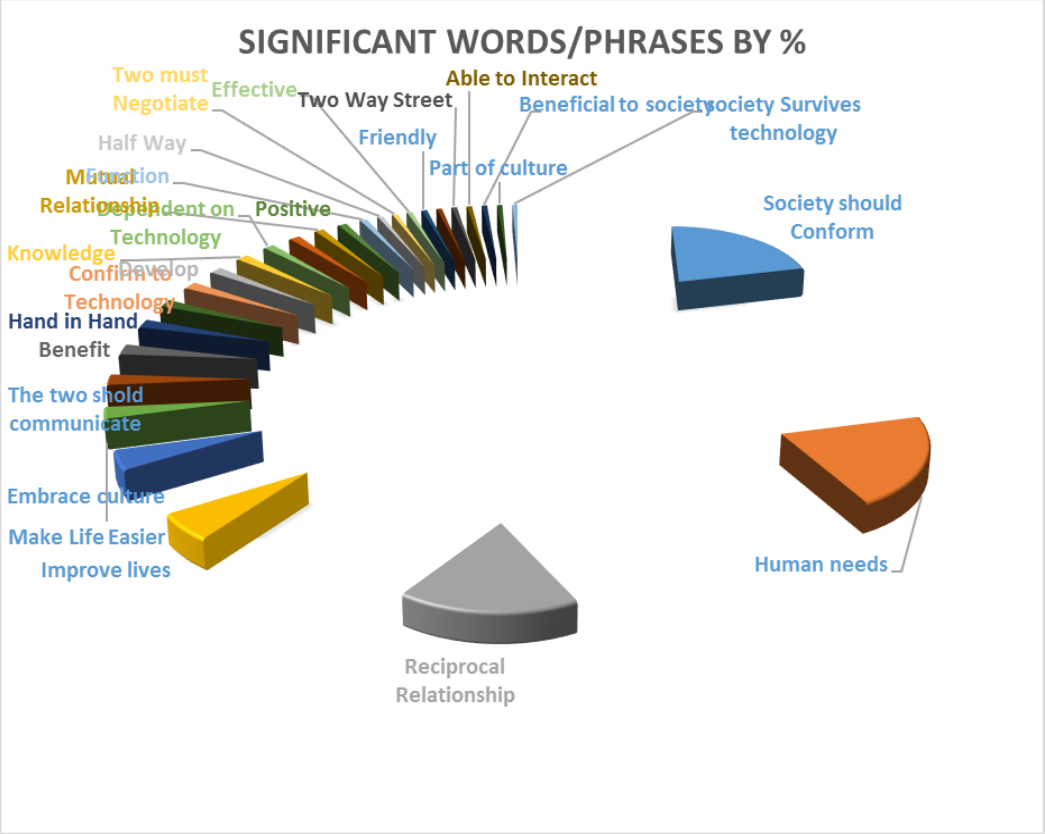

Fig 3. Socio-technical relationship

On the same question of relationship between technology and society, another researcher had the following to say:

"Technology should not be a garget but a solution to a problem. That is the solution. Therefore, any piece of technology that does not answer to problems of society at

hand then it's not useful. Therefore society should come first in every case. Technology should come to fill a gap but at the end, the solution should benefit society. Eg etolls in SA, it's a good
Technology but it's not filling the gap. Society does not need it. There should be another model."

The above quote emphasizes reciprocal shaping of the two with special reference to values. This points to culture. The experts gave pre-eminence to human values. The researcher interprets to mean the need of consultations or market research before implementing some technologies.

The expert quoted above focuses on the ultimate end and that is in the final analysis, any technology should fill a gap in society otherwise it is irrelevant. In terms of how technology can fill the gaps without compromising existent societal norms and values, there are trade-offs that can be done, hence the need for consultations.

Figure 2 attempts to summarize the responses on this question On technology-society relationship, the result reveals that the majority of respondents are of the opinion that society should take credence over technology. The researcher therefore has reason to accept that in SADC society takes precedence over technology

VI. CONCLUSIONS AND RECOMMENDATIONS

In conclusion, it has been evidenced that a socio-technical environment like broadband has inherent, negative unintended ramifications that come with it. Such ramifications can be provided for by enacting policies aimed at reducing their effects. These two variables have been explored within the context of SADC where broadband is provided for as a public good. Lastly, the relationship between technology and society has been interrogated and as much as some participants suggest one of reciprocal shaping, most of them concur that society should take preeminence over technology. It is recommended that further research can done on each of the aspects of the research questions separately and concrete results for each be discussed separately. A times series research of the same phenomenon is also recommended to establish if the socio-technical environment of broadband changes significantly with time.

REFERENCES

[1] L. A. Suskie, *Questionnaire Survey Research: What Works Paperback*, [retrieved: October, 2019 from http://www.amazon.com/Questionnaire-Survey-Research-WhatWorks/dp/1882393058

[2] World Bank Group, *Broadband Strategies Toolkit*, [retrieved: 12 September 2019], from http://broadbandtoolkit.org/0.

[3] A. Picot, and, C. Wemick, "The role of government in broadband access", Telecommunications Policy, Volume 31, Issues 10–11, pp. 660-674, November–December 2007.

[4] S. Khan, "South Africa Connect", ITU broadband Policy, [retrieved October 2019], from https://researchictafrica.net/presentations/Presentations/2015%20Khan_Safia_ITU%20Broadband%20Policy%20Presentation.pdf

[5] C. A. Firth, and D. Mellor, "Broadband: benefits and problems", volume 29, Issues 2–3, pp. 223-236, March–April 2005.

[6] K.Junghyun and P. M. Haridakis, "The Role of Internet User Characteristics and Motives in Explaining Three Dimensions of Internet Addiction", Journal of Computer-mediated Communication, Volume 14, Issue 4, pp. 988–1015 July 2009,.

[7] T. Reynolds, "Broadband Promotion", ITU, [retrieved: October 2019], from https://www.itu.int/osg/spu/ni/promotebroadband/presentations/01-reynolds.pdf

[8] J.E. Katz and R.E. Rice, "Public views of mobile medical devices and services: a US national survey of consumer sentiments towards RFID healthcare technology.", [retrieved: October 2019], from https://www.ncbi.nlm.nih.gov/pubmed/18619897.

[9] R. Crandal, W. Lehr, and R. Litan, "The Effects of Broadband Deployment on Output and Employment: A Cross-sectional Analysis of U.S. Data" ITU, [retrieved: September 2019], from, https://www.brookings.edu/research/the-effects-of-broadband-deployment-on-output-and-employment-a-cross-sectional-analysis-of-u-s-data/

[10] T. Kelly and S. Raja, "Building Broadband: Strategies and Policies for the Development. Global Information and Communication Technologies Department of World Bank", [retrieved: September 2019], from, http://siteresources.worldbank.org/extinformationandcommunicationandtechnologies/Resources/282822-1208273252769/Building_broadband.pdfS.

[11] WHO, "Make every mother and child count", World health organization report 2005, [retrieved: October 2019], form https://www.who.int/whr/2005/whr2005_en.pdf

[12] World Bank Group, "Broadband Strategies Toolkit", [retrieve: 12 September 2019], from http://broadbandtoolkit.org/0

[13] ITU, *New global broadband study: national plans and competitive markets are crucial*, [retrieved: August 2019], from http://www.itu.int/net/pressoffice/press_releases/2013/27.aspx#.U5DphvmSx1Y

[14] UN, *E-Government Survey 2010*, [retrieved: September 2019], from https://publicadministration.un.org/egovkb/Portals/egovkb/Documents/un/2010-Survey/unpan038851.pdf

[15] T. Kelly and S. Raja, *Building Broadband: Strategies and Policies for the Development. Global Information and Communication Technologies Department of World Bank*, [retrieved: September 2019], from http://siteresources.worldbank.org/extinformationandcommunicationandtechnologies/Resources/282822-1208273252769/Building_broadband.pdfS.

[16] T. Kelly and M. Rossotto, *Broadband strategies handbook*, [retrieved: August 2019], from https://books.google.co.za/books?id=4xru2lluqzyc&pg=pa5&dq=buttkereit+et+al.+2009&hl=en&sa=x&ved=0ahukewixhvnkk9plahvoqxuihamabccq6aeimdab#v=onepage&q=buttkereit%20et%20al.%202009&f=false

[17] Q. Zhang, L. Cheng, and R. Boutaba, "Cloud computing: state-of-the-art and research challenges", [retrieved: September 2019], from https://u.cs.biu.ac.il/~ariel/download/ds590/resources/cloud/cloud_sota.pdf

[18] B. Sanou, "ICT facts and figures", [retrieved: August 2019], from https://www.itu.int/en/ITU-D/Statistics/Documents/facts/ICTFactsFigures2013-e.pdf

 ISBN: 978-1-61208-758-0

[19] G. B Mugeni1, G. W. Wanyembi, and J. M. Wafula, "Evaluating factors affecting broadband intensity in Kenya", [retieved: September 2019], from https://www.academia.edu/5066315/Evaluating_Factors_Affecting_Broadband_Intensity_in_Kenya

 ISBN: 978-1-61208-758-0

Optical Coding Label Reuse Scheme to Support More Routing Paths over Multi-Protocol Label Switching Networks

Chun-Chieh Liu, Jen-Fa Huang*, En-Sheng Cheng
Institute of Computer and Communications Engineering,
Department of Electrical Engineering,
National Cheng Kung University,
Tainan, Taiwan.
*e-mail: huajf@ee.ncku.edu.tw

Chao-Chin Yang
Department of Electro-Optical Engineering
Kun Shan University
Tainan, Taiwan
e-mail: ccyang@mail.ksu.edu.tw

***Abstract*—In a Multi-Protocol Label Switching (MPLS) network based on Optical Code Division Multiplexing (OCDM), each core switching node is assigned one code sequence with N chips for each specific input/output pair. With optical code division multiplexing, it creates a new way to utilize optical codes as optical labels. As the users and Internet traffic continue to grow rapidly, it is expected that optical networks will support a larger number of users in the future. However, there is a scalability problem that the large the number of core nodes, the more code sequences are needed. To solve this critical problem, we consider a situation that can reuse label in order to save the number of utilized labels. Under this structure, there is a significant increase in the number of users that can be supported compared to the original ones. In this paper, we compare the relationship of the number of utilized labels and supported LSPs (label switching paths) in both situations with and without reusing labels. We also discuss the issue of cost efficiency and bandwidth efficiency. Further, the discussion of BER performance is also included.** *(Abstract*)

***Keywords- Optical code division multiplexing (OCDM); multi-protocol label switching (MPLS); label stacking; spectral amplitude coding (SAC) (key words*)**

I. INTRODUCTION

Multi-Protocol Label Switching (MPLS) is a switching protocol between data link layer (layers 2) and network layer (layer 3), which labels are added in packet headers and the labelled packets are forwarded in corresponding paths using label switching [1]. The term 'multi-protocol' has the meaning that it can be used in different network layer protocols. MPLS maps IP addresses into simple fixed-length protocol-specific identifiers called 'labels' which are distinguishing forwarding information (label) from the content of the IP headers [2], in other words, MPLS enables the forwarding of packets based on looking up the labels rather than the IP addresses [3].

Many MPLS techniques based on different multiplexing methods have been proposed in optical domain, such as Time-Division Multiplexing (TDM) [4], Wavelength-Division Multiplexing (WDM) [5], Subcarrier-Division Multiplexing (SDM) [6] and Optical Code Division Multiplexing (OCDM) [7]. With OCDM, it creates a new way to utilize optical codes as optical labels [8]. In [9], author proposes a method to check the label in the core node with the function of optical correlation, because logic operations corresponding a look-up table is the toughest challenge for optical processing.

Some researches had been proposed, focusing on increasing the user capacity in OCDMA system [10][11]. However, in the OCDM-based MPLS network, the length of a label is mainly related to the number of nodes of core network [12]. The bigger the core network is, the more core nodes are needed. When more nodes are required, the more code sequences are needed, which means the code length must be increased due to the reason that the number of code sequence is limited by the code length [13]. Therefore, we consider a scenario which can reuse labels in order to save the number of utilized labels when the number of core nodes is limited. We will compare the relationship of the number of utilized labels and supported LSPs in the situation with and without reusing labels; BER performance, cost efficiency and bandwidth efficiency in both situations are also discussed.

Spectral-Amplitude Coding (SAC) has the advantages of low-cost implementation and high switching speed. It is easy to eliminate the Multiple-Access Interference (MAI) when code sequences are with fixed in-phase cross correlation (such as M-sequence or MQC code) [14][15]. However, we use the method of label stacking based on SAC, which is compatible with label stacking, to generate labels [16]. With the label stacking method, the size of forwarding tables can be reduced, and the speed of routing process can also be increased, moreover, the repeated process of label swapping can be avoided. In our proposed system architecture, we use Arrayed Waveguide Grating (AWG) as the codec in order to generate labels and do the optical correlation.

The rest of this paper is organized as follows. Section II introduces the label stacking method base on SAC, and the system structure we used. Section III describes the concept of label reuse and we will first mention the problems from the aspect of OCDMA, then we discuss these problems when applying OCDMA to MPLS. In Section IV, we compare the relationship of the number of utilized labels and supported LSPs when labels are with or without reused, also, the cost

 ISBN: 978-1-61208-758-0

efficiency and bandwidth efficiency are also included in the discussion. Finally, conclusions are presented in Section V.

II. Label Stacking Based On Spectral-Amplitude Coding

A label stacking method based on SAC is first proposed in [16]. With this approach, each label is assigned to each intermediate node rather than link. Here, one label means a specific bond, in other words, the forwarding information of two links adjacent to an intermediate node. At the ingress node, it chooses the path and sends all the labels corresponding to the intermediate node attached to the payload, and the intermediate node only needs to check a short label that is assigned to it. This approach reduces the size of forwarding tables and increases the speed of routing processing; moreover, the repeated process of label swapping can be avoided.

Here, we take an example of simple MPLS network in order to introduce the concept of label stacking based on SAC with the proposed scheme that AWG is used as the codec. The example is shown in Figure 1, which we assume that the ingress node has chosen two Label Switching Paths (LSPs) and each of them contains three core nodes. In one LSP, each core node is assigned with a specific code sequence (label), in this example, labels $\boldsymbol{C}_1$ to $\boldsymbol{C}_3$ belong to LSP1 and $\boldsymbol{C}_4$ to $\boldsymbol{C}_6$ belong to LSP2.

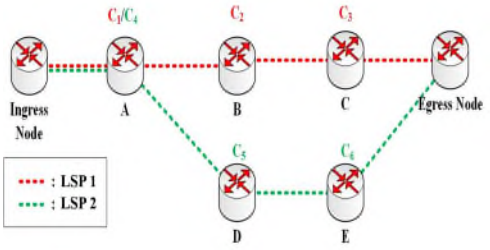

Figure 1. Example of a simple MPLS network topology.

Figure 2 illustrates the system structure of the ingress node. The broadband light source will be sent to the splitter, then, the light source will be encoded on the spectrum in order to generate the corresponding code sequences. Here, we utilize AWG as the codec to encode and decode code sequences, and the M-sequence with code length 7, code weight 4 and correlation value 2 is also used as the label. On the other hand, the electrical header has the information of the desired LSP for the user and it determines the corresponding code sequences to be encoded into a label stack.

After the label stack has been chosen, the label stack will modulate the payload bit with intensity modulation in order to generate the labelled packet. Therefore, each bit in the labelled packet includes the information of label stack, in other words, the payload and the label stack occupy the same bandwidth in the labelled packet, which also increases the bandwidth efficiency. Figure 3 shows the spectrums of the labelled packet bit of LSP1 and LSP2.

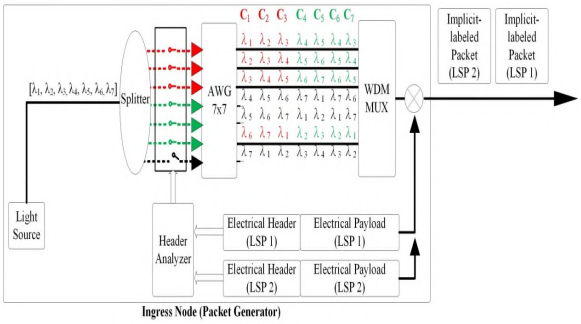

Figure 2. System structure of ingress node.

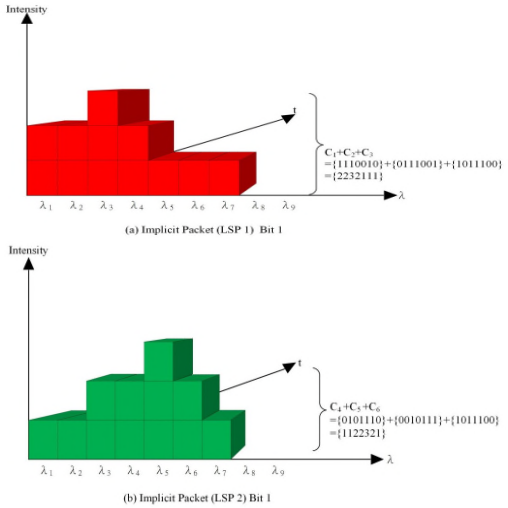

Figure 3. Spectrum of the labelled packet bit of (a). user of LSP1; and (b). user of LSP2.

As shown in Figure 4, at the core node, the bit of the labelled packet is first sent to the splitter, and the label processor will do the optical correlation by the optical decoder, also, the optical switch will forward the packet to the correct output. The structure of the decoder ($\boldsymbol{C}_1$) is illustrated in Figure 5, it will remove the power of undesired code sequences by the balanced detector, and the output of the decoder is used as the control signal to order the corresponding optical switch to forward the packet to the correct output port.

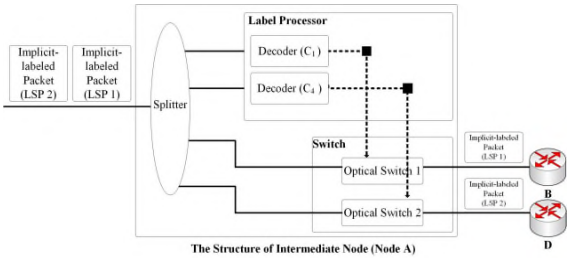

Figure 4. The structure of core node (node A).

 ISBN: 978-1-61208-758-0

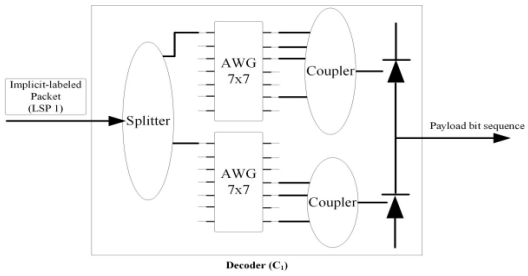

Figure 5. The structure of decoder (C1).

III. Concept Of Label Reuse

From the aspect of OCDM, the most direct method to support more users is increasing the code length. Most Optical Orthogonal Codes (OOCs) have limited number of users for a reasonable code-length and code-weight, for example, the M-sequence codes with code length 3 and code weight 2 can only support 3 users, as shown in Figure 6. If we want to support more users, then the code length must be increased for the reason that the code length increases with the increase in the number of users.

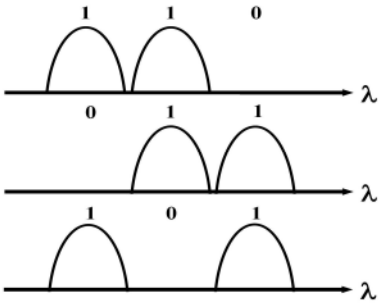

Figure 6. M-sequence code (length 3, weight 2).

When the bandwidth of the broadband light source is fixed and we increase the code length, as shown in Figure 7, the port numbers of AWG codec will also increase, resulting in a higher cost. In second case, the bandwidth of the wavelength channels is fixed and two times the bandwidth of broadband light source is used than before increasing the code length, as shown in Figure 8. This situation causes a lower bandwidth efficiency.

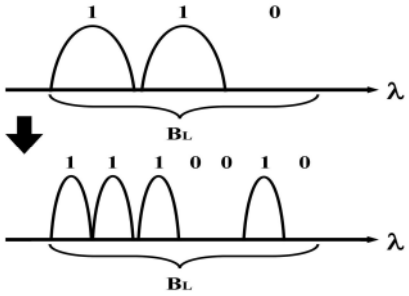

Figure 7. Increasing code length when the bandwidth of the broadband light source is fixed.

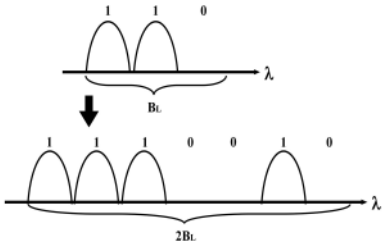

Figure 8. Increasing code length when the bandwidth of the wavelength channels is fixed.

As mentioned above, from the aspect of OCDM, the discussions are focused on how to increase the number of supported users. However, when applying OCDM to MPLS, the point will be how to save the number of utilized labels and support more LSPs when the number of available labels is limited. The following will describe the concept of label reuse with a simple example. The concept of label reuse is quite intuitive. When one intermediate node is not intersected with other LSP, a specific label which has been assigned to other node can be reused by this intermediate node. An example is shown in Figures 9 and 10.

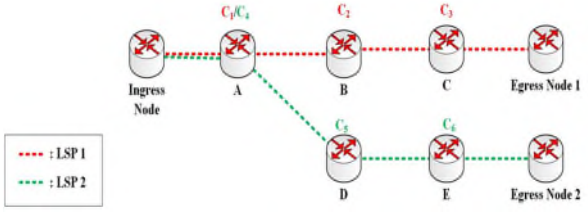

Figure 9. Example of MPLS network (without label reuse).

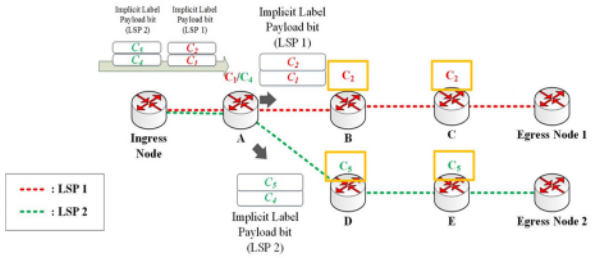

Figure 10. Example of MPLS network (with label reuse).

Two LSPs are assumed. Two payload bits, each with different label stack. Except intermediate node A, the nodes in LSP1 and those in LSP2 are independent. Therefore, as illustrated in Figure 10, it is intuitive that $\boldsymbol{C}_2$ and $\boldsymbol{C}_5$ can be reused in LSP1 and LSP2, separately.

IV. Comparison And Discussion

We want to know the difference between the label-reused scenario and the situation without reusing the labels. In the following examples of grid topology, we assume that every LSP has only three intermediate nodes, and only one of them intersects by other LSPs, in other words, the rest two nodes are not related to other LSPs. Here, we discuss

 ISBN: 978-1-61208-758-0

the relationship between the number of utilized labels and supported LSPs when labels are with or without reused. We first fix the number of supported LSP to compare the number of utilized labels between the label-reused scenario and the situation without reusing labels. It is assumed that the number of supported LSPs is 2, and we take examples of the grid topology to illustrate this case in Figures 11 and 12. As illustrated in Table I, according to Figures 11 and 12, we can save two labels from being utilized when reusing labels (case 1 in Table I).

In order to see a more obvious change, we consider two more cases that the fixed number of supported LSPs is set as 6 and 10. As shown in Table I, in case 2, the number of utilized labels is 18 without label reused, however, we can save four labels when reusing labels. On the other hand, in case 3, the number of utilized labels will be decreased down to 20 when reusing labels, in the contrast, it is 30 when labels without reused.

Here, we fix the number of utilized labels to compare the number of supported LSP between the label-reused scenario and the situation without reusing labels. We assume that the number of utilized labels is 2, and we take examples of the grid topology to illustrate this case in Figures 11 and 13 (case 1 in Table II). Table II shows that, in case 1, only two LSP can be supported when labels are not reused, however, in the label-reused scenario, the number of supported LSP reaches to 4.

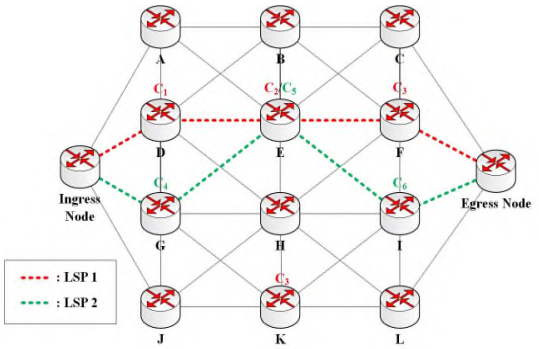

Figure 11. Grid topology (without label reuse).

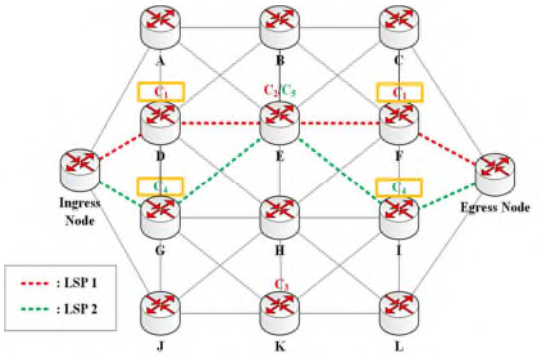

Figure 12. Grid topology (with label reuse / fixed number of supported LSPs).

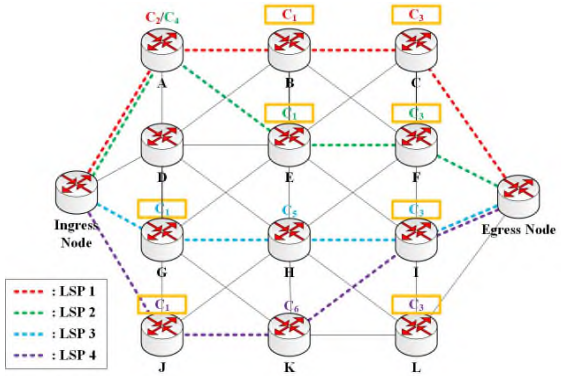

Figure 13. Grid topology (with label-reuse / fixed number of utilized labels).

TABLE I. NUMBER OF UTILIZED LABELS AND SUPPORTED LSP WITH AND WITHOUT LABELS REUSING WHEN THE FIXED NUMBER OF SUPPORTED LSP IS 2/6/10.

Case		The number of utilized labels	The number of supported LSPs
Case1	***Lwor***	6	2
	Lwr	4	2
Case2	***Lwor***	18	6
	Lwr	12	6
Case3	***Lwor***	30	10
	Lwr	20	10
Lwor: Labels without reuse / *Lwr*: Labels with reuse.			

TABLE II. NUMBER OF UTILIZED LABELS AND SUPPORTED LSP WITH AND WITHOUT LABELS REUSING WHEN THE FIXED NUMBER OF SUPPORTED LSP IS 6/15/30

Case		The number of utilized labels	The number of supported LSPs
Case1	***Lwor***	6	2
	Lwr	6	3
Case2	***Lwor***	15	5
	Lwr	15	8
Case3	***Lwor***	30	10
	Lwr	30	15
Lwor: Labels without reuse / *Lwr*: Labels with reuse.			

In addition for viewing a more explicit change, we also consider other two cases that the fixed number of utilized labels is set to be 15 and 30. In case 2, we let the number of utilized labels be 15. If labels are not reused, the number of supported can only be 5, however, it can be up to 8 when reusing labels. On the other side, in case 3, the number of supported LSPs increases from 10 to 15.

From the cases of comparison above, we can derive the mathematical relationship between the number of utilized labels and supported LSPs in a intuitive way. First, we assume the following parameters:

n: The number of core nodes in every LSP.

α: The number of core nodes which intersect with other LSPs in each LSP.

K: The number of utilized labels.

L: The number of supported labels.

As mentioned, from the cases of comparison above, we can derive the mathematical relationship intuitively. The mathematical relationship between the number of utilized labels and supported LSPs is as follows:

$$K = n \cdot L. \quad (1)$$

$$K = \text{ceiling}(\alpha \cdot L + L) = \text{ceiling}(L \cdot (\alpha + 1)). \quad (2)$$

where ceiling(x) is the ceiling function which gives the smallest integer greater than or equal to x.

Equation (1) denotes the relationship between the numbers of utilized labels and supported LSPs when labels are without reused. On the other hand, (2) is for the case that labels are reused. For example, if labels are without reused and there are two LSPs (L=2), every of them has five core nodes (n=5), one of these nodes are intersected with other LSPs (α = 1), then from (1), we can obtain the number of utilized labels K is 10 ($K = n \cdot L = 5 \cdot 2 = 10$). On the other hand, if in the label-reused scenario, we can obtain from (2) that the number of utilized labels K is 4 ($K = L \cdot (\alpha+1) = 2 \cdot (1+1) = 4$).

Based on the assumption that every LSP has only three intermediate nodes and only one of them intersects by other LSPs, under the situation that the bandwidth of the broadband light source is fixed, if we let the number of supported LSPs is 10, then the number of utilized labels will be 30, which means we need the codes with code length at least 30. However, in the label-reused scenario, we only need code with code length with at least 20. This situation is related to the cost of AWG codecs. In other words, if we use codes with longer code length as the labels, then we need AWG codecs with more ports which increases the cost. Therefore, the situation with label-reused is more cost efficient.

Based on the same assumption that every LSP has only three intermediate nodes and only one of them intersects by other LSPs, if we let the number of supported LSPs is 10 and the bandwidth of wavelength channel of AWG is fixed, then we need the codes with code length at least 30, therefore, the bandwidth of broadband light source will be 30 times the one of wavelength channel. However, in the label-reused scenario, we only need code with code length with at least 20, in other words, the bandwidth of broadband light source will only need to be 20 times the one of wavelength channel. So, the bandwidth of the broadband light source will not be wasted too much when labels are reused, therefore, the bandwidth efficiency is better.

We analyze the BER performance in both situations that with and without label reuse. It is assumed that the number of core nodes in every LSP is 6 (n=6), the number of core nodes which intersect with other LSPs in each LSP is 1 (α=1) and the number of supported labels is 4 (L=4). Besides, we use M-sequence code with code length 15, code weight 8 and correlation value 4 as the label sequence. As illustrated in Figure 14, when labels are without reuse, the BER is higher for the reason that the label stack contains six code sequences. However, if labels are reused, the BER performance becomes better, because when reusing labels, the number of code sequences in the label stack will decrease. For example, in this case, the number of code sequences in the label stack is two when reusing labels. In the previous research [17], the BER performance between labels coded with stuffed quadratic congruence (SQC) codes and conventional M-sequence codes had been discussed. The BER of M-sequence label in [17] at the power level of -16 dBm is about 10^{-11}, however, as seen in Figure 14, at the same power level, the BER of M-sequence labels with label reuse is about 10^{-67} theoretically, which is much better than the result derived in [17].

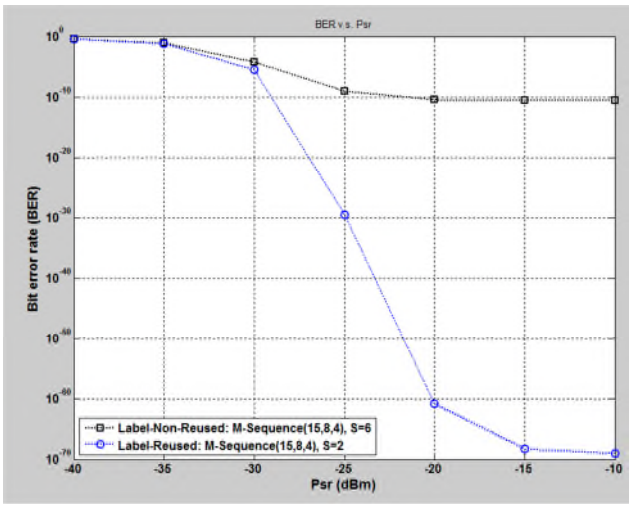

Figure 14. BER vs. effective received power when labels are with and without reuse.

V. CONCLUSION

Mathematical relationship of the number of utilized labels and supported LSPs when labels are reused or not reused were well derived. Some advantages with label reuse were found out as following: (1). If the number of utilized labels was limited, then the number of supported LSPs increased when labels were reused; (2). If the number of supported LSPs was limited, then we can save more labels being utilized when reusing labels; (3). When labels were reused and the bandwidth of broadband light source was fixed, the cost of AWG codecs will be decreased due to the smaller code length of the utilized code which was because the number of utilized labels was smaller; and (4). When the labels are reused and the bandwidth of wavelength channels of AWG codecs was fixed, more bandwidth can be saves due to due to the smaller code length of the utilized code. It was concluded that the number of code sequences in one label stack can be reduced when labels were reused. Therefore, the BER performance in the label-reused scenario will be better than the situation without reusing labels.

 ISBN: 978-1-61208-758-0

REFERENCES

[1] R. Xu, Q. Gong and P. Ye, "A novel IP with MPLS over WDM-based broadband wavelength switched IP network," *IEEE J. Lightwave Technology*, vol. 19, pp. 596–602, 2001.

[2] H. Ghafouri-Shiraz and M. Massoud Karbassian, Optical CDMA Networks: Principles, Analysis and Applications. John Wiley & Sons Ltd, United Kingdom, 2012.

[3] L. D. Ghein, MPLS Fundamentals. Cisco Press, USA, 2007.

[4] R. K. Singh and Y. N. Singh, "An overview of photonic packet switching architectures," *IETE Technical Review*, vol. 23, pp. 15–34, 2006.

[5] N. Wada, H. Harai, W. Chujo, and F. Kubota, "Photonic packet switching based on multi-wavelength label switching using fiber Bragg gratings," ECOC'2000, Munich, Germany paper P10.4.6, 2000.

[6] J. Capmany, D. Pastor, S. Sales, and B. Ortega, "Subcarrier multiplexed optical label swapping based on subcarrier multiplexing: a network paradigm for the implementation of optical Internet," *The 5th International Conference on Transparent Optical Networks* (ICTON) , Warsaw, Poland, pp. 154-157, 2003.

[7] K. Kitayama, N. Wada, and H. Sotobayashi, "Architectural considerations for photonic IP router based on optical code correlation," *IEEE J. Lightwave Technology*, vol. 18, pp. 1834–1844, 2000.

[8] T. Khattab and H. Alnuweiri, "Optical CDMA for all-optical sub-wavelength switching in core GMPLS networks," *IEEE J. on Selected Areas in Commu*., vol. 25, pp. 905–921, 2007.

[9] N. Wada and K. Kitayama, "10 Gb/s optical code division multiplexing using 8-chip optical bipolar code and coherent detection," *IEEE J. Lightwave Technology*, vol. 17, pp. 1758–1765, 1999.

[10] M. K. Eghbal, F. Aminian and M. Shadaram, "Effect of different optical codes on a W-band WDM-over- OCDMA system," *The 19th International Conference on Transparent Optical Networks* (ICTON), Girona, Spain, pp. 1-4, 2017.

[11] D. Jia, C. Du, Z. Ji, H. Zhang, T. Liu, and Y. Zhang, "An Approach for Increasing User Capacity of OCDMA System Based on Vernier Effect" *IEEE J. Lightwave Technology*, vol. 34, pp. 4877-4883, 2016.

[12] W. H. Yang and C. S. Wu, "Optical CDMA Label Encoding for Optical Packet Switching in All-Optical Networks," *The 14th International Conference on Networks*, Singapore, vol. 2, pp. 1-5, 2006.

[13] A. Borude and S. Krishnan, "Simulation of Optical CDMA using OOC Code," International Journal of Scientific and Research Publications, vol. 2, pp1-5, 2012.

[14] A. A. Isaac, C. Yongsheng, C. Fushen, and A. E. Ampoma, "Performance of 40, 80 and 112 Gb/s PDM-DQPSK optical label switching system with spectral amplitude code labels," *the 22nd Asia-Pacific Conference on Communications (APCC)*, Yogyakarta, Indonesia, pp. 161-166, 2016.

[15] S. H. Meng, K. S. Chen, J. F. Huang, and C. C. Yang, "Orthogonal stacked composite M-sequence labels for quick packet routing over optical MPLS network," *the 28th Canadian Conference on Electrical and Computer Engineering (CCECE)*, Halifax, NS, Canada, pp. 908-913, 2015.

[16] P. Seddighian, S. Ayotte, J. B. Rosas-Fernandez, J. Penon, L. A. Rusch, and S. LaRochelle, "Label Stacking in Photonic Packet-Switched Networks With Spectral Amplitude Code Labels," *IEEE J. Lightwave Technology*, vol. 25, pp. 463-471, 2007.

[17] K. S. Chen, C. C. Yang, and J. F. Huang, "Stuffed Quadratic Congruence Codes for SAC Labels in Optical Packet Switching Network, " *IEEE Communications Letters*, vol. 19, pp. 1093-1096, 2015.

 ISBN: 978-1-61208-758-0